Inflammation- and infection-related alterations in the structure, biomechanics, and lytic susceptibility of fibrin

PhD Thesis

Ádám Zoltán Farkas

Molecular Medicine Doctoral School

Semmelweis University

Supervisor:	Krasimir Kolev, MD, D.Sc
Official reviewers:	Zsolt Oláh, MD, Ph.D
	János Fazakas, MD, Ph.D

Head of the Final Examination Committee: Gyula Domján, MD, Ph.D

Members of the Final Examination Committee: György Blaskó, MD, D.Sc
                                           Gábor Bőgel, MD, Ph.D

Budapest

2021

List of abbreviations

AIS	Acute ischemic stroke
ASA	Acetylsalicylic acid
CAD	Coronary artery disease
cH3	Citrullinated Histone H3
CitFg	Citrullinated fibrinogen
CRP	C-reactive protein
DVT	Deep vein thrombosis
FII-XIII(a)	(Active) factor II-XIII
FD50	Median fibrin/DNA ratio
FH50	Median fibrin/citrullinated H3 histone ratio
G-CSF	Granulocyte colony-stimulating factor
HEPES	4-(2-hydroxyethyl)-1-piperazine-ethane-sulfonic acid
IVC	Inferior vena cava
LSM	Laser scanning microscopy
MPO	Myeloperoxidase
NET(s)	Neutrophil extracellular trap(s)
NE	Neutrophil elastase
Nox	NADPH-oxidase
PAD	Peripheral arterial disease
PAD2,4	Peptidyl-arginine-deiminase 2 or 4
PT	Prothrombin
Plg	Plasminogen
SAXS	Small-angle X-ray scattering
SCG	Staphylocoagulase
SCG-PT	Staphylocoagulase-prothrombin=Staphylothrombin
SCG-T	Staphylocoagulase-thrombin
SEM	Scanning electron microscopy
TAFI(a)	(Active) thrombin activated fibrinolysis inhibitor
tPA	Tissue type plasminogen activator
uPA	Urokinase type plasminogen activator

VTE	Venous thromboembolism
vWFbp	Von Willebrand Factor binding protein
WBC	White blood cell

1. Introduction

According to the statistics of the World Health Organization, cardiovascular-, infectious diseases and malignant tumors remain the leading cause of death worldwide (1). Thrombus formation is a critical step in the pathophysiology of these diseases. Therefore, the prognosis of these diseases might highly depend on how we can fine-tune the hemostatic balance. There is an excellent development in the treatment of thromboembolic disorders, but their mortality remains high.

For better prognosis, novel therapeutic targets are needed. To identify such, it is necessary to understand the structural, mechanical, and lytic behavior of thrombi and determine their (easily accessible) predictors.

The interplay between the hemostatic- and the immune system is long known, but many aspects remain unclear. On the host's side, immune cells actively participate in thrombus formation, e.g., by neutrophil granulocytes releasing neutrophil extracellular traps (NETs). The altered structure of the formed clots and the antifibrinolytic effects caused by this network is well described (2). Thus, it is of interest to determine the NET content and its predictors in thrombi in different thromboembolic diseases.

On the other hand, intruders can also use the hemostatic system for their own agenda: bacteria often switch the hemostatic balance to a procoagulant state to form a barrier and evade the immune response of the host. *Staphylococcus aureus* expresses staphylocoagulase (SCG) to form a fibrin barrier. Characterizing this unique hemostatic shield would further our knowledge of the pathomechanism and complications of infectious diseases.

In our study, we examined *ex vivo* and *in vitro* thrombi focusing on NET content, predictors of clot structure, fibrinogen citrullination, and the effects of staphylocoagulase on thrombus composition, mechanical and lytic properties.

Before presenting our methods and results, this chapter summarizes the formation, structure, and mechanical aspects of fibrin; staphylocoagulase, neutrophil extracellular traps, and their known role in hemostasis.

1.1. Formation, structure, and mechanics of fibrin network

1.1.1. Activation and structure of thrombin

The enzymatically active serine protease α-thrombin is generated from its inactive precursor by the prothrombinase complex, which consists of a serine protease (factor Xa), a non-enzymatic cofactor (Va), and Ca^{2+} ions assembling on a phospholipid surface. α-Thrombin has two different chains: the A and B chains, while prothrombin (PT) also contains fragments 1 and 2 (3, 4). There are two distinct pathways for thrombin activation. 1) The initial cleavage at Arg271 yields the inactive prethrombin-2 intermediate, and for α-thrombin generation, a subsequent cleavage by factor Xa is necessary at Arg320 (5). 2) If the first reaction happens at Arg320, enzymatically active meizothrombin is generated, and the subsequent step at Arg271 results in α-thrombin (Figure 1).
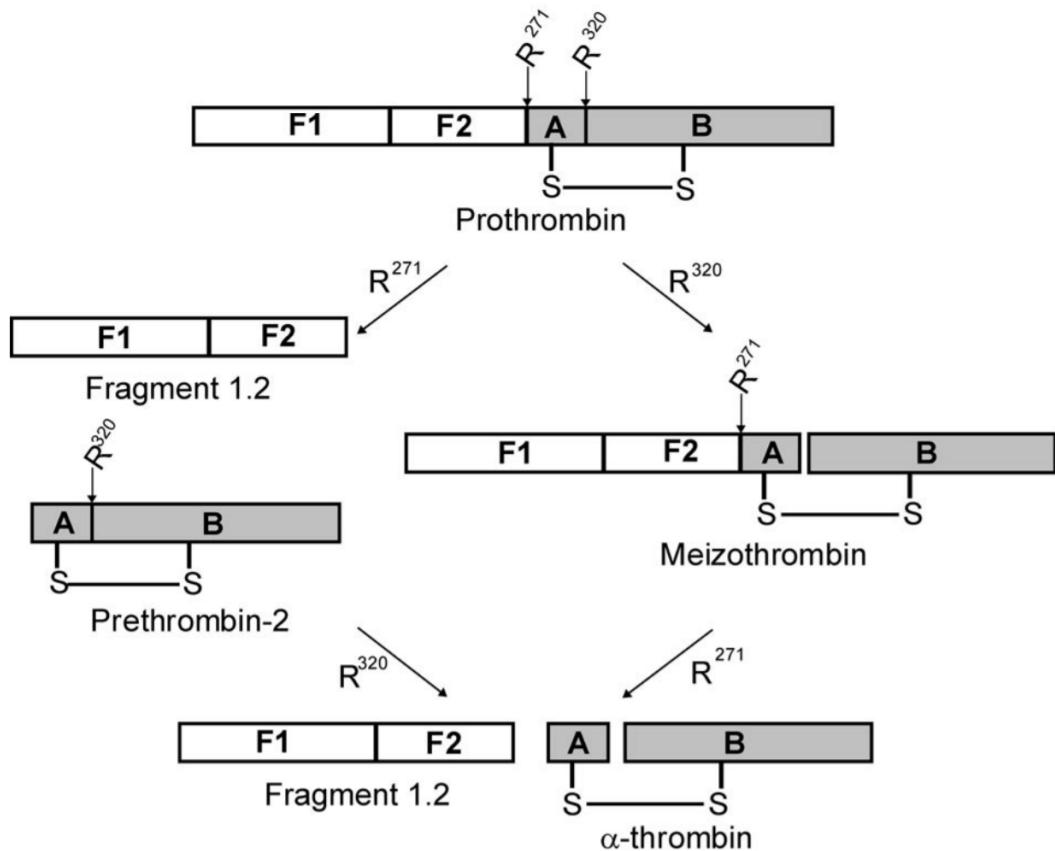
Figure 1. Thrombin generation. Human prothrombin consists of four main domains: the fragment 1, 2 and the A, B chains. Following cleavage at Arg271, Prethrombin-2 (enzymatically inactive) is formed along with fragment 1.2. A subsequent cleavage at Arg320 results in the production of α-thrombin. Alternatively, meizothrombin (an active intermediate) may be formed, if the first cleavage happens at Arg320. After the removal of fragment 1.2 (cleavage at Arg271), α-thrombin is generated. Figure adapted from (3).

In α-thrombin, a disulfide-bridge holds the A and B chains together, which consist of 36 and 259 amino acid residues, respectively (6).

Near the active site, exosite I – consisting of a 30s and 70s loop – has a role in binding fibrinogen, thrombomodulin, and in recognition of all further substrates of thrombin (PAR1, FV, FVIII, protein C, FXIII (7-15)). The role of exosite II is to bind heparin and platelets (through GpIbα receptor), but it also participates in the binding of FV, FVIII (16-20).

Most endogenic inhibitors of thrombin belong to the family of serine-protease inhibitors, also known as serpins. Serpins are proteins that contain a reactive center loop (7). Serine

proteases such as thrombin attack the reactive center loop, which is followed by the disintegration of an Arg-Met peptide bond. The N-terminal of the reactive center loop goes through a conformational change, which results in the movement of the protease to the opposite side of the inhibitor (21-23). This sudden alteration distorts the active center of the protease and slows down the lysis of the acyl-enzyme bond, inhibiting the dissociation of the enzyme from the inhibitor (24-27). Antithrombin, protein C inhibitor, heparin cofactor II, protease nexin I are able to inhibit thrombin. Glycosaminoglycans (heparan-sulfate, heparin) bind to both exosite II of thrombin and the serpins, increasing their inhibitory effect (7, 28-34).

1.1.2. Fibrinogen structure and formation of fibrin network

Fibrinogen is a 340 kDa glycoprotein, which can be found normally at approximately 1.5-4 g/L concentration in human blood plasma (35). It is an elongated, rod-shaped, 45 nm long molecule, consisting of three pairs of polypeptide chains (Figure 2): (Aα, Bß, γ)$_2$ (36, 37).
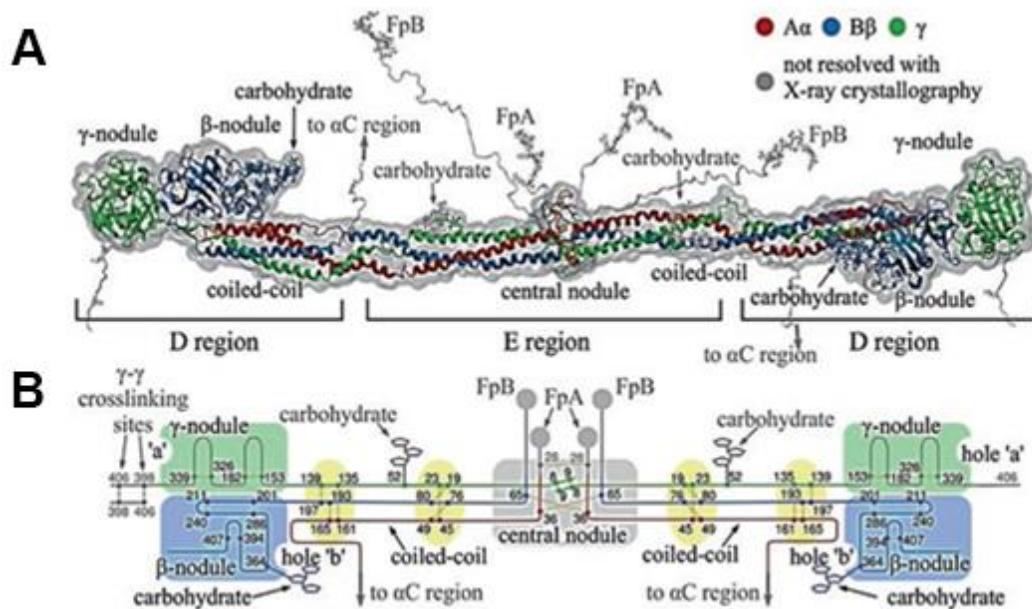
Figure 2. The structure of fibrinogen. The first panel (A) shows the structure of fibrinogen with the three dimeric polypeptide chains (Aα, Bß, γ)$_2$, which form the two distal D and the central E regions. The schematic structural figure (B) shows the disulfide bonds, holes 'a' and 'b'. For a more detailed description, see the text below. FpA, FpB: Fibrinopeptide A and B. αC: C-terminal of the α-chain. Adapted from (38).

The Aα chain has 621, the Bß 461, and the most common γ form 411 amino acids (39). The chains are stabilized with altogether 29 disulfide bonds (40). The E region can be found in the center of the protein, while the two distal parts participate in the formation of two D regions.

The cleavage of fibrinopeptide A at the N-terminal of fibrinogen Aα chain is the initiator of fibrin polymerization (41). As fibrinogen has a dimeric structure, two "A-knobs" are formed, which are able to attach to "a-holes" on γ-chains (Figure 3). This leads to the formation of a double-stranded, end-to-side attached fibrin protofibril. As the monomers are aligned in a half-staggered manner, a lateral periodicity of 5-10 nm and a longitudinal of 22.5 nm can be observed (42-49). This initial step is followed by the cleavage of fibrinopeptide B at the N-terminals of the Bß chains. Thus, two "B-knobs" are formed. The B-knob-b-hole interactions are thought to have a role in the lateral aggregation of fibrin (50). The C-terminal of α- and γ-chains, the so-called ß-nodules (see Figure 2), coiled coils, and N-glycans on fibrin monomers also have a role in lateral aggregation (51-53). The αC domains normally interact with the central portion of the molecule. During fibrin formation, αC domains dissociate from the central region and are available for intermolecular interaction. Thus, they are important for the enhancement of lateral aggregation during fibrin polymerization (54). As a result, thicker fibrin fibers are formed, with a diameter of 100-200 nm (55). The fibrin network also possesses branching points. These are made up of three distinct fibrin fibers of similar diameters (56).
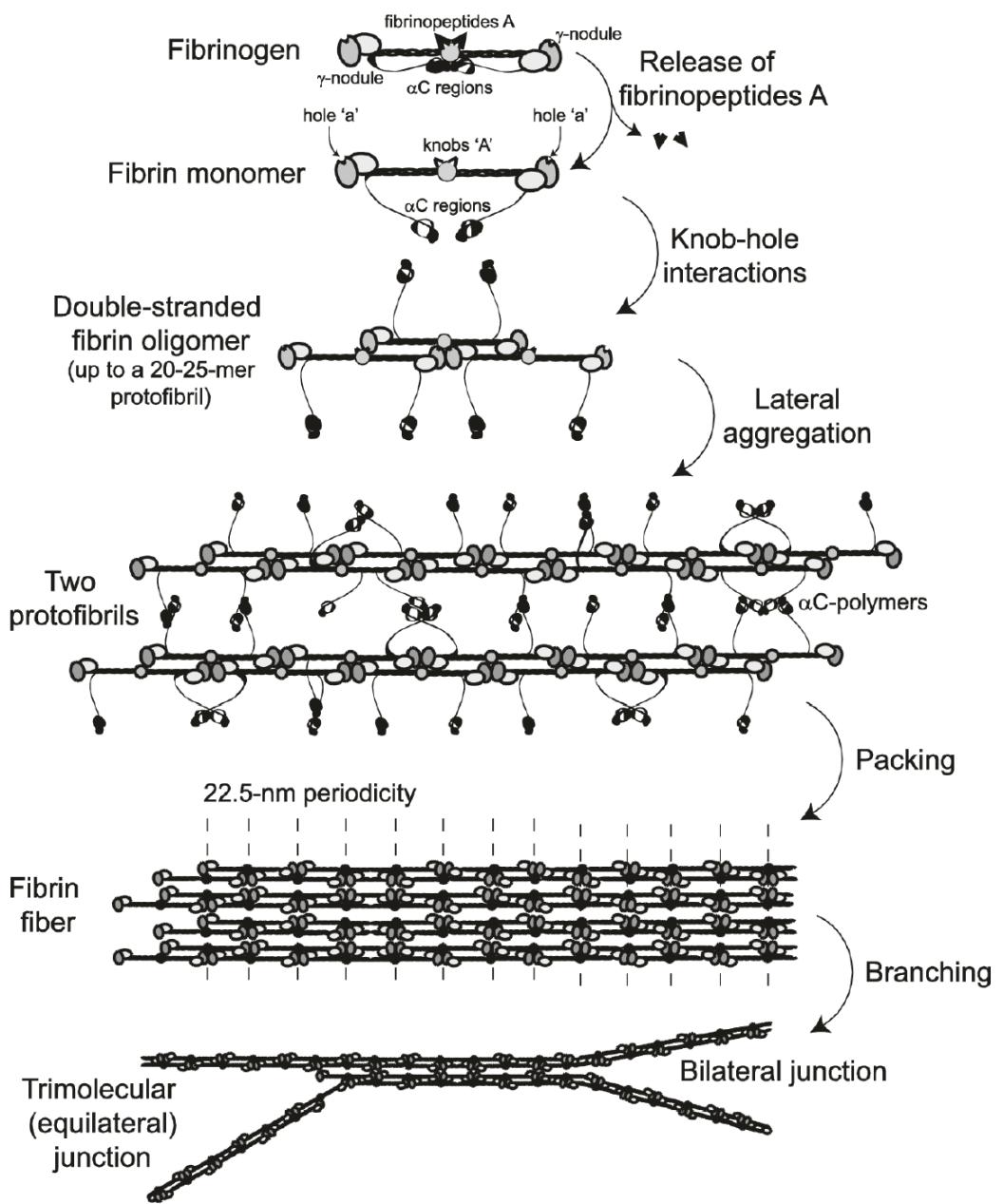
Figure 3. Fibrin polymerization. Following the cleavage of fibrinopeptides A, A-knobs can attach to the a-holes found on the γ-chain in fibrin monomers, forming a double-stranded, half staggered fibrin oligomer. After the removal of fibrinopeptides B, lateral aggregation starts, in which αC-regions also have an important role. As a result, fibrin fibers are formed. Branching points are formed with either trimolecular or bilateral junctions. For more details, see the text. Figure adapted from (57).

Fibrin fibers and branch points form pores of different sizes (0.1-5 μm), which allow the permeation of proteins, fluid, and nanoparticles through the clot (58-61).

Fibrin structure is highly dependent on thrombin activity, as clots with higher thrombin concentration have thinner fibers, smaller pores, more branch points. Lowering thrombin activity has opposing effects (58, 62).

1.1.2.1. Mechanical properties of fibrin

Polymerized fibrin is viscoelastic, as it goes through a reversible mechanical deformation (elasticity), but also a slow irreversible deformation (viscosity) following mechanical impact. The elastic response is measured by the so-called shear storage modulus (G'), while the viscous response is characterized by the shear loss modulus (G"). The relative viscosity and stiffness of a clot are measured by the ratio G"/G' (35).

Each of the above-mentioned (D-E-D) regions of fibrinogen contains α-helical coiled coils (42), of which three right-handed coiled coils form a left-handed supercoil (63). These structures provide the ability for fibrin to undergo partial untangling and reversible extension-contraction (38). This enables the adaptation to tensile stress, although following stronger impact, the α-helices are converted into ß-sheets (64, 65). During mechanical stress, the unfolding coiled coils allow fibrin to elongate more than 5-fold, up to about 250 nm (66, 67).

Increasing fibrinogen concentration leads to the formation of more rigid clots (increased G'), which is the result of higher fibrin fiber- and branchpoint density (56). The effect of thrombin- and $CaCl_2$ concentration is more complex: clots are most rigid at a peak concentration of 0.25 IU/ml thrombin and 1.5 mM $CaCl_2$. This is the result of optimal fiber diameter and branching point density (56).

1.2. Fibrinolysis

Once clots fulfilled their purpose, their main fibrin scaffold must be eliminated. This process is called fibrinolysis and has two main steps (Figure 4). The activation of plasminogen (Plg, I) is followed by the digestion of fibrin (II) (68).
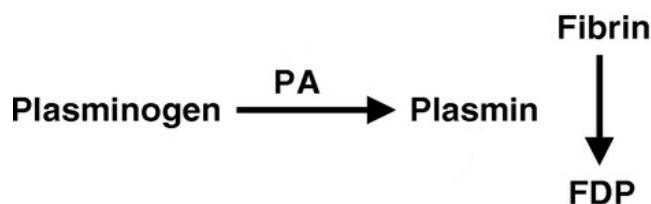
Figure 4. The schematic diagram of fibrinolysis. Fibrinolysis has two main steps. First, plasminogen is activated by plasminogen activators (PA) to form plasmin. The active serine-protease plasmin can degrade fibrin, and the reaction yields fibrin degradation products (FDP). For more details, see the text below. Modified from (69).

1.2.1. Activation of plasminogen

The activation of Plg is carried out by endogenous and exogenous Plg activators. Tissue-type plasminogen activator (tPA) with a 70 kDa weight is mainly secreted by vascular endothelial cells (70, 71). Fibrinolytic enzymes have homologous domains. In tPA, a finger-like domain, an epidermal growth factor-like domain, two kringle (K1, K2) domains, and a C-terminal trypsin-like catalytic domain can be found (72). The protein is secreted as a proenzyme in a single-chain form (sc-tPA). If plasmin cleaves the molecule next to an arginine residue, the activity of the formed two-chain tPA (tc-tPA) is about ten-fold higher (73), but in the presence of fibrin(ogen) this difference disappears (74). tPA can attach to fibrinogen via its finger- and K2 domains (75, 76). Following the fibrinogen-fibrin conversion, high-affinity lysine-dependent and low-affinity lysine-independent binding sites become available for tPA (77). tPA is a fibrin selective plasminogen-activator, as it is only able to activate fibrin-bound Plg. Both enzymes can bind to fibrin, which provides them a scaffold for activation. Furthermore, binding to fibrin increases the enzymatic activity of tPA more than 100-fold (73).

The urokinase-type plasminogen activator (uPA) is also secreted as a single-chain 53 kDA proenzyme by endothelial cells, monocytes, leukocytes, epithelial cells, and

14

fibroblasts (78-82). uPA has a growth factor-like domain, a kringle domain, and a C-terminal serine protease domain (72). Plasmin, FXIIa, trypsin, and cathepsins are able to cleave single-chain uPA to the active two-chain form (78, 83, 84). The growth factor-like domain has a role in uPA receptor-mediated activation (85). Once active, uPA is able to activate Plg without the presence of fibrin (86, 87).

Streptokinase is an exogenous activator of Plg, produced by ß-hemolytic *Streptococci*. The 47 kDa protein forms a stoichiometric 1:1 complex with Plg. Streptokinase itself is a non-enzymatic activator, but the newly formed complex binds further Plg molecules and activates them to plasmin following proteolytic cleavage (88-92).

Another Plg activator of bacterial origin is staphylokinase, which is secreted by *Staphylococcus aureus* (see chapter 1.3.3) (93). This nonenzymatic activator also forms a 1:1 complex with Plg, which induces a conformational alteration in the active center of the proenzyme, and the newly formed complex serves as a Plg activator (94, 95). Fibrin acts as a cofactor in the process, as it not only protects the activator complex from the fibrinolysis inhibitor α_2-antiplasmin, but also increases the activity of the staphylokinase-plasmin activator complex (95-97).

Plasminogen is a 92 kDa glycoprotein secreted by the liver and has a blood plasma concentration of 2 μM (98, 99). The amino acid sequence of the enzyme starts with glutamate (Glu-Plg), which is part of the N-terminal preactivation peptide. During limited proteolysis catalyzed by plasmin, the preactivation peptide is removed, while lysine-Plg is formed. The N-terminal part is followed by five kringle domains (K1-5) stabilized by three disulfide bonds in each domain (100). The C-terminal is the catalytic domain. Upon activation, His603, Asp646, and Ser741 are brought together, forming the active site characteristic of serine proteases, which can degrade fibrin (72).

In Lys-Plg, the N-terminal is removed; thus, the new conformation supports the binding and activation of the proenzyme with tPA or uPA. Furthermore, Lys-Plg can attach to fibrin easier than Glu-Plg (101, 102). K1-2 and K4-5 are able to bind to C-terminal Lys-residues (K1 and K4 have the highest affinity to fibrin(ogen)) (103-106).

The activation of plasminogen during the lysis of a clot is rather complex. First, Plg molecules embedded in fibrin will be activated. As plasmin cleaves fibrin next to Lys-residues, new C-terminal Lys amino acids become available. This potentiates the recruitment of further Plg-molecules and also tPA (which can attach to fibrin with its

kringle domain) (72). Plg and tPA are brought to close contact, and after a peptide bond between Arg561 and Val562 is cleaved near K5 by Plg activators, the two-chained active plasmin is formed (107). Fibrin serves as a cofactor in Plg activation, as upon binding to fibrin, Plg goes through a conformational change, which facilitates its conversion to plasmin (108).

1.2.2. The molecular process of fibrinolysis

Activated plasmin initiates fibrinolysis as described in the previous chapter. First, free C-terminal Lys residues are liberated, which is followed by the subsequent binding of further plasmin and tPa molecules, which leads to positive feedback. On the clot surface, numerous Lys binding sites are found (at least one per fibrin monomer), and the affinity of plasmin and tPa for fibrin is rather high ($K_D \sim 10^{-8}$ M) (68, 109). Thus, tPa attaches to fibrin mainly on the surface – although the pores in fibrin would allow tPa to diffuse deeper (68, 72). The initial lysis happens in a few micrometers depth from the surface (110-112). Later, according to the concentration gradient of fibrinolytic enzymes, deeper parts of the thrombi also begin to dissolve (112, 113).

The binding site of plasmin is near the end-to-end binding site of fibrin monomers. The flexible protein is able to reach the cleavage site on the adjacent protofibrils; thus, it "crawls" from strand to strand while cleaving fibrin fibers (114). In the lateral direction, there are only 5-10 nm wide gaps, which allows K2 of plasmin to bind to the second fibrin strand before it releases the previous one with K1. Thus, first, a bridge is formed, and when the lysis of the fibrin strand bound by K1 is complete, the enzyme crawls to the next strand, bound by K2 (115, 116).

During plasmin-mediated lysis, soluble fibrin degradation products are formed: fragments E and D. According to the structure of fibrin, fragment E is from the central, and D fragments are from the lateral domains. FXIIIa-crosslinked fibrin monomers yield D-dimers (117). The total dissolution of clots requires approximately 25% degradation of E-D interactions (118).

Fibrin fiber diameter has a great impact on fibrinolysis. Although single fibers are cleaved faster when they are thinner, whole fibrin matrices with thicker fibrin fibers tend to be lysed faster (119). In clots with thicker fibers, fibrinolytic enzymes have to cut through

fewer fibrin strands, and the movement of t-PA "frontline" is faster, leading to increased plasminogen activation (120).

1.2.3. The inhibitors of fibrinolysis

Plasminogen activator inhibitor 1 (PAI-1) is a serpin secreted by endothelial cells, platelets, and also hepatocytes (29, 121-124). The main targets of PAI-1 are tPA and uPA (forming a 1:1 stochiometric complex), but it is also able to inhibit plasmin itself (121, 125). The rapid, spontaneous inactivation of PAI-1 is inhibited by binding to vitronectin in blood plasma (126-128). As vitronectin is found at the site of vascular injury, PAI-1 can bind to the glycoprotein and inhibit early clot lysis (129, 130). Following inhibition, the enzyme-inhibitor complex is eliminated from the circulation, which is followed by intracellular degradation (131).

Plasminogen activator inhibitor 2 (PAI-2) also belongs to the family of serpins. This inhibitor is secreted by monocytes, placental trophoblasts (132-134). The inhibiting effect of PAI-2 on uPA and tc-tPA is lower than PAI-1 (10-50-fold lower rate constant compared to PAI-1) (135). There is a Gln-rich region in PAI-2 that serves as a substrate for the transglutaminase FXIIIa (136). Thus, PAI-2 can be attached covalently to the α chain of fibrin during transglutamination with an isopeptide bond (137).

The serpin α_2-plasmin inhibitor (α_2-PI) is secreted by the liver. The main inhibitor of plasmin has a blood plasma concentration of approximately 1 μM (138, 139). α_2-PI can inhibit plasmin in many ways: 1) It can bind covalently to fibrin (this process is similar to the binding of PAI-2 to fibrin, (140-143), which renders clots more resistant to fibrinolysis. 2) As the inhibitor has surface Lys-residues, it competitively inhibits plasmin. 3) It forms an inactive enzyme-inhibitor complex with high affinity, as the C-terminal of α_2-PI can bind to the kringle domains of Plg of plasmin ($K_D = 2 \times 10^{-10}$ M) (144). α_2-macroglobulin is a homotetrameric glycoprotein that can inhibit many proteinases. In the central region of the protein, the "bait" can be cleaved by almost all endopeptidases. Cleavage of the bait sequence is followed by a conformational change that traps the enzyme (145, 146). When this cage is closed, an internal ß-cysteinyl-γ-glutamyl thiol ester bond is available to form a covalent bond with the enzyme (147, 148). The enzyme-inhibitor complex goes through receptor-mediated internalization (with LDL-receptor related protein 1) and intracellular degradation (149).

17

Thrombin activated fibrinolysis inhibitor (TAFI) is a metallo-carboxypeptidase secreted by the liver as a zymogen (150, 151). To gain maximal activity, the enzyme has to go through proteolysis (yielding TAFIa), the removal of an activation peptide catalyzed by thrombin (or plasmin) (150, 152-154). Thrombin activates TAFI efficiently when bound to thrombomodulin, as its activity increases more than 1000-fold (155, 156). Thrombin catalyzed TAFI-activation is Ca^{2+}-dependent (157, 158). Plasmin does not require Ca^{2+} to activate TAFI, but the efficiency of the process is ten-fold lower compared to the thrombin-thrombomodulin complex (159). Removing C-terminal lysine residues from fibrin, TAFI decreases binding sites for fibrinolytic enzymes (157, 160). TAFIa also inhibits the conversion of Glu-Plg to Lys-Plg (161, 162). Removing Lys-residues also decreases the half-life of plasmin, as Lys-bound plasmin is more resistant to α_2-macroglobulin (163). TAFIa can be crosslinked to fibrin by FXIIIa, which increases the half-life of the enzyme (164). The soluble form is rather unstable, and the enzyme loses its activity in minutes following an intrinsic structural alteration (165, 166). Inner regions are exposed that can bind to α_2-macroglobulin, which is followed by the elimination of TAFIa (109).

1.3 *Staphylococcus aureus*

S. aureus is a Gram-positive coccal bacterium, a member of the human normal microbial flora, which can cause a broad palette of pathologies – from localized skin infections to life-threatening invasive diseases (167, 168). The spreading of antibiotic-resistant strains poses an increasing burden on healthcare (169). *S. aureus* infections can be coupled to the formation of abscesses or valvular vegetation in infective endocarditis (168), which exemplifies the interplay between bacterial pathogenic factors and the blood coagulation and innate immunity systems of the host. In endocarditis, bacteria colonize the endocardium – either following endothelial layer injury or endothelial cell activation – and the bacterial products, as well as the inflammatory process, can destroy the heart valve tissue (170).

1.3.1 Staphylocoagulase

S. aureus has a remarkable number of virulence factors, some of which are specifically designed to alter and exploit the host coagulation system to its own advantage for propagation in the host organism. One of these factors is staphylocoagulase, a protein that binds to prothrombin, and the formed SCG-PT complex (staphylothrombin) expresses thrombin-like proteolytic activity through a non-proteolytic zymogen activation of prothrombin (171, 172).

SCG is a single-chain molecule with an approximately 61.000 Da molecular weight (173). In the N-terminal region, it contains D1-D2 α-helical domains, followed by a linker region (Figure 5). In the C-terminal region, the R-domain contains several 27-amino acid repeats. The N-terminal region, mainly the D2 domain is responsible for binding with high affinity to exosite I on thrombin or proexosite I on prothrombin/prethrombin-2 (171, 174). Each repeat in the R-domain is available to bind a fibrinogen molecule, which retains the enzyme to the growing clot or bacterial vegetation (175-177).
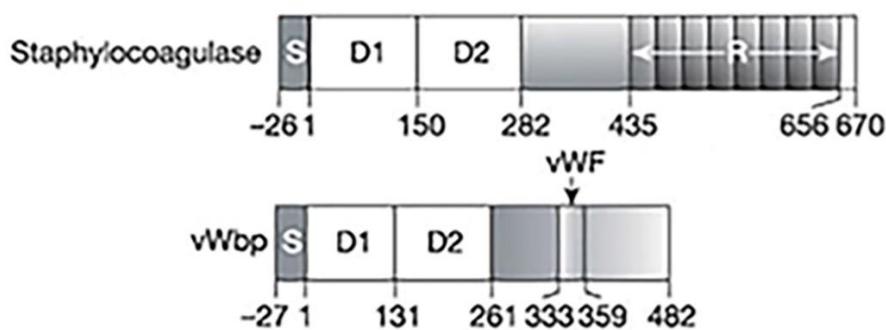
Figure 5. The schematic structure of staphylocoagulase and von Willebrand factor binding protein (vWFbp). S indicates a signal peptide sequence. D1-D2, R are domains of staphylocoagulase and vWFbp, as detailed in the text. The arrow near vWFbp indicates the binding site of von Willebrand factor (vWF). Modified from (171).

SCG is able to form a stoichiometric 1:1 complex with prothrombin, which is followed by the insertion of the N-terminal peptide sequence (D1 domain and the N-terminal dipeptide, which is similar to that found on cleaved thrombin (171)) of SCG into the activation pocket of PT (Figure 6). The formed complex (SCG-PT) can convert fibrinogen to fibrin without the proteolytic activation of PT (171).
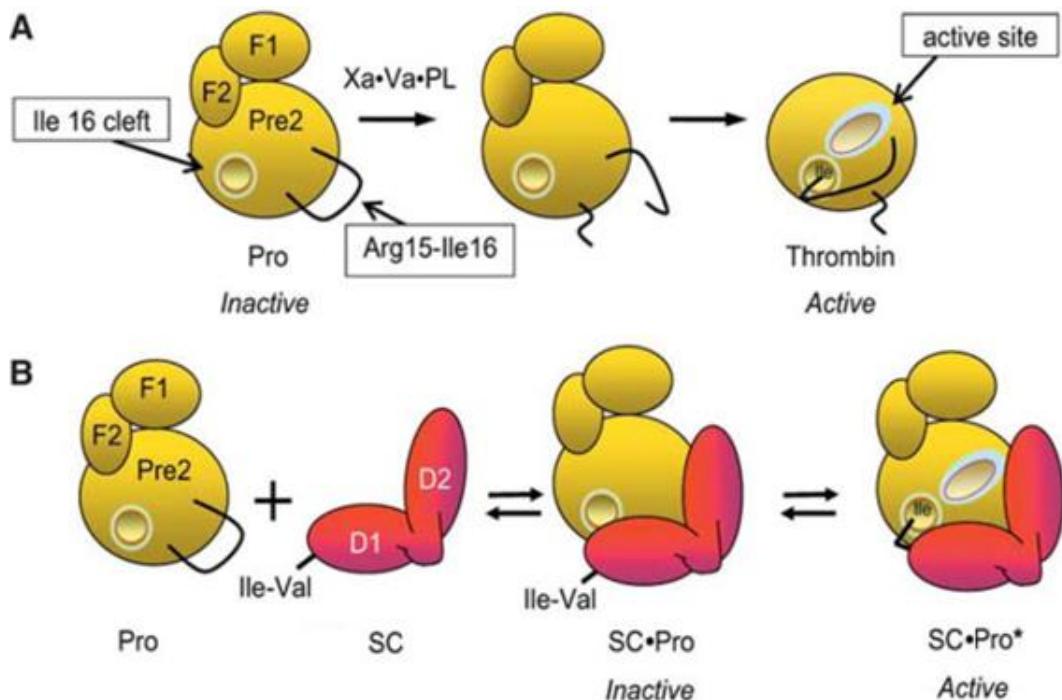
Figure 6. Schematic view of prothrombin activation by FXa (A) or staphylocoagulase (B). Panel A shows the physiological route of prothrombin activation by factor Xa-Va-Phospholipids (PL) from prothrombin (Pro). Pre2 indicates prethrombin-2 found in the structure of prothrombin along with F1, 2: fragments 1 and 2. The staphylocoagulase (SC) mediated activation of prothrombin can be seen on panel B. After SC is attached to prothrombin, the N- terminal Ile residue is inserted into the activation pocket of prothrombin. For more details, see the text above. Modified from (174).

SCG-PT has a high specificity toward fibrinogen and is unable to bind other physiological substrates of thrombin, including its plasma inhibitors (174, 178). Furthermore, conventional antithrombotic therapy is usually ineffective against SCG-PT; only small-molecular inhibitors might be used (e.g., argatroban, dabigatran (179)). Hirudin and bivalirudin are bivalent, potent thrombin inhibitors. The binding of these molecules to exosite I is blocked (see in the text above). The resulting uncontrolled fibrin formation is thought to play a role in abscess development and bacterial attachment to cardiac valves in acute endocarditis or vascular implants (177, 178, 180). A common complication in endocarditis is the occurrence of septic embolisms (181), but in the absence of data on the characteristics of the fibrin matrix formed by SCG-PT, the exact contribution of this fibrin to the fragmentation and embolization of the bacterial vegetations is not clear (181).

1.3.2. von Willebrand factor binding protein, the other coagulase of *S. aureus*

von Willebrand factor binding protein (vWFbp) is anchored to the bacterial cell wall by clumping factor A (another virulence factor of *S. aureus*) (182). The protein has structural similarities to SCG, as they share the N-terminal and D1-2 domains (Figure 5). Thus, vWFbp can also activate prothrombin, as discussed in the previous chapter (180). Besides activating prothrombin, vWFbp also binds to the A domain of vWF, tethering *S. aureus* bacteria to the vessel wall upon injury, as on the C-terminal binding sites for vWF and fibrinogen are available. (183-186). With the coagulase activity, bacteria released from the primary infection site form bacteria-fibrin-platelet aggregates that can adhere to the vessel wall, making it possible to form metastatic infections or infective endocarditis (186).

1.3.3. Haemostasis and *S. aureus*

S. aureus infection is often accompanied by biofilm and/or abscess formation, in which fibrin is an abundant structural element. This network shields bacteria from the immune system, thus the experimental genetic removal of SCG or vWFbp from the pathogen (or pharmacologically inhibiting their effect with dabigatran) significantly reduced its ability to cause skin- or catheter infections, making them potential therapeutic targets (187, 188). In bacterial endocarditis, fibrin and platelets form a matrix in which *S. aureus* is embedded (189). Infection with SCG-vWFbp mutant *S. aureus* results in lower pathogenicity and increased survival (177); in rats, dabigatran has a preventive effect against *S. aureus* endocarditis (190).

1.4. Neutrophil extracellular traps (NETs)

NETs are net-like structures composed of decondensed chromatin and embedded antimicrobial peptides emitted by polymorphonuclear cells to the extracellular space (191).

1.4.1. NETosis

1.4.1.1. Suicidal NETosis

Brinkman et al. described a novel cell death, where neutrophils – following different stimuli (e.g., Phorbol 12-myristate 13-acetate *in vitro*) – are activated, and minutes later, cells become flat (191-194). The nucleus loses its lobulation, the chromatin becomes decondensed, the inner-, and outer nuclear membrane separates, and they form vesicles. The intracellular granules disintegrate; thus, the cytoplasm and nucleoplasm form a homogenous mass. Cells become rounded and shrink until the cell membrane bursts and the cell content is released to the extracellular space (194). This phenomenon was named NETosis (194-196). The process is different from apoptosis or necrosis, as the cell membrane remains intact (194), no phosphatidyl-serine exposure, membrane blebbing, chromatin-condensation, or DNS-fragmentation is observable (194, 197), and the process does not require caspase activity (198). This so-called suicidal NETosis requires 2-3 hours (194).

1.4.1.2. Vital NETosis

Another distinct form of NET formation is vital NETosis, during which neutrophils survive NET-release, the cell membrane remains intact, and the cells further function as antimicrobial cytoplasts (199-201). This process is faster compared to suicidal NETosis, occurs in 5-60 minutes, and involves either nuclear or mitochondrial DNA (191, 199, 200).

1.4.2. Structure of NETs

The main scaffold of NETs is composed of 15-17 nm wide DNA threads, which are "decorated" with 25-50 nm globular domains (191, 202). These can organize into thicker fibers with a diameter of 15-25 nm, mimicking thin fibrin fibers (Figure 8) (203). According to transmission electron microscopic images, these structures are not

surrounded by membranes proving the extracellular localization (191). When hydrated, NETs are cloud-like structures, with a volume 10-15 fold bigger than the emitting cell (204, 205).
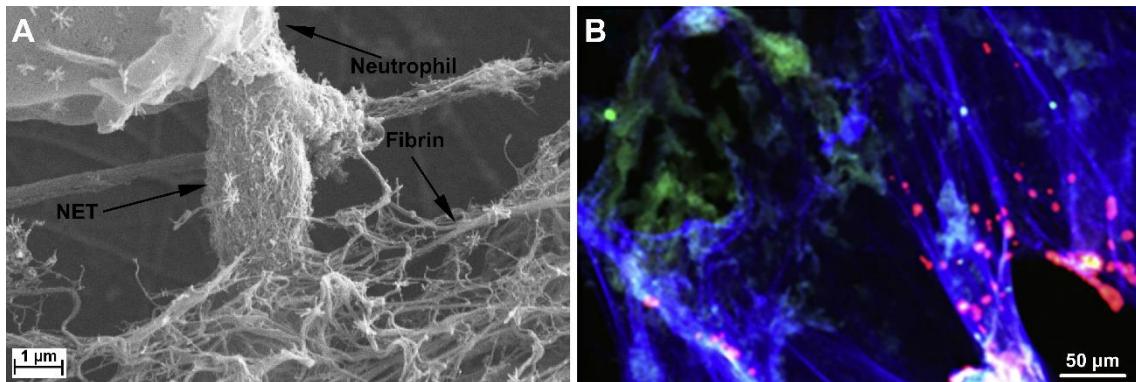
Figure 8. Intertwined fibrin and neutrophil extracellular trap (NET) scaffolds of thrombi. A: Scanning electron micrograph of NETs released by phorbol myristate acetate-activated isolated neutrophils in a fibrin clot. B: Confocal micrograph of a coronary thrombus removed with percutaneous coronary thromboaspiration from a 39-year old female patient with acute myocardial infarction and immunostained for fibrin (green) and citrullinated histone H3 (red) and stained for DNA with TOTO-3 (blue). Modified from (206).

Antimicrobial peptides are bound to the extracellular scaffold. Both core (H2A, H2B, H3, H4) and linker (H1) histones but also their degradation products (buphorines) attach to DNA (191, 193, 207). In NETs, H2A- and H2B histones are bound to DNA, but H3, H4 histones have a lower affinity, which leads to their dissociation. The peptidyl-arginine-deiminase 4 (PAD4, see in chapter 1.4.3.3 and 1.5) processed H1 histone is also prone to dissociate from extracellular DNA (205, 208). Along with the nuclear histones, cytoplasmatic (calprotectin) and many granular proteins (including enzymes, serine proteases) can be found in NETs: neutrophil elastase (NE), myeloperoxidase (MPO), cathepsin G, defensines, azurocidine, lactoferrin, gelatinase, proteinase 3, proteoglycan recognizing proteins, neutrophil serine protease 4, bactericidal permeability-increasing protein (205, 209-217).

1.4.3. NET formation

1.4.3.1. Triggers of NET formation

NET formation can be induced by pathogens, antigen-antibody complexes, activated cells, and other endogenous, non-endogenous factors (Table 1, (209, 218-228). The amount of NETs is often proportional to the amount of the activator. The stimulatory effect of microbial components is less effective than that of whole microorganisms (193, 194). Many receptors are included in the signal transduction, such as Toll-like receptors, Fc immunoglobulin receptors, cytokine receptors, or the Mac-1 integrin receptor (191, 218, 229-231). HIV-1 virus can initiate NET formation through endosomal Toll-like receptors 7 and 8 (232).

Table 1. Microbial and non-microbial inducers of NET-formation. Based on (209, 218-228).

Microbial stimuli		
Bacteria	**Fungi**	**Viruses**
Staphylococcus aureus *Streptococcus pyogenes* *Streptococcus dysgalactiae* *Escherichia coli* *Shigella flexneri* *Haemophilus influenzae* *Yersinia enterocolica* *Yersinia pseudotuberculosis* *Mannheimia haemolytica* *Mycobacterium tuberculosis* *Mycobacterium canettii* *Klebsiella pneumoniae* *Listeria monocytogenes* *Porphyromonas gingivalis* *Pseduomonas aeruginosa* *Enterococcus faecalis* *Helicobacter pylori* *Lactococcus lactis* *Serratia marcescens*	*Candida albicans* *Aspergillus fumigatus* *Aspergillus nidulans* *Cryptococcus gattii/neoformans*	SARS-CoV-2 Feline leukemia virus HIV-1 Influenza A
Microbial particles		**Protozoa**
Lipopolysaccharide Lipophosphoglycane Formil-methionyl-leucil-phenylalanine δ-toxin of *S. epidermidis* Glucose-oxidase		*Leishmania amazonensis* *Leishmania donovani* *Leishmania major* *Leishmania chagasi* *Toxoplasma gondii*

M1 protein-fibrinogen complex	
Panton-Valentin leukocidin	
Non-microbial inducers	
Endogenous factors	**Non-physiological factors**
Interleukin-1ß/8/23	
Autoantigens	
Antigen-antibody complexes	
TLR4-activated platelet	
Activated endothelial cell	
NO	
Na-urate crystal	Phorbol 12-myristate 13-acetate
Ca^{2+}	Phorbol 12-myristate 13-acetate + ionomycin
Granulocyte-monocyte colony-stimulating factor + Complement 5a or lipopolysaccharide	Cholesterol-lowering statins
Interferone + eotaxine	
Interferon-α/γ + Complement 5a	
Interleukin-5 + Interferon-γ or lipopolysaccharide	
H_2O_2	
Tumor necrosis factor α	
Platelet-activating factor	

1.4.3.2. The NADPH-oxidase (Nox)-dependent pathway

During suicidal NETosis, various agonists may induce Nox-dependent NET formation in two different pathways (191, 233). Following stimulation, Ca^{2+} enters the cytosol from the endoplasmatic reticulum increasing the activity of protein kinase C. This results in the phosphorylation of gp91phox/Nox2, which is necessary for the assembly of Nox (234). Nox has a role in generating free oxygen radicals: it reduces molecular oxygen to superoxide-anion with an electron from NADPH. This is further converted by superoxide-dismutase to H_2O_2, a substrate of myeloperoxidase. Myeloperoxidase (MPO) catalyzes the formation of HOCl (235). These reactive oxygen species (ROS) have a role in the disintegration of granular and nuclear membranes (194, 235). As neutrophil elastase (NE) and MPO are liberated from granules, they can get into close contact with nuclear

27

proteins, resulting in the degradation of histones, facilitating chromatin decondensation (235). H1 and core histones are cleaved by NE, of which the degradation of H4 seems to have the most prominent effect on chromatin-decondensation (235). MPO travels to the nucleus in the first 30 minutes of NETosis, following NE, and potentiates chromatin-decondensation non-enzymatically by chlorination (235, 236). The swelling nucleus leads to the disappearance of nuclear lobules (237, 238). The cytosolic and nuclear content is mixed together, DNA becomes decorated with antimicrobial (granular) content and is later released to the extracellular place (191, 235).

Upstream of Nox activation, there can be substantial differences in signal transduction. Following activation with phorbol 12-myristate 13-acetate, the Raf-Mek-Erk and Rac2 pathway lead to Nox-activation (239, 240). However, following stimulation with lipopolysaccharide, a separate pathway is initiated, mediated by c-Jun N-terminal kinases (241).

1.4.3.3. Nox-independent NETosis

Nox-independent NETosis is a puzzle yet to be solved. Parker et al. showed that calcium ionophores (e.g., ionomycin) could induce NETosis, independently of the Nox pathway (227). PAD4 has an essential role in the process, as the calcium influx initiated by the non-physiological ionophores activates the enzyme, which is translocated to the nucleus (as it has a nuclear localization signal in its structure, (242)). Here, the enzyme catalyzes the deimination of Arg into citrulline, accompanied by the loss of a positive charge (237). Substrates of PAD4 include lamin C, core, linker histones, and PAD4 itself (which may lead to decreased activity) (208, 237, 243-245). The result is DNA-histone dissociation and the detachment of heterochromatin protein 1ß, leading to chromatin decondensation (234, 237, 246-248).

Calcium-activated potassium channels and mitochondrial ROS also seem to have an essential role in Nox-independent NET formation, as inhibiting these potassium channels or mitochondrial ROS production decreases NETosis (247). Ravindran et al. reviewed that mitochondria in neutrophils play only a minimal role in ATP synthesis (249); therefore, mitochondria could have a novel role and serve as a ROS generator for Nox-independent NET-formation (202).

1.4.4. The degradation of NETs

The clearance of NETs is a two-step, complicated process, as each component requires distinct mechanisms for breakdown. First, NETs have to be fragmented, and later, the remnants are removed by phagocytic cells. The degradation is mediated by DNases, proteolytic enzymes, and macrophages, neutrophils that clear the debris (250). DNase I is secreted into human blood plasma by several exo-, endocrine organs (251-253), while DNase-I-like-3 is produced by hepatocytes, cells of the kidney, spleen, and also macrophages (254). Their role is to break down the main scaffold of NETs. Plasmin has a supportive role in the process, as it facilitates DNase activity by breaking down histones (255). However, such cooperation is not possible between plasmin and DNase-I-like-3, as the latter one is a substrate of plasmin (256).

Histones are degraded by NE, thrombin, and activated protein C (257). The efficacy of activated protein C might be reduced when histones are bound to DNA (258, 259).

During debris phagocytosis, macrophages secrete resolvins and protectins, which reduce further neutrophil activation (260).

1.4.5. NETs and hemostasis

The immune- and hemostatic systems often cooperate in fighting bacteria, and thrombus formation is often coupled with NET production, leading to "immunothrombosis" (261). NETs and fibrin networks become intertwined (Figure 8) in clots leading to functional and structural consequences.

1.4.5.1. The effects of DNA, the backbone of NETs

The DNA network of NETs is highly negatively charged with the potential to enhance the activation of FXII (262). Polyphosphates released to the extracellular space also lead to FXII activation following histone-mediated platelet activation during NETosis (263, 264). DNA also has a role in clotting initiation through the extrinsic pathway and serves as a cofactor for thrombin-dependent FXI activation (265, 266).

Cell-free DNA also has antifibrinolytic effects. The formation of PAI-1 - tPA complexes is more prominent; DNA and fibrin may form an inactive complex with plasmin; tPA-mediated plasminogen activation is inhibited (258, 267, 268). Plasmin mediated lysis rate is lower. Once fibrin is digested, the release of fibrin degradation products is also slower

(258, 269). These findings are supported by the fact that the lysis of *ex vivo* and *in vitro* clots is enhanced in the presence of DNases (258, 270, 271).

1.4.5.2. The effects of histones on hemostasis

Histones may bind to phospholipid membranes, leading to prolonged clotting time *in vitro* (272, 273). During NETosis, histones can bind to endothelial cells *in vivo*, leading to pore formation, ion influx, and endothelial activation (or even cell death) (259, 274, 275). Positive feedback can be initiated, due to H_2O_2 release from the activated cells, leading to neutrophil activation and NETosis (194). Von Willebrand factor is released from Weibel-Palade bodies, leading to platelets binding to collagen (276).

Histones may bind to other cells, including neutrophils, leading to further NETosis (277), and also to red blood cells, platelets. Binding to platelets is followed by the activation of the GpIIbIIIa integrin receptor due to calcium influx, and the result is platelets binding to fibrin (278-280). Histones also potentiate thrombin mediated-, and Toll-like receptor 2, 4 mediated platelet activation (263, 281). These processes are further facilitated by the binding of histones to fibrinogen (258). Through all these effects *in vivo* histones lead to rapid thrombosis and thrombocytopenia (259, 282, 283). Red blood cells can expose phosphatidylserine, which is enhanced upon histone binding, leading to increased thrombin generation (284, 285).

Histones also interfere with the protein components of the coagulation system, they can be "built-into" fibrin fibers during polymerization, which renders clots more resistant against lysis and shear stress (269). Histones not only increase prothrombin activation but inhibit antithrombin-mediated thrombin inactivation (258, 286). The formation of activated protein C is decreased as histones inhibit thrombin-thrombomodulin interaction (259, 287). Activated protein C is further inhibited by neutrophil elastase and oxidases, which reduces NET degradation (see in chapter 1.4.4.) (288, 289). Hindered thrombin-thrombomodulin interaction also leads to lower TAFIa activity leading to the increased number of plasminogen binding sites, maintaining the hemostatic balance (155, 157).

Interestingly, SCG-PT mediated fibrin formation is facilitated when polylysine (mimicker of H1 lysine-rich histone) is present (290).

1.4.5.3. The role of neutrophil elastase

Neutrophil elastase may interfere with clotting and fibrinolysis. It can lead to the formation of miniplasminogen (formed from plasminogen), which can digest covalently cross-linked fibrin more efficiently, and it is also easier to be activated to miniplasmin (291, 292). NE itself is able to degrade fibrin; furthermore, it inactivates α_2-plasmin inhibitor (291, 293). Cleaving vWF by NE results in platelet release under high shear rates (294)**.** Thrombin and FX can also be cleaved by NE, which is accompanied by the formation of antimicrobial peptides (295).

The procoagulant effects of NE include cleaving antithrombin, thrombomodulin, tissue factor pathway inhibitor, and subendothelial proteins, resulting in a more thrombogenic pattern (155, 296-298). By cleaving uPA and tPA, NE also presents antifibrinolytic properties (299).

1.4.5.4. The effect of NETs on hemostasis

The effects of the most important components of NETs are discussed above. However, when they are emitted together to the extracellular space during immunothrombosis, their effects might be modified. DNA and histones have synergizing effects in increasing the mechanical stability of clots, but cell-free DNA does not further modify the effects of histones on tPA-mediated clot lysis (258, 269). NE may degrade histones in the extracellular space – reducing their effects – which is potentiated by the inactivation of the NE inhibitor α1-antitrypsin by MPO (300). DNA-bound NE may also be hard to reach for inhibitors.

1.4.5.5. Effects of the hemostatic system on NETs

It is now well-known that during immunothrombosis, the hemostatic system affects NET production and stability. FXIIa can lead to NET formation through a uPA receptor-mediated process (301). When thrombin cleaves complement C5 and C3, their active forms result in leukocyte migration and NETosis (302). Cross-linking of fibrin leads to increased mechanical stability. Histones in NETs might also be cross-linked and stabilized through neutrophil-derived transglutaminases, increasing their stability (303). As vWF is secreted from endothelial cells upon histone-mediated cell injury, it links DNA

and histones to the fibrin network through platelets (304, 305). Thus, vWF forms a third scaffold in thrombi (beside fibrin and NETs) (306).

1.4.6. NETs and cancer

Cancer patients have a 4- to 7-fold increased risk of venous thromboembolism (VTE) compared with the general population (307). However, the rates of VTE vary in different cancer types. For instance, breast cancer has a low rate, whereas pancreatic cancer has a high rate of VTE (308). This variability suggests that there may be cancer-type-specific mechanisms of VTE (309).

Leukocytosis is often observed in cancer patients, particularly patients with lung and colorectal cancer (309). Leukocytosis is also associated with VTE in cancer patients and is a component of the Khorana Risk Score for predicting chemotherapy-associated thrombosis in ambulatory cancer patients (310-312). In addition, some patients have increased circulating levels of hematopoietic cytokines, such as granulocyte-colony stimulating factor (313). The coagulation cascade is activated by pathogens as part of the innate immune system to limit the dissemination of infection (314). Activated monocytes can trigger thrombosis by expressing tissue factor (315). Activated neutrophils release proteases, such as neutrophil elastase, which enhance thrombosis by degrading the anticoagulant protein tissue factor pathway inhibitor (296). In addition, neutrophils also release NETs. PAD4 is also expressed by the human breast cancer cell line MCF7.31 Citrullinated histones, such as citrullinated histone H3, are widely used as a biomarker of NET formation. In mice, it has been proposed that PAD4 is required for NET formation (237). Indeed, PAD4−/− mice have smaller thrombi in the inferior vena cava (IVC) stenosis model (316). Interestingly, a recent study found an association between plasma levels of cH3 and VTE in patients with pancreatic and lung cancer but not in those with other types of cancer, such as breast cancer (317). In another study, plasma levels of nucleosomes and cell-free DNA were higher in cancer patients than in healthy controls, but these are not NET-specific biomarkers (318).

Neutrophilia was observed in mice bearing murine breast 4T1 tumors and human pancreatic BxPc-3 tumors (319-322). In addition, mice bearing 4T1 breast tumors had increased levels of circulating markers of neutrophil activation and NET, such as cH3 and myeloperoxidase (321, 322). Furthermore, tumor-bearing mice had more rapid

thrombotic occlusion in a jugular vein Rose Bengal/laser-induced injury model (322). Interestingly, administration of DNase I to degrade cell-free DNA and NET did not affect thrombotic occlusion in control mice but provided protection from the enhanced venous thrombosis observed in tumor-bearing mice (322). These studies suggest that neutrophils and NET contribute to venous thrombosis in a murine breast cancer model.

In view of recent clinical data suggesting a role of NET in VTE in patients with pancreatic cancer (317), it is of interest to investigate the contribution of neutrophils and NET to venous thrombosis.

1.5. Citrullination of fibrinogen

Intracellular citrullination of histones by PAD4 was identified as a hallmark of chromatin decondensation during NET formation, and circulating biomarkers of NETosis (extracellular DNA, citrullinated histone H3) showed association with venous thromboembolism risk (237, 317, 323). However, NET-forming neutrophils also secrete PAD4 and PAD2 (324). Furthermore, PAD4 has been detected on the surface of neutrophils, and PAD2 may be spontaneously released from neutrophils independently of NETosis (325). Both PAD4 and PAD2 catalyze citrullination of fibrinogen, according to *in vitro* data (326).

The structure of the fibrin matrix is a major determinant of the lytic susceptibility of clots (327). Consequently, posttranslational modifications of fibrin(ogen) (oxidation, glyoxilation, carbamylation, glycation) that alter fibrin structure, modify fibrin stability (327-329). Citrullination – another posttranslational modification potentially converting 23 peptidyl-arginyl residues of fibrinogen into peptidyl-citrulline – is a proven phenomenon in inflammatory joint diseases as well as in atherosclerotic plaques (330-332).

Some of the modified Arg residues of fibrin include thrombin recognition sites, which renders fibrinogen more resistant to thrombin-mediated digestion. The release of fibrinopeptide A and B is impaired, citrullinated fibrinogen is resistant to fibrin monomer polymerization. Furthermore, the presence of citrullinated fibrinogen inhibited the polymerization of native fibrinogen in a dose-dependent manner (333, 334). At the same time, the significance of citrullinated fibrinogen (CitFg) in intravascular thrombosis is unknown, and studies concerning the structure of fibrin formed in the presence of CitFg provide little or no insight into the mechanical and lytic susceptibility of such clots (333-335). However, mounting research on neutrophil extracellular traps (NETs) from the last decade has made a compelling case to direct attention to the effects of CitFg on clot stability (306).

There are other substrates for PAD2, 4 in the hemostatic system. Citrullinating antithrombin leads to a decreased inhibitory effect (336). Other substrates include the activators and inhibitors of the fibrinolytic system (337). The activity of ADAMTS13 (a vWF cleaving protease) also decreases upon citrullination leading to the increased half-life of vWF multimers (338).

2. Objectives

2.1. The effects of staphylocoagulase on fibrin- and plasma clot structure, viscoelastic parameters, and fibrinolysis

1. To improve our understanding of clot structure formed in the presence of staphylothrombin.
2. To characterize the viscoelastic properties of such clots.
3. To monitor changes in fibrinolytic properties.
4. To assess whether staphylocoagulase also has an impact on thrombin.

2.2. Neutrophil extracellular traps and the structure of *ex vivo* arterial and venous thrombi

1. To determine fibrin content, fibrin fiber thickness, and semi-quantitatively analyze the content of neutrophil extracellular trap components in *ex vivo* thrombi.
2. To introduce clinical determinants of clot structure and neutrophil extracellular trap content.
3. To study the neutrophil extracellular trap content in cancer-associated venous thrombi (from human pancreatic tumor-bearing mice, compared to control mice).
4. To characterize clot structure, viscoelastic properties, and lysis of clots formed in the presence of citrullinated fibrinogen.

3. Methods

3.1. Staphylocoagulase

Recombinant SCG was expressed and purified by our collaborators. The protein concentration of the pooled batch was 380 nM.

3.2. Neutrophil extracellular traps and the structure of *ex vivo* thrombi

3.2.1. Patient characteristics

Between 2014 and 2016, 208 consecutive patients (66 coronary artery disease, CAD patients; 64 peripheral artery disease, PAD patients, and 78 acute ischemic stroke, AIS patients) were prospectively enrolled. Clinical characteristics and basic laboratory findings of the patient cohort are summarized in Table 2 on the next page. Atherosclerosis was diagnosed if atherosclerotic plaques were visible during the procedure or via carotid ultrasound (B mode). The patients were considered dyslipidemic if they had elevated fasting blood cholesterol or triglyceride levels or were on lipid-lowering therapy. Thrombophilia was determined from patient history.

Table 2. Patient characteristics. Values are provided as mean ± SD or percentages, median values with lower and upper quartiles in brackets followed in parenthesis by the number of subjects included in the analysis. CAD=coronary artery disease, PAD=peripheral artery disease, AIS=acute ischemic stroke, WBC=white blood cell count, CRP=C-reactive protein, ASA=acetylsalicylic acid.

	CAD (66)	**PAD** (64)	**AIS** (78)	**All** (208)
Patient characteristics				
Male	68.2% (45/66)	56.3% (36/64)	61.5% (48/78)	62% (129/208)
Patients' age (years)	63±14.9 (66)	68.7±10.8 (64)	60±10.5 (78)	63.6±12.6 (208)
Laboratory findings				
WBC (10^3/μL)	12.4±4.9 (66)	10.1±3.5 (62)	10.6±4.1 (78)	11±4.3 (206)
CRP (mg/L)	12.9±25.6 (65)	29.2±49.5 (33)	12±22.7 (62)	15.9±31.6 (160)
Fibrinogen (g/L)	3.7±1.1 (49)	4.1±1.2 (36)	2.4±1.3 (29)	3.5±1.4 (114)
Etiology				
Thrombophilia	0% (0/66)	0% (0/17)	5.2% (4/77)	2.5% (4/159)
Cardiac embolization	0% (0/66)	11.8% (2/17)	49.4% (38/77)	25.2% (40/159)
Atherosclerosis	100% (66/66)	70.6% (12/17)	26% (20/77)	61% (97/159)
Dissection	0% (0/66)	0% (0/17)	3.9% (3/77)	1.9% (3/159)
Cryptogenic	0% (0/66)	17.6% (3/17)	15.6% (12/77)	9.4% (15/159)
Data of thrombi				
Symptom to intervention time (hours)	3 [2-8.75] (58)	24 [12-48] (57)	5.3 [4.4-6.5] (77)	6 [4-12] (192)
Medication prior to intervention				
ASA	100% (62/62)	41.9% (26/62)	24.7% (18/73)	53.8% (106/197)
Clopidogrel	100% (62/62)	22.6% (14/62)	12.3% (9/73)	43.1% (85/197)
Oral anticoagulant	-	6.7% (1/15)	19.5% (15/77)	-
Statin	13% (8/64)	42% (22/52)	25% (16/63)	(46/179)
Comorbidities and risk factors				
Atherosclerosis	100% (66/66)	79.4% (50/63)	50.6% (39/77)	75.2% (155/206)
Diabetes	25.8% (17/66)	31.7% (20/63)	20.8% (16/77)	25.7% (53/206)
Hypertension	69.7% (46/66)	79.4% (50/63)	79.2% (61/77)	76.2% (157/206)

Hyperlipidaemia	50% (33/66)	55.6% (35/63)	35.1% (27/77)	46.1% (95/206)
Tumor	18.2% (12/66)	11.1% (7/63)	15.6% (12/77)	15% (31/206)
Smoking				
Never	54% (34/63)	41.3% (26/63)	12.5% (2/16)	43.7% (62/142)
Former	7.9% (5/63)	0% (0/63)	6.3% (1/16)	4.2% (6/142)
Currently smoking	38.1% (24/63)	58.7% (37/63)	81.3% (13/16)	52.1% (74/142)

3.2.2. Thrombus collection

In the case of CAD and PAD patients, thrombi were collected during acute therapeutic catheter interventions and operations, as previously described (339): Coronary patients were referred to primary PCI after developing symptoms of ST-elevation myocardial infarction or Non-ST-elevation (inclusion criteria: definite diagnosis of acute myocardial infarction, eligibility for percutaneous coronary intervention, no previous thrombolytic therapeutic approach and TIMI (Thrombolysis In Myocardial Infarction) thrombus grade ≥ 3). Angiography and thromboaspiration were performed from radial or femoral access with QuickCat (Spectranetics Int., Leusden, Netherlands), Export (Medtronic Inc, Minneapolis, MN), or Eliminate (Terumo, Gifu, Japan) aspiration catheters. All patients were pre-treated immediately before revascularization with aspirin (500 mg), an intravenous bolus of unfractionated heparin (5000 IU), abciximab (unless an absolute contraindication was present), and clopidogrel (600 mg). Patients already taking any antiplatelet agents on a regular basis were given a reduced dose (100-300 mg of ASA, 300 mg of Clopidogrel). Peripheral artery thrombosis patients presenting with acute symptoms were treated by thrombendarterectomy by Fogarty catheter and semi-closed endarterectomy by Vollmar ring stripper in local or general anesthesia (inclusion criteria: definite radiographic and clinical diagnosis of arterial occlusion, eligibility for surgery). In AIS, thrombi were removed via stent-retriever thrombectomy from acutely occluded large vessels of the circle of Willis. All patients with a definite diagnosis of AIS eligible for mechanical thrombectomy were included during the study period providing that a clot was successfully removed. Prior to mechanical thrombectomy, recombinant tissue-type plasminogen activator was administered to patients who were eligible for intravenous

thrombolysis (10 mg/kg of body weight, but maximum 100 mg). All thrombi were removed by qualified clinicians. The study was approved by the institutional and regional ethical board (Ref.#8/2014/18.09.2014), and informed written consent was obtained from all participants or their legal guardians. The research also conforms to the principles outlined in the Declaration of Helsinki.

3.3. Thrombi from mice bearing human pancreatic tumors

3.3.1. Cells and the mouse tumor model

Our collaborators used a human pancreatic cancer cell line BxPc-3 expressing the firefly luciferase reporter (319). BxPc-3 tumors were grown in the pancreas of Crl:NU-Foxn1nu male mice (nude mice) and monitored by measuring luciferase expression (319). They used mice with tumors weighing from 1.5 to 3.9 grams. All animal studies were approved by the University of North Carolina at Chapel Hill Animal Care and Use Committee and complied with National Institutes of Health guidelines.

3.3.2. Thrombosis model

Our collaborators used the IVC stasis model to produce a consistent clot size (340-342). A limitation of this model is that there is reduced delivery of circulating factors to the growing thrombus. The IVC was exposed, carefully separated from the aorta, and fully ligated with 5-0 silk suture below the left renal vein. Any side branches close to the IVC ligation site were also ligated, and the back branches were cauterized. They used the Vevo® 2100 Imaging System (FUJIFILM VisualSonics Inc., Toronto, Ontario, Canada) to monitor the development of clots at 3, 6, 24, and 48 hours after IVC ligation. Clots were harvested at 48 hours and weighed. Clots were frozen at -80°C or fixed in 10% formalin and then stored in 70% ethanol.

3.4. Citrullination of fibrinogen

PAD4 concentrations and incubation times were adjusted according to the highly variable needs of various experimental setups. E.g., for the purposes of permeability measurements, shorter incubation times had to be chosen (compared to those for SEM and turbidimetry) since more extensive citrullination made clots mechanically too unstable to withstand the pressure of the fluid column. Generally, human fibrinogen at a standard concentration of 8 µM was incubated with PAD4 (GST (glutathione S-

transferase) tagged, Sigma-Aldrich) concentrations ranging between 0.25-1.15 µg/mL or PAD4 vehicle (50 mM Tris-HCl, pH 7.5, 150 mM NaCl, 10 mM glutathione, 0.1 mM EDTA, 0.25 mM DTT, 0.1 mM PMSF, 25% (v/v) glycerol) in 100 mM Tris-HCl 10 mM $CaCl_2$ 1 mM DTT pH 7.5, where Tris: Tris(hydroxymethyl)aminomethane; EDTA: Ethylenediaminetetraacetic acid, DTT: Dithiothreitol; PMSF: Phenylmethylsulfonyl fluoride) for 1-8 h at 37 °C. Reactions were stopped by the addition of PAD4-inhibitor Cl-amidine at 60 µg/mL.

3.5. Structural studies

3.5.1. Scanning electron microscopy (SEM)

Fibrin, plasma clots and *ex vivo* thrombi were fixed according to a previously published method (343): clots were placed into 100 mmol/L Na-cacodylate pH 7.2 buffer for 24 h at 4 °C. After repeated washes with the same buffer, samples were fixed in 1% (v/v) glutaraldehyde. The fixed samples were dehydrated in a series of ethanol dilutions [20–96% (v/v)], 1:1 mixture of 96% (v/v) ethanol/acetone and pure acetone followed by critical point drying with CO_2 in E3000 Critical Point Drying Apparatus (Quorum Technologies, Newhaven, UK). The specimens were mounted on adhesive carbon discs, sputter-coated with gold in an SC7620 Sputter Coater (Quorum Technologies). SEM images were taken from randomly selected regions (to control for composition heterogeneity) of clots/thrombi at 5,000× and 20,000× magnification with SEM EVO40 (Carl Zeiss GmbH, Oberkochen, Germany). The diameter of 300 fibrin fibers was measured from each image using the Image Processing Toolbox of Matlab R2018a (Mathworks, Natick, MA), and the size distribution was evaluated according to a previously described algorithm (343, 344). Surface occupancy of cellular components fibrin network was determined in typically five images (exceptionally four) at the lower magnification after dividing the images to 864 equal-sized square regions of interest using Photoshop 7.0.1 CE (Adobe, San José, CA, USA) and based on morphological characteristics each region was classified as occupied by fibrin, other blood cells or their combinations. Thrombus composition was then calculated as a percentage of regions occupied by each component out of the total area of the image as previously described (269).

3.5.2. Small-angle X-ray scattering (SAXS)

SAXS is a procedure that provides information about the internal structure of the fibrin fibers (345). For these measurements, fibrin clots were prepared in thin-walled borosilicate capillaries of 1.5 mm outer diameter (0.01 mm wall thickness). After sealing one end of the capillary with flame, fibrinogen was clotted, the content of the capillary was stirred for 5 s with a piece of nylon fiber for complete mixing. Finally, the other end of the capillary was sealed with a cylindrical glass plug, and quick-setting two-component epoxy resin and SAXS measurements were carried out on "CREDO", the SAXS camera of the Research Centre of Natural Sciences, Hungary (346). Samples were inserted into the vacuum space of the sample chamber. Cu Kα radiation was produced by a GeniX3D Cu ultra low divergence integrated beam delivery system equipped with a FOX3D parabolic graded multilayer mirror (Xenocs SA, Sassenage, France). The X-ray beam was shaped using a three-pinhole collimating system (347). SAXS patterns were collected using a Pilatus-300k CMOS hybrid pixel detector (Dectris Ltd, Baden, Switzerland), situated 534 mm downstream from the sample. A second measurement sequence was done using the same procedure but with a 1,305 mm sample-to-detector distance. In order to assess sample and instrument stability during the experiment, the exposures were made in 5 min units, with frequent sample change and reference measurements. Raw images were corrected for measurement time, sample self-absorption, geometrical effects, and instrumental and environmental background with the on-line data reduction routine implemented in the instrument control software. Intensities have been scaled into absolute units (differential scattering cross-section) using a glassy carbon secondary reference measured along with the samples. One-dimensional scattering curves have been derived from the fully corrected and calibrated scattering patterns by azimuthal averaging (258, 347). The angular dependence of the scattering has been expressed in terms of q, the momentum transfer (defined as $q = 4\pi \sin\theta/\lambda$ where 2θ is the scattering angle and $\lambda = 0.1542$ nm is the X-ray wavelength). After merging the resulting scattering curves from the two sample-to-detector distances, the final datasets covered the range $0.08 < q < 6$ nm^{-1}. Solvent background has been subtracted from all scattering curves.

3.5.3. Clot permeability

To characterize the porosity of the clots, fluid permeation studies were performed according to a previously described procedure (258). Fibrinogen (in some cases pretreated) or diluted, recalcified plasma (1:1, in HEPES buffered saline pH 7.4 containing 150 mM NaCl; where HEPES: 4-(2-hydroxyethyl)-1-piperazineethanesulfonic acid) was clotted in 1 mL plastic pipette tips, and plasma samples were supplemented with fibrinogen to a 4 g/L final concentration. HEPES buffered saline was permeated through the clots kept under constant hydrostatic pressure. Porosity (Darcy constant, K_S) was determined from the equation (348)

$$K_S = \frac{Q * L * \eta}{t * A * \Delta P}$$

where Q = permeated volume of buffer (cm^3); L = clot length (1.5 cm); η = viscosity of buffer (10^{-2} poise = 10^{-7} N s cm^{-2}); t = time (s); A = average cross-sectional area of the clot (0.09 cm^2); ΔP = pressure drop (0.170 N cm^{-2} for fibrin clots, 0.054 N cm^{-2} for plasma clots).

3.5.4. Immunofluorescent imaging

Thrombus samples were placed in isopentane immediately after removal and stored at -80°C until further processing. Cryosections of 6 μm thickness were made from 6 to 15 different areas of the thrombi, depending on thrombus size. Extracellular DNA, citrullinated histone H3 (cH3), and fibrin network were identified using dimeric cyanine nucleic acid dye TOTO-3 for DNA (T-3604, Life Technologies, Budapest, Hungary), mouse anti-human fibrin (ADI311, Sekisui, Pfungstadt, Germany), and rabbit anti-human citrullinated histone H3 monoclonal antibodies (ab5103, Abcam, Cambridge, UK). To visualize fibrin and cH3 Alexa Fluor 488 goat anti-rabbit IgG (A11008, Life Technologies, Budapest, Hungary) and Alexa Fluor 546 goat anti-mouse IgG (A11003, Life Technologies, Budapest, Hungary) antibodies were used. Fifteen images were taken from each thrombus using confocal laser scanning microscopy (LSM; Zeiss LSM 710, EC Plan-Neofluar 20x/0.50 M27 objective, Carl Zeiss, Jena, Germany) with the following excitation/emission wavelengths: fibrin: 543/589, cH3: 488/516 and DNA: 633/670. To quantify the area of different fluorescent signals, Image J software (NIH, Bethesda, MD, USA) was used as previously described (339), median values of fibrin/DNA (FD50) and fibrin/citrullinated histone H3 ratio (FH50) distribution were determined.

Human fibrinogen at 3.6 μM (citrullinated with 0.4 μg/mL PAD4 for 0/3/4 h) supplemented with 15 μg/ml Alexa Fluor® 546-conjugated fibrinogen was clotted with 16 nM thrombin for 30 min at room temperature in sterile, uncoated IBIDI VI 0.4 μ-slides (Ibidi GmbH, Martinsried, Germany). Confocal fluorescent images (Z-stack mode) were taken using a Zeiss LSM710 confocal LSM (Carl Zeiss, Jena, Germany) with a 63x oil immersion objective lens at an excitation wavelength of 543 nm and emission wavelength of 575 nm. Images were analyzed based on a protocol modified from Duval et al. (349). Fiber density was determined as the average of the number of fibers crossing 2 arbitrary lines of fixed length (120 μm) drawn through a single optical section. Each fibrin clot was prepared in duplicate, and two density measurements were performed in each one.

3.6. Rheometry: viscoelasticity and mechanical stability studies

Fibrinogen or plasma was clotted in a 450 μL final volume, and 410 μL of this mixture was quickly transferred into the gap space between the stationary and the oscillating plate of a Haake Rheostress 1 oscillation rheometer (Thermo Scientific, Karlsruhe, Germany). In case of plasma clots before setting the cone to measurement position, mineral oil (light, white color mineral oil from Sigma Aldrich, Budapest, Hungary) was applied around the sample to prevent desiccation. Oscillatory strain (γ) of 0.015 at 1 Hz frequency was imposed on the fibrin clot 2 min after the initiation of clotting, and storage modulus (G') and loss modulus (G'') were determined (269). At the end of the clotting phase, G' and G'' plateaued, and flow curves for the same samples were registered by applying increasing shear stress (τ) from 0.01 up to 1000 Pa stepwise in 250 steps within 300 s and measuring the resulting strain values (269). Flow curves are presented as calculated clot viscosity vs. applied stress, where the collapse of the clot structure is mirrored as a sharp decline of its viscosity, and critical shear stress (τ_0) for the gel/fluid transition is determined from an extrapolation of this decline to a theoretical zero viscosity value. All measurements were performed in 3-5 replicas for each combination of additives in the fibrin clots.

3.7. Fibrinolysis assays

SCG was synthetized and fibrinolysis assays were investigated by our collaborators in microtiter plates on purified fibrin or human plasma clots (100 μl) formed with human

thrombin (01/578), SCG-PT, and SCG-T (0.5, 5.0, and 50 nM). Each reaction contained purified fibrinogen, or human plasma (06/158) supplemented with purified fibrinogen, to a final concentration of 3.0 g/L, with 60 nM Glu-plasminogen (Hyphen Biomed, Neuville-sur-Oise, France) and a range (5.0–40.0 IU/ml) of tPA concentrations (WHO 3rd IS, 98/714, NIBSC, South Mimms, UK). Lysis was monitored at 405 nm, and time courses were analyzed using a Shiny app for analyzing lysis curves (350) to calculate time to 50% lysis from the maximum clotting absorbance. Potency estimates for tPA activity against SCG-(P)T clots were calculated relative to thrombin-formed clots using a parallel line bioassay analysis and semi-weighted combination (351).

Fibrinogen (6 µmol/L, native, pre-treated with 1.15 µg/L PAD4 for 8 h, or a 1:1 mixture of the two) was clotted with 15 nmol/L thrombin, and lysis was initiated by the addition of 1 µmol/L plasmin to the surface of the formed fibrin. Processes were monitored at 37 °C using a Zenyth 200rt microplate spectrophotometer (258). For adequate comparison of lytic rates from measurements, in which different maximum turbidity values were reached despite the identical quantities of fibrin, the absorbance values were normalized as $(A\text{-}A_0)/A_{max}$ where A_{max} is the maximal- and A_0 is the final absorbance at 340 nm after complete lysis. The time needed to reduce the turbidity of the clot to a given fraction of the maximal value (T0.5 to reach $0.5A_{max}$) was used as a quantitative parameter of fibrinolytic activity.

tPA-induced lysis was examined in IBIDI VI 0.4 µ-slides. Human plasma recalcified with 12.5 mmol/L $CaCl_2$ and supplemented with 1 µmol/L fibrinogen (pretreated with 1.15 mg/L PAD4 for 0/3/4 h) was mixed with 16 nmol/L thrombin and 1.5 µmol/L plasminogen. Mixtures were quickly transferred in 30-µL channels of IBIDI slides and incubated at 37°C for 60 min. Lysis was initiated with 60 µL 0.3 µmol/L tPA and followed by time-lapse photo-scanning of the fluid/opaque clot boundary. Results are presented as distance run by the lysis front at 45 min in relative units (1 RU = the length of the channel between the centers of opposite orifices, 13 mm).

3.8. Statistical procedures

The optimal continuous theoretical distributions were fitted to the fiber diameter values from the SEM images, and these were compared according to Kuiper's test using Monte Carlo simulations as previously described (343, 344). Two-tailed t-tests were used when

comparing the averages of two datasets. On datasets with three or more compared subsets, ANOVA was performed. If the normal distribution of obtained data could not be confirmed by the Shapiro-Wilk test, non-parametric statistical tests were applied. The Kolmogorov-Smirnov test was chosen because of its robust power to compare distributions of two data sets independently of their distribution, while for the comparison of three or more datasets, the Kruskal-Wallis test was used. Statistical tests were performed using GraphPad Prism 6 and 7 (GraphPad Software, La Jolla California USA) and the Statistical Toolbox 7.3 of Matlab. The critical P-value of 0.05 was used for all statistical tests.

Each patient was characterized by an array of routine clinical data, immunofluorescent data, fiber diameter, and surface occupancy data from typically five (exceptionally four) SEM images. The data were analyzed using regression analysis and/or hypothesis testing for identifying characteristics and dependencies of the different features of the patients. If the analyzed dependencies did not include the occupancy data, the sample sets are crisp because each patient's data forms one observation in the sample. However, if occupancy data were analyzed, the sections of a thrombus could not be treated as separate observations because the intra-individual heterogeneity would have been neglected and the patients with larger sets of SEM data would be ascribed a higher weight in the conclusion derived. That is why the sets of occupancy data were treated as fuzzy samples. The so formed fuzzy sample accounted for inter-individual heterogeneity in thrombus occupancy because each patient would influence the conclusions equally. A Kuiper statistical test for equality of distribution (352) and a one-tail statistical test for median equality (339) were used to identify differences in the characteristics of two one-dimensional continuous populations. In order to achieve highly confident estimates of the statistical significance of differences of data showing large dispersions within samples of relatively small size, bootstrap procedures that do not use any parametric assumptions were implemented with 10,000 pseudo-realities (353) and equal size generation over empirical cumulative distribution function as previously described (354). The linear regression models with response variable described as quadratic function of one or two explanatory variables were built using previously described algorithms (339). The false discovery rate was assumed 10% (355).

4. Results

4.1. Staphylocoagulase

4.1.1. Clot Structure

Because fibrin structure is an essential determinant of the lytic susceptibility of the clots [reviewed in (356)], we evaluated clot structure. To this end, we applied SEM, SAXS, and pressure-driven permeation techniques.

According to the SEM images (Figure 9), increasing thrombin concentration resulted in thinner fibrin fibers (Table 3) both in pure fibrin and in plasma clots. These trends were the same when either SCG-T or SCG-PT was used. Generally, the presence of SCG increased the fiber median with both SCG-T and SCG-PT when compared to thrombin, except for SCG-PT in plasma, which showed fiber thickening only at 100 nM SCG-PT.
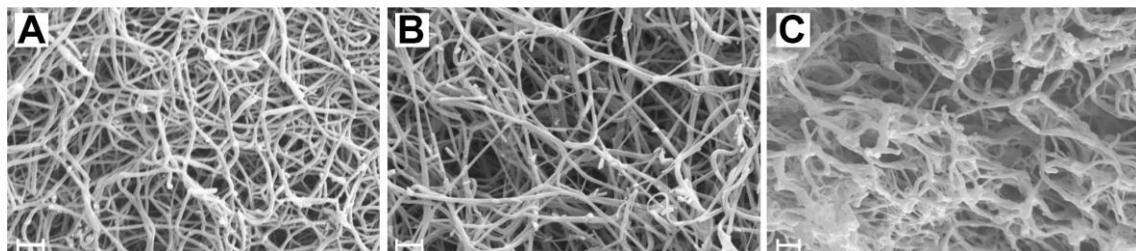
**Figure 9. Scanning electron microscopic images of fibrin clots.** Fibrin clots (3-4 with each enzyme) were formed with 2.9 g/L human fibrinogen and 5 nM human thrombin (A), staphylocoagulase-thrombin (B), and staphylocoagulase-prothrombin (C), and 4–6 images were taken from each clot as described in chapter 3.5.1. This was followed by a morphometric analysis, the results of which are presented in Table 3. Scale bar = 1 μm.

Table 3. Fiber diameter in fibrin and plasma clots. Fibrinogen (2.9 g/L) or recalcified (12.5 mM CaCl$_2$) plasma was clotted with the indicated enzyme, and SEM images were taken as illustrated in Figure 9. The diameter of 300 fibrin fibers was manually measured on 4–6 images of each clot (3-4 clots were formed with each enzyme). The table presents the median values (in nm) of the measured diameters with bottom and top quartiles in brackets. SCG-T, staphylocoagulase-thrombin; SCG-PT, staphylocoagulase-prothrombin. All differences between thrombin and the respective concentration of the SCG-T or SCG-PT are significant (indicated with *) according to Kuiper's test except for the 5 nM thrombin/SCG-PT in plasma. **Thrombin control for plasma SCG-T (0.6 g/l fibrinogen). ***Thrombin control for plasma SCG-PT (1.7 g/l fibrinogen).

[enzyme] nM	Fibrin			Plasma			
	Thrombin	SCG-T	SCG-PT	Thrombin**	SCG-T	Thrombin***	SCG-PT
0.5	121 [92-159]	139* [101-184]	132* [96-182]	-	-	-	-
5	100 [80-127]	114* [89-143]	111* [87-142]	75 [63-90]	106* [87-130]	104 [81-133]	103 [82-128]
50	66 [55-80]	84* [58-106]	86* [69-108]	66 [54-79]	77* [63-93]	92 [73-116]	81* [63-103]
100	51 [42-62]	83* [65-104]	82* [64-104]	66 [54-81]	70* [58-84]	76 [64-90]	79* [64-98]

The increase in fiber diameter could be caused either by a larger lateral distance between the protofibrils of polymerizing fibrin monomers or by a higher number of monomers per cross-section of the fiber. Our SAXS measurements (Figure 10) showed that the scattering peak corresponding to the 7 nm periodicity in the lateral alignment of fibrin monomers (51, 269) was increased in height and area in the SCG-PT-formed clots. The increase in this scattering peak indicated that the average size of the regions containing a consistent 7-nm repeat became typical (larger), suggesting that the typical lateral alignment (and thus density) of protofibrils within the fibers was preserved, but the number of protofibrils per cross-section was increased. Importantly, the structure of SCG-PT-formed fibrin was the only one that showed a SAXS peak for periodicity of about 22

nm (Figure 10) corresponding to higher-order alignment in cluster units of the fibers according to the model of Yang et al. (51).
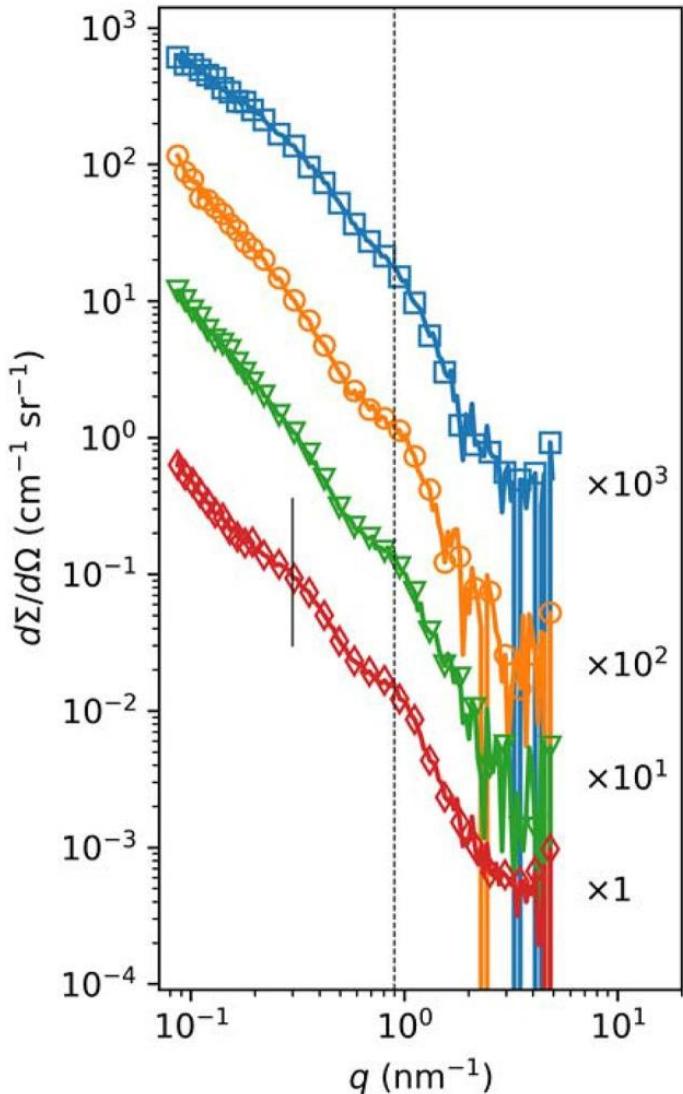
Figure 10. Small-angle X-ray scattering in fibrin clots. Fibrinogen (3.6 mg/mL) was clotted with 50 nM thrombin (orange circles), SCG-T (green triangles), or SCG-PT (red diamonds) under the conditions described in chapter 3.5.2. Fibrinogen solution was used as a reference (blue squares). Three independent measurements were performed. The normalized scattering intensity ($d\Sigma/d\Omega$) is plotted as a function of the momentum transfer (q), and empirical curves are fitted to the raw data. Curves are shifted vertically by the indicated factors for better visualization. The dashed vertical line indicates the position of the scattering peak corresponding to a periodicity of ~7 nm, whereas the solid vertical line points to the peak for periodicity of about 22 nm observed only in the SCG-PT fibrin.

Although fiber thickness is typically related to clot porosity (357), more direct characterization of the pore size in the fibrin matrix can be achieved with fluid permeation assays. Using thrombin at increasing concentrations, thinner fibers were associated with a smaller pore size (lower K_S, Table 4). With SCG-T, a reverse trend was noticeable; 100 nM SCG-T resulted in the loosest fibrin matrix. The presence of SCG-T generally increased porosity at least 2-fold except at 0.5 nM. With SCG-PT, the tendencies were more complex; 0.5 or 50 nM concentration of SCG-PT both increased porosity, but at 5 nM SCG-PT, strikingly denser clots were found compared to the respective thrombin controls.

Table 4. Permeability in fibrin and plasma clots. Clots were formed using thrombin, staphylocoagulase-thrombin (SCG-T), and staphylocoagulase-prothrombin (SCG-PT) at different concentrations, and the permeability constant was determined and compared to the respective thrombin controls. The table presents mean ± SD values of the permeability constant K_S (10^{-9} cm^2) from 3 to 4 independent measurements with 3–5 parallel samples each. *Indicates a $P<0.05$ statistical significance compared to the respective thrombin control according to Kolmogorov-Smirnov hypothesis test.

	T				SCG-T			
Fibrin clot	**0.5 nM**	**5 nM**	**50 nM**	**100 nM**	**0.5 nM**	**5 nM**	**50 nM**	**100 nM**
	8.90± 3.03	2.57± 1.35	2.41± 0.88	2.7± 1.04	5.18± 2.06*	6.69± 6.00*	6.79± 4.25*	13.40± 5.02*
	T				**SCG-PT**			
	0.5 nM	**5 nM**	**50 nM**		**0.5 nM**	**5 nM**	**50 nM**	
	3.43± 2.60	2.24± 1.15	0.64± 0.29		20.60± 1.67*	0.50± 0.37*	5.72± 1.97*	
Plasma clot	**T**				**SCG-T**			
		5 nM	**50 nM**	**75 nM**		**5 nM**	**50 nM**	**75 nM**
		9.83± 4.33	4.57± 1.64	4.14±0.69		10.50± 4.14	10.20± 6.71*	8.67± 1.89*
	T				**SCG-PT**			
		5 nM	**50 nM**	**100 nM**		**5 nM**	**50 nM**	**100 nM**
		6.91± 2.00	4.14± 1.36	3.52± 0.48		5.91± 3.98*	5.3± 2.91	6.04± 1.80*

In plasma clots, we detected similar tendencies with SCG-PT (Table 4): 5 nM SCG-PT decreased pore size compared to 5 nM thrombin, and a significantly increased porosity was detected at the highest, 100 nM SCG-PT concentration. SCG-T-induced plasma clots also followed the patterns seen in fibrin, but significant differences were observed only at higher concentrations (50 and 75 nM SCG-T).

4.1.2. Viscoelastic Properties

Because the primary biological function of fibrin is to form a scaffold, the mechanical stability of which is determined by its structure (56), the observed structural features of the SCG-PT-formed fibrin incited the evaluation of its viscoelastic parameters.

According to the rheological measurements, the presence of SCG (either as SCG-T or SCG-PT) resulted in softening of the fibrin clots (decrease in storage modulus, G', Figures 11A, 12A).
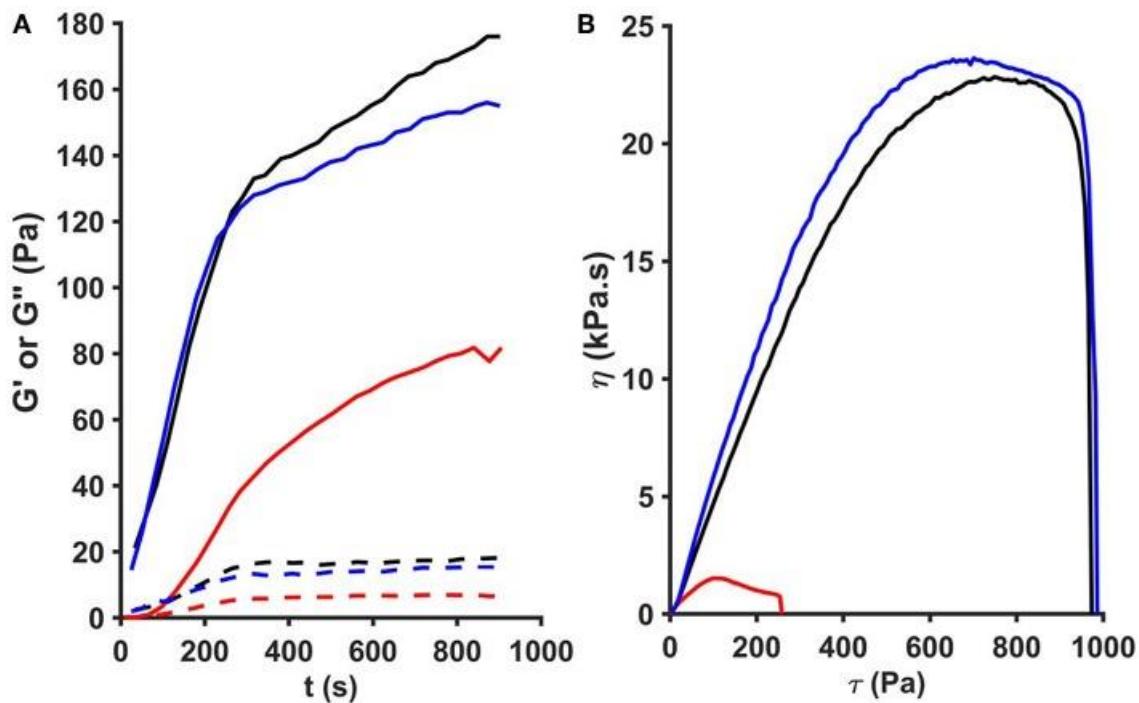
Figure 11. Oscillation rheometer assay of fibrin clots. Fibrinogen (2.9 g/L) was mixed with 5 nM thrombin (black), staphylocoagulase-thrombin (blue), or staphylocoagulase-prothrombin complex (red), and the storage modulus (G′, continuous line) and the loss modulus (G″, dashed line) were measured using an oscillation rheometer (A). Following the 15-min clotting phase, stepwise increasing shear stress (τ) was applied to the clot, and viscosity (η) was measured (B). The gel/fluid transition of the clots is characterized by the critical shear stress (τ_0) at which the value of η falls to zero. n=3, three parallel samples.
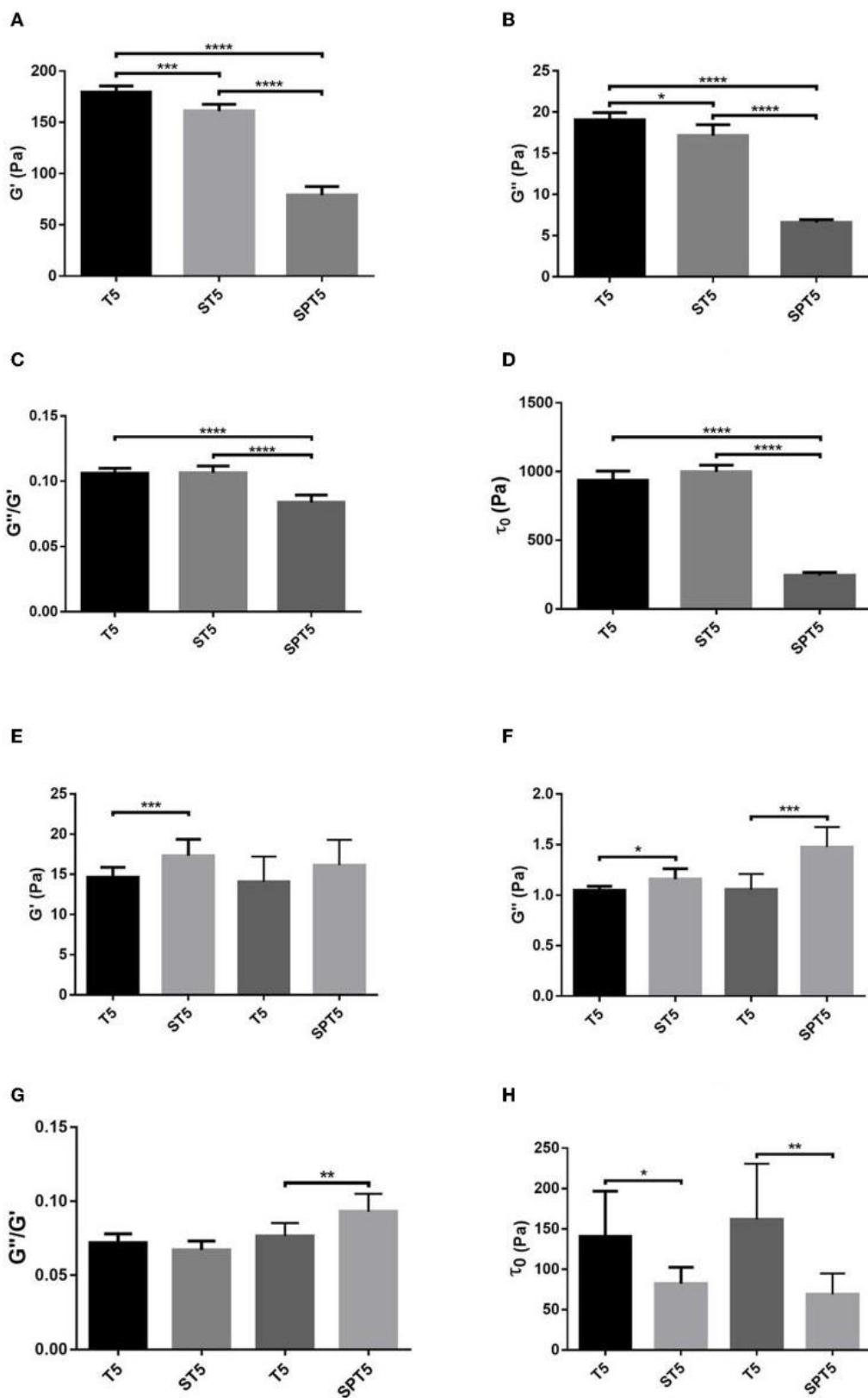
Figure 12. Viscoelastic properties of fibrin and plasma clots. Fibrin (from fibrinogen at 2.9 g/L) **(A–D)** and plasma **(E–H)** coagula were formed with thrombin/SCG-(P)T with

the indicated concentrations as described in chapter 3.6., and their viscoelastic parameters were determined as illustrated in Figure 11. Bars represent mean and SD following three independent measurements with three replica samples each. In the case of plasma clots, two different batches were used. Thus, we applied two control groups for our measurements. The different plasma batches showed no significant differences in their viscoelastic properties. G′, Storage modulus; G″, Loss modulus; τ_0, Critical shear stress; T, thrombin; ST, staphylocoagulase-thrombin; SPT, staphylocoagulase-prothrombin. The numbers after the abbreviations represent the respective concentrations in nM. *P<0.05; **P<0.01 ***P<0.001; ****P<0.0001 statistical significance according to Kolmogorov-Smirnov hypothesis test.

The modifying effect of SCG-PT was stronger, generating softer fibrin clots than those formed by thrombin or SCG-T. The loss modulus (G″) of SCG-PT and SCG-T fibrin followed a similar trend of decreased values, representing lower viscosity (Figure 12B). The viscosity component (G″) of the SCG-PT fibrin showed a bigger drop relative to elasticity (G′, Figure 12C). Similar trends in the modulation of the viscoelastic properties of fibrin were observed at higher enzyme concentrations (Figure 13).
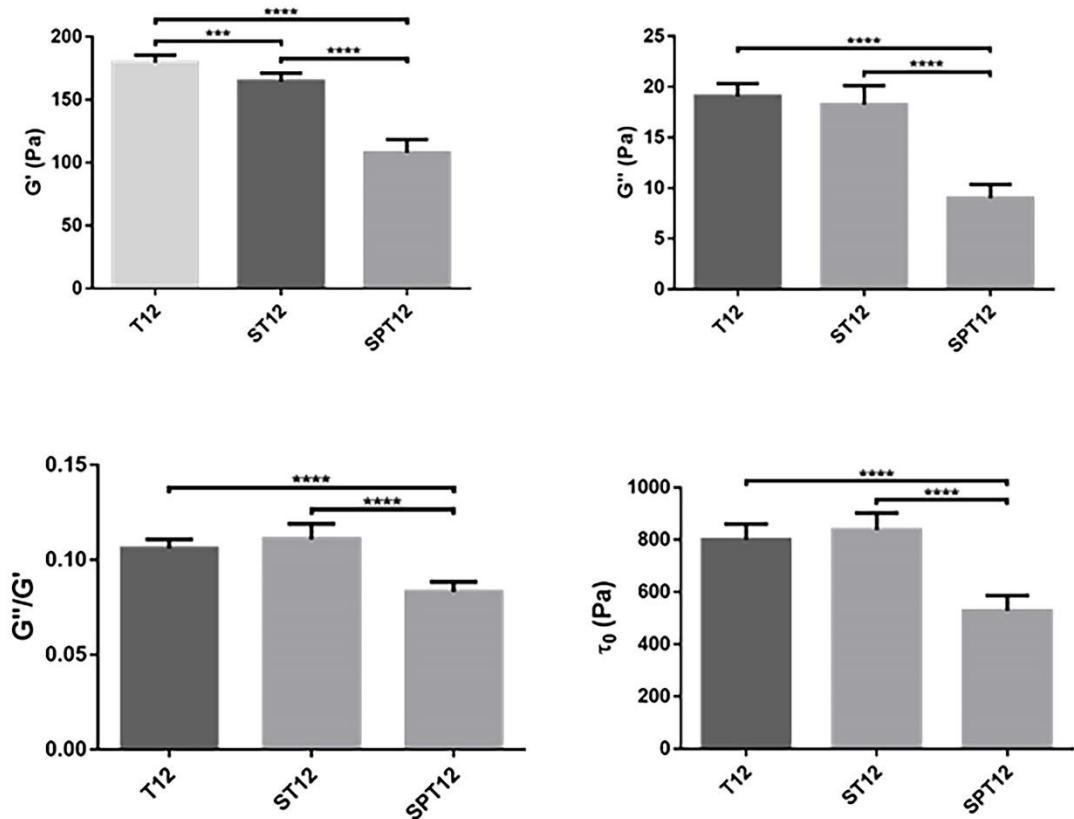
Figure 13. Viscoelastic properties of fibrin clots formed with 12 nM thrombin/staphylocoagulase-thrombin or staphylocoagulase-prothrombin complex. The bars represent mean and SD following three independent measurements with three parallel samples. G'=Storage modulus; G''=Loss modulus; τ_0=Critical shear stress; T=thrombin; ST=staphylocoagulase-thrombin; SPT=staphylocoagulase-prothrombin. The numbers after the abbreviations represent the respective concentrations in nM. ***$P<0.001$; ****$P<0.0001$ statistical significance according to Kolmogorov-Smirnov hypothesis test.

The mechanical stability of fibrin can be characterized by the critical shear stress needed for the disintegration of clots (τ_0, Figure 11B). The least stable clot was formed by SCG-PT (Figure 12D) with a 4-fold decline in this parameter compared to T or SCG-T. The mechanical stability of T and SCG-T fibrins was rather similar.

Plasma clots showed a different pattern of viscoelastic properties compared to pure fibrin formed by the different clotting enzymes (Figures 14E–H). In contrast to pure fibrin, plasma clots generated by SCG-T were consistently more rigid (higher G′, Figure 12E), and SCG-PT also significantly raised the storage modulus at higher enzyme concentration (Figure 14A). The trend of viscosity changes was also the opposite of the one observed for pure fibrin; the loss modulus (G″) was consistently higher for SCG-T and SCG-PT at all evaluated concentrations (Figure 12F, Figure 14B). Concerning the matrix resistance to shear forces (reflected in the values of τ_0, Figure 12H), both SCG-PT and SCG-T plasma clots were consistently less stable than thrombin clots, mirroring the SCG-PT effect in pure fibrin clots.
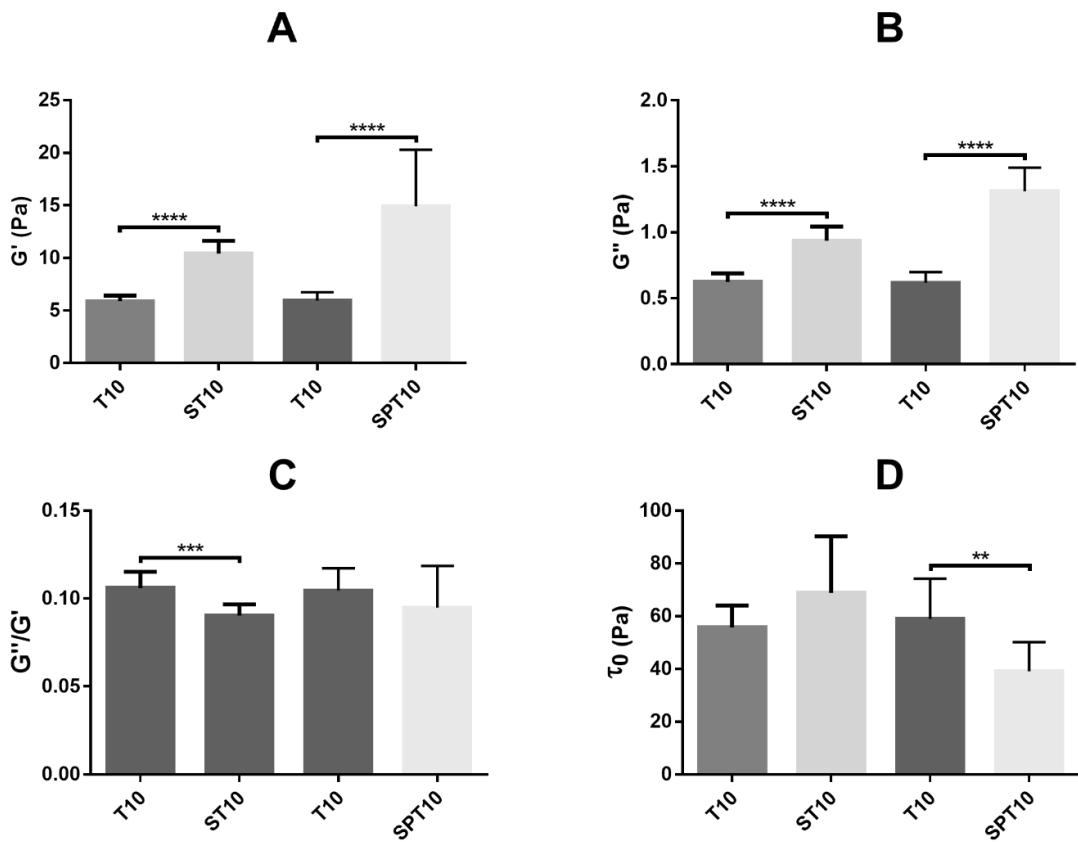
Figure 14. Viscoelastic properties of plasma clots with 10 nM thrombin/staphylocoagulase-thrombin or staphylocoagulase-prothrombin complex. The bars represent mean and SD following three independent measurements with three parallel samples. G'=Storage modulus; G"=Loss modulus; τ_0=Critical shear stress; T=thrombin; ST=staphylocoagulase-thrombin; SPT=staphylocoagulase-thrombin. The numbers after the abbreviations represent the respective concentrations in nM. **P<0.01; ***P<0.001; ****P<0.0001 statistical significance according to Kolmogorov-Smirnov hypothesis test.

4.1.3. Fibrinolysis

We addressed experimentally the susceptibility of SCG-induced clots to lysis. tPA potency estimates of clots formed by SCG-(P)T, with both purified fibrinogen and human plasma, were made relative to thrombin-generated clots using a parallel line analysis of a logarithmic transformation of lysis rates (time to 50% lysis from maximum clot formation) against tPA concentration. The fibrinolytic potential of clots formed by SCG-

(P)T, expressed as % tPA potency relative to thrombin-formed clots, is shown in Table 5. In purified fibrinogen, the tPA concentration range used (5.0–40 IU/ml) failed to produce a measurable clot with 0.5 nM SCG-PT, and so a lower range (0.3–2.5 IU/ml) was used. A 2-fold increase in tPA potency was observed at 0.5 nM SCG-PT concentration compared to thrombin. Higher SCG-PT concentrations reduced the fibrinolytic potential to no measurable difference at 50 nM. For SCG-T in fibrinogen, a moderate increase in fibrinolysis was only observed at 5.0 nM, with no apparent difference at 0.5 or 50 nM.

In plasma, enhanced fibrinolysis was only observed with SCG-T at 50 nM. For SCG-PT, both 0.5 and 50 nM plasma clots showed increased fibrinolysis, with no measurable difference at 5.0 nM compared to thrombin.

Table 5. Fibrinolysis on fibrin and plasma clots. Fibrinogen or plasma was clotted with the indicated enzyme in the presence of plasminogen and a range of tPA concentrations. Potency estimates for tPA were made for SCG-(P)T clots relative to thrombin-formed clots and are expressed as a percentage of the labeled potency on the WHO 3rd International Standard for tPA (10,000 IU) with 95% confidence limits in brackets (n ≥ 3, with 4 parallel samples). Differences are considered statistically different if the confidence intervals do not overlap. SCG-T: staphylocoagaluse-thrombin, SCG-PT: staphylocoagulase-prothrombin.

Enzyme (nM)	Fibrin		Plasma	
-	**SCG-T**	**SCG-PT**	**SCG-T**	**SCG-PT**
0.5	108 [99-117]	211 [174-256]	107 [95-121]	145 [132-158]
5	122 [113-132]	142 [132-153]	109 [99-121]	103 [92-114]
50	95 [74-121]	92 [76-111]	158 [144-173]	156 [145-168]

4.2. Neutrophil extracellular traps and the structure of *ex vivo* thrombi

4.2.1. Extracellular DNA and cH3

Our work confirmed the presence of NET components in AIS thrombi, but we also demonstrated that extracellular DNA content – the major meshwork-forming constituent of NETs – of AIS (median FD50 of 0.208) thrombi is similar to CAD and 2.5-fold lower than in PAD thrombi (median FD50 of 0.082, P=0.0013, Figure 15).
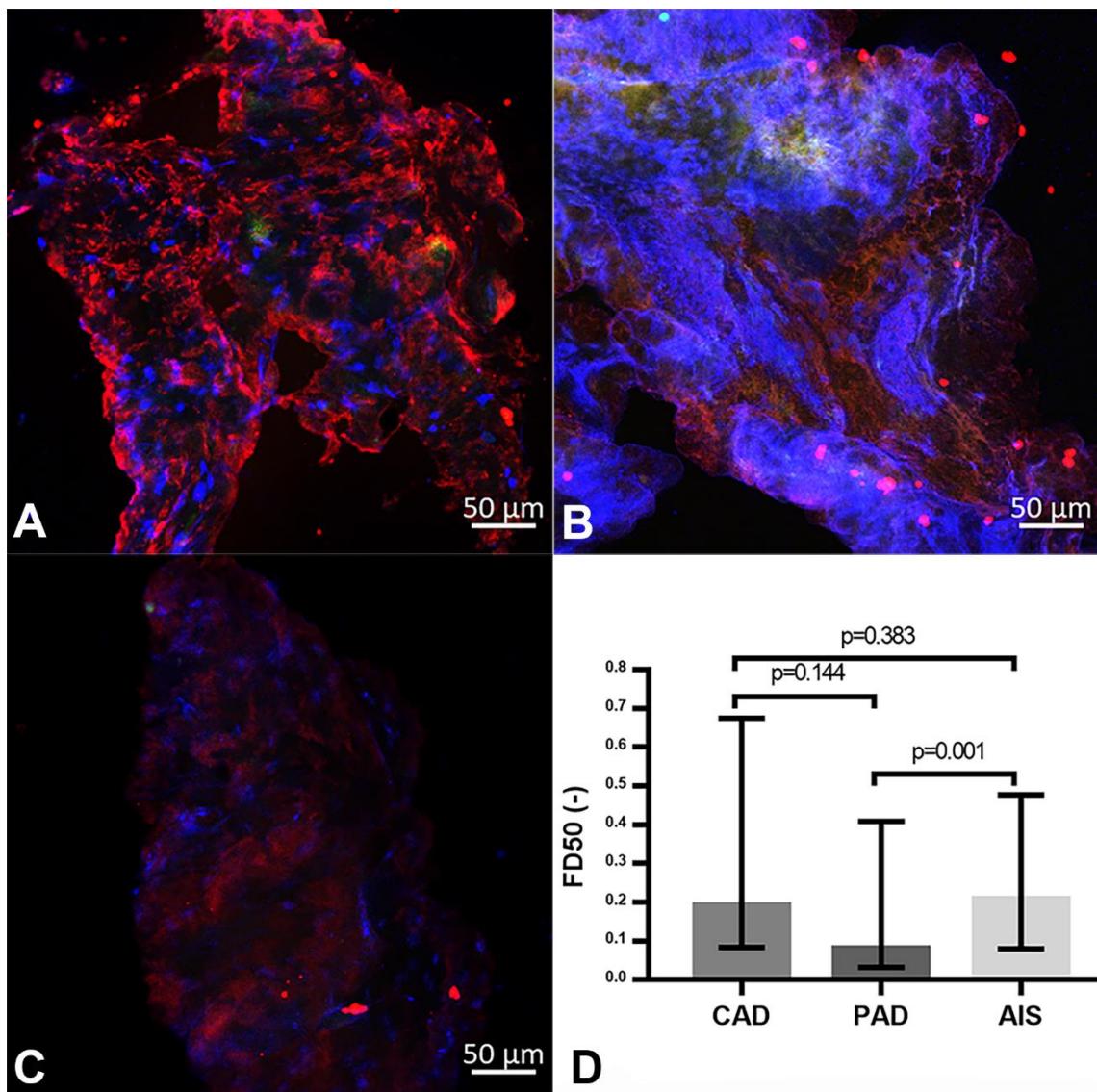
Figure 15. Indirect immunofluorescent imaging and fibrin/DNA area ratio in arterial thrombi from coronary (CAD), peripheral artery disease (PAD), and acute ischemic stroke (AIS). Following interventional extraction of thrombi from coronary artery disease (A), peripheral artery disease (B), and acute ischemic stroke (C) patients, cryosections were prepared and treated with the fluorescent DNA dye TOTO-3, mouse anti-human fibrin, and rabbit anti-human cH3 antibodies followed by the respective species-specific fluorescent anti-IgG antibodies as described in chapter 3.5.4. Images were taken with a confocal laser microscope (red, fibrin; green, cH3; blue, extracellular DNA). Based on the fluorescent signal, the ratio of cross-section area occupied by fibrin and DNA was determined in 6-15 regions of each thrombus, and the median values of these ratios for each thrombus (FD50) were evaluated (D). A lower value FD50 indicates

a higher relative DNA content in clots. The columns and bars represent median and IQR values. The patient number in each group was n_{CAD}=49, n_{PAD}=57, and n_{AIS}=64. P-values result from one-tailed hypothesis testing for medians (significant if P-value less than 0.05) using Bootstrap resampling of n'=10,000 for each statistical test.

cH3 antigen was present in all clots (FH50, Figure 16); however, no significant quantitative differences were observed between cH3 content at different vascular locations.
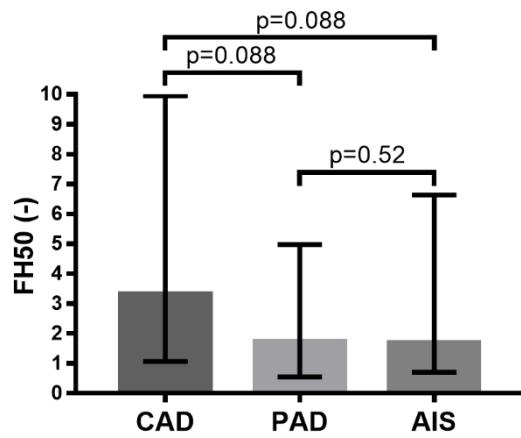
Figure 16. Fibrin/citrullinated histone H3 (cH3) area ratio in arterial thrombi from different localizations. Based on the fluorescent signal (Figure 15), the ratio of cross-section area occupied by fibrin and cH3 was determined in 6-15 regions of each thrombus, and the median values of these ratios for each thrombus (FH50) were evaluated. A lower value FH50 indicates a higher relative cH3 content in clots. The columns and bars represent median and IQR values. The number of patients in each group was n_{CAD}=49, n_{PAD}=57, and n_{AIS}=64. CAD=coronary artery disease, PAD=peripheral artery disease, AIS=acute ischemic stroke. P-values result from one-tailed hypothesis testing for medians (significant if P-value less than 0.05) using Bootstrap resampling of n'=10,000 for each statistical test.

The treatment with oral anticoagulants lead to a two-fold higher relative cH3 content in all thrombi (FH50 decreased from 1.431 to 0.665, P=0.0174). Because of the common use of statins in hypercholesterolemia, we evaluated the effects of these drugs on the NET markers in dyslipidemic patients: neither FH50 nor FD50 was changed by this

cholesterol-lowering medication. Both the DNA and the cH3 content, as hallmarks of NETs, correlated positively with the patients' age (except for cH3 in AIS). The regression models used to evaluate the associations are described in Table 7 at the end of this chapter. FD50 showed an inverse correlation in all main groups up to the age of 57 years (R^2_{adj}=0.30 and 0.33 in AIS and PAD and a stronger association in CAD, R^2_{adj}=0.99) (Table 6, Figure 17).
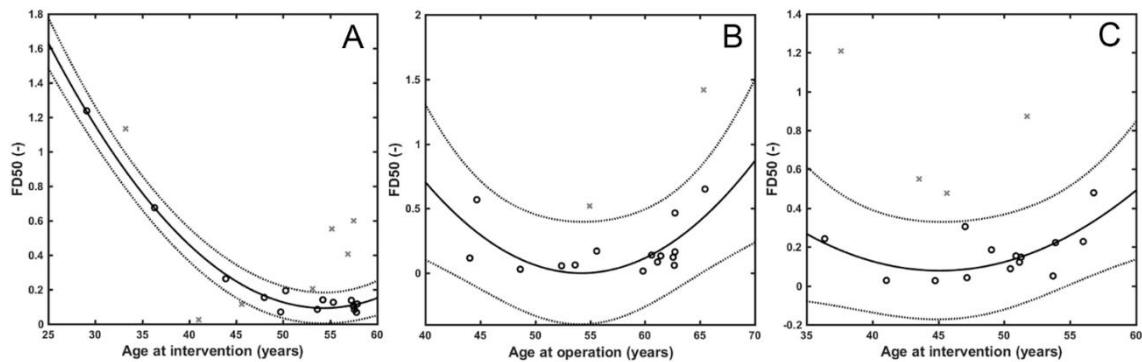
Figure 17. Associations between the median of fibrin/extracellular DNA ratios (FD50) and the age of patients in coronary artery disease (A), peripheral artery disease (B), and acute ischemic stroke (C). Regression curve (solid line) according to the model equation in Table 7 with 95% confidence intervals (dashed lines) is shown for data points (o) after outlier (x) rejection (2 outliers are not shown because they are out of the chosen ordinate scale).

Table 6. Strength of association between median fibrin/DNA ratio (FD50), median fibrin/cH3 ratio (FH50), and patient age or inflammatory laboratory markers. The regression models and their coefficients for each dependence are presented in Table 7. WBC=white blood cell count, CRP=C-reactive protein, n=sample size, R^2_{adj}=adjusted coefficient of determination, P_{ANOVA}=P-value of the analysis of variance (significant if P-value less than 0.05), (-), no considerable dependence ($R^2_{adj}<0.3$), n=sample size constrained to variable range for which the dependence is valid (defined in Table 7).

	FD50			FH50		
	R^2_{adj}	n	P_{ANOVA}	R^2_{adj}	n	P_{ANOVA}
All patients						
Neutrophil count	-	-	-	0.38	28	1.22×10^{-3}
Coronary artery disease						
Age at intervention	0.99	21	2.98×10^{-11}	0.71	21	6.09×10^{-5}
WBC	0.48	35	1.50×10^{-5}	-	-	-
Neutrophil count	0.89	13	1.81×10^{-4}	-	-	-
Fibrinogen level	0.58	22	6.19×10^{-4}	-	-	-
Peripheral artery disease						
Age at operation	0.33	18	3.68×10^{-2}	0.39	41	4.33×10^{-5}
CRP	0.75	12	6.31×10^{-3}	-	-	-
Acute ischemic stroke						
Age at intervention	0.3	18	5.71×10^{-2}	-	-	-
Neutrophil count	-	-	-	0.63	23	3.36×10^{-5}

In AIS, no further associations with FD50 were revealed, but in CAD, an inverse correlation was found between FD50 and fibrinogen level, and a parabolic association between FD50 and white blood cell (WBC) count with a minimum at $11\times10^3/\mu L$ (Figure 18B). A parabolic regression model described the dependence of FD50 on C-reactive protein (CRP) in the range of 0-7.2 mg/L in PAD thrombi (Figure 18C).
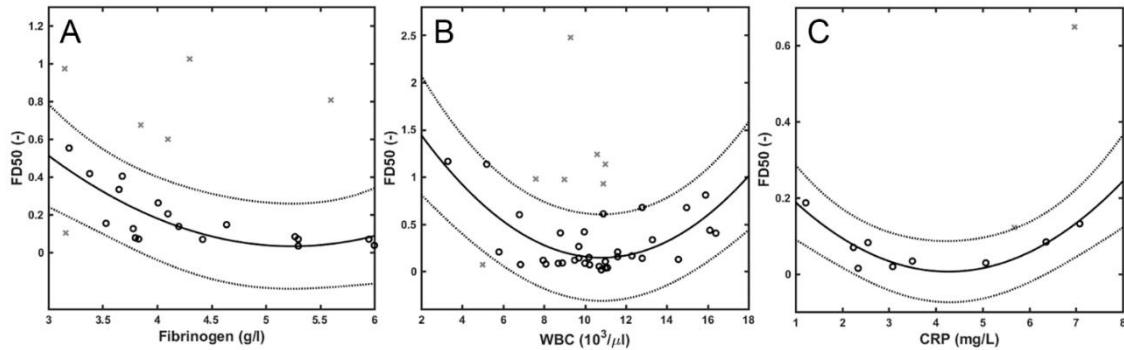
Figure 18. Associations between the median of fibrin/extracellular DNA ratio (FD50) and blood fibrinogen level (A), white blood cell (WBC) count (B) in coronary artery disease, and C-reactive protein (CRP) in peripheral artery disease (C). Regression curve (solid line) with 95% confidence intervals (dashed lines) is shown for data points (o) after outlier (x) rejection (2 outliers are not shown because they are out of the chosen ordinate scale).

The absolute neutrophil count showed a similar parabolic interrelation with FH50, with a minimum at about 5 to $8 \times 10^3/\mu L$ (Figure 19 and Table 7).
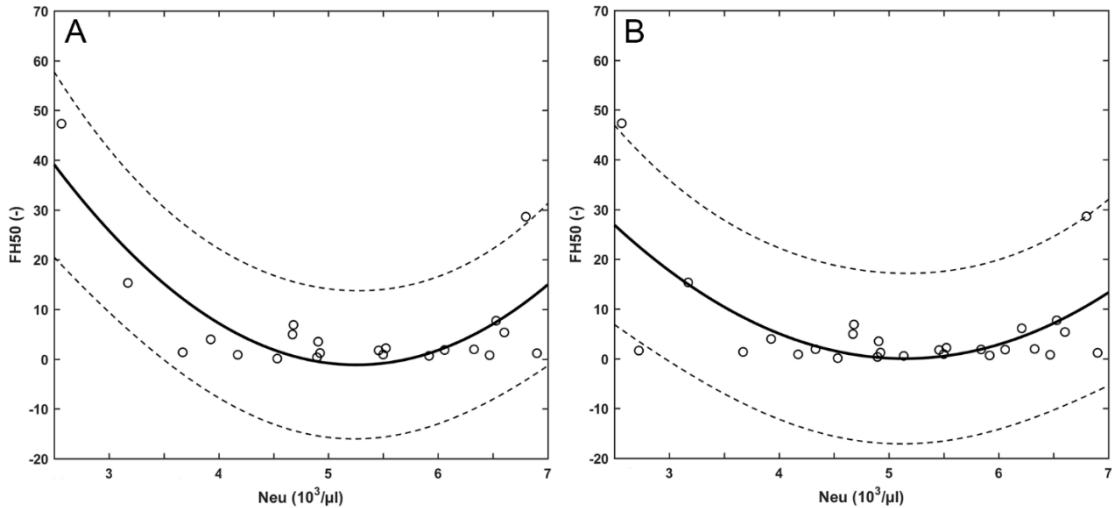
Figure 19. Associations between absolute neutrophil count (Neu) and fibrin/citrullinated histone H3 ratio (FH50) in acute ischemic stroke (A) and in all disease groups without any constraints (B). Regression curve (solid line) with 95% confidence intervals (dashed lines) is shown for data points (o) after outlier (x) rejection (2 outliers are not shown because they are out of the chosen ordinate scale).

In AIS, no significant association was found between FH50 and age at intervention, whereas in the CAD group, FH50 showed an inverse correlation with age (R^2_{adj}=0.71). The same association pattern could be observed in PAD between age 50 to 80, and a positive correlation above 80 years (n=11, R^2_{adj}=0.52, P_{ANOVA}=1.7×10^{-2}). In addition, in PAD, the strength of association between the NET content of thrombi and patients' age was increased by atherosclerotic etiology or systemic indicators of inflammation (CRP, leukocytosis, plasma fibrinogen) (Table 7). The age trend in FH50 of AIS patients was reinforced by malignant co-morbidities to an R^2_{adj} value of 0.90 (Table 7). Generally (evaluating all main groups together), the interrelation of the local NET-marker FH50 and the systemic inflammatory indicators followed a rather complex trend in thrombi from patients with malignancy (Figure 20). Although FH50 correlated positively with WBC count at fibrinogen levels less than 4 g/L, the correlation was inverted at higher fibrinogen concentrations (n=20, R^2_{adj}=0.65, P_{ANOVA}=1.9×10^{-4}).
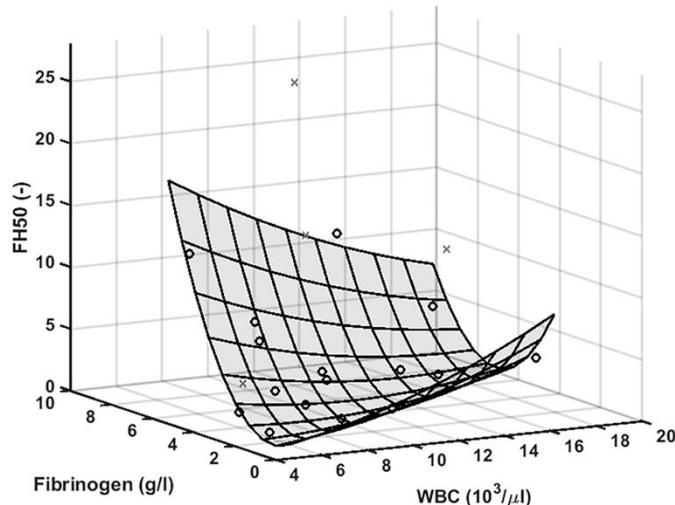
Figure 20. The joint impact of fibrinogen and white blood cell count on the ratio of fibrin/cH3 in thrombi extracted from patients with malignancy. Regression surface is shown for data points (o, n=20) after outlier (x) rejection. FH50=The median of fluorescent signal ratio of fibrin/cH3, WBC=White blood cell count. The equation for the 3D regression model was $y=A_0+A_{10}*x_1+A_{01}*x_2+A_{20}*x_1^2+A_{11}*x_1*x_2+A_{02}*x_2^2+e$, where y=FH50, x_1=Fibrinogen concentration, x_2=white blood cell count, A_0, A_{10}, A_{11}: non-significant, A_{20}=6.7x10^{-2}, A_{11}=-0.46, A_{02}=0-87. The adjusted coefficient of determination R^2_{adj} =0.65. P_{ANOVA} (P-value of the analysis of variance (significant if P-value less than 0.05))=0.8×10^{-4}.

Table 7. Relationship between fibrin fiber median, fibrin/extracellular DNA ratio (FD50), fibrin/citrullinated histone H3 ratio (FH50), and age of patients or inflammatory laboratory markers. CAD=coronary artery disease, PAD=peripheral artery disease, AIS=acute ischemic stroke; FD50= median of fibrin/DNA ratio; FH50= median of fibrin/citrullinated H3 histone ratio; ASA= acetylsalicylic acid; WBC=white blood cell; CRP=C-reactive protein; x, y=independent variables for 2D regression model; n=sample size, R^2_{adj}=adjusted coefficient of determination, P_{ANOVA}=P-value of the analysis of variance (significant if P-value less than 0.05), A_0, A_1, A_2: coefficients of the 2D regression model; equation for 2D regression model: $y=A_0+A_1*x+A_2*x^2+e$. Only clinical constraints that increase the strength of association (R^2_{adj}) of the y,x pairs are presented with the respective modified R^2_{adj} values.

Main group	y	x	Limitation of variable x	n	R^2_{adj}	P_{ANOVA}	A_0	A_1	A_2	Constraints	R^2_{adj}
All	Fibrinogen level (g/L)	Symptom-to-intervention time	<24	35	0.34	8.3×10^{-8}	3.9	-4.0×10^{-1}	3.0×10^{-2}	Male	0.53
										ASA	0.35
										Atherosclerotic	0.42
										Smoker	0.47
			<6.0	20	0.45	9.1×10^{-6}	2.2	1.06	-0.2095	Male	0.55
	FH50	Neutrophil count (10^3/µL)	<7.0	28	0.38	1.2×10^{-3}	101.8	-4.0×10^{-1}	3.8×10^{-4}	Female	0.86
										Hypertensive	0.50
CAD	Fibrin fiber median	Fibrinogen level (g/L)	>2.0	35	0.35	1.9×10^{-4}	1.9×10^{-1}	-5.9×10^{-2}	7.3×10^{-3}	ASA	0.45
										Clopidogrel	0.45
										Hypertensive	0.77
										Smoker	0.36
	FD50	Age at intervention (years)	<59	21	0.99	3.0×10^{-11}	5.4	-2.0×10^{-1}	1.8×10^{-3}	-	-

				N							
		Fibrinogen level (g/L)	>3.1	22	0.58	6.2×10^{-4}	2.6	-1.00	9.5×10^{-2}	Male	0.69
										Female	0.74
		WBC count ($10^3/\mu L$)	<16.9	35	0.48	1.5×10^{-5}	2.1	-3.6×10^{-1}	1.7×10^{-2}	ASA	0.54
										Clopidogrel	0.54
										Elevated fibrinogen	0.71
	FH50	Age at intervention (years)	<59	21	0.71	6.1×10^{-5}	87.8	-3.1	2.8×10^{-2}	Male	0.86
										ASA	0.79
PAD	FD50	Age at operation (years)	<66	18	0.33	3.7×10^{-2}	10.3	-3.8×10^{-1}	3.5×10^{-3}	Atherosclerotic	0.47
										Hypertensive	0.39
										Smoker	0.41
		CRP (mg/L)	<7.2	12	0.75	6.3×10^{-3}	3.2×10^{-1}	-1.5×10^{-1}	1.71×10^{-2}	-	-
	FH50	Age at operation (years)	50-80	41	0.39	4.3×10^{-5}	15.0	-1.9×10^{-1}	-	Female	0.98
										ASA	0.87
										Clopidogrel	0.47
										Diabetic	0.90
										Hypertensive	0.47
										Elevated CRP	0.90
			>80	11	0.52	1.7×10^{-2}	-	-1.7×10^{-1}	2.1×10^{-3}	Hypertensive	0.61
AIS	Fibrin fiber median	CRP (mg/L)	<24	16	0.48	1.1×10^{-6}	7.2×10^{-2}	-3.7×10^{-3}	3.4×10^{-4}	Male	0.56
										Leukocytosis	0.82
	FD50	Age at intervention (years)	<57	18	0.30	5.7×10^{-2}	3.9	-1.7×10^{-1}	1.9×10^{-3}	Male	0.81

	FH50	Age at intervention (years)	-	64	0.02	-	-	-	3.8×10^{-3}	Tumor	0.90
		Neutrophil count ($10^3/\mu L$)	<7.0	23	0.63	3.4×10^{-5}	145.2	-5.6×10^{-1}	5.3×10^{-4}	Hypertensive	0.81

4.2.2. Fibrin content and fibrin fiber thickness

Although the fibrin fiber occupancy was statistically higher in PAD thrombi (98.1±5.6%) compared to AIS (97.1±7.93%, P=0.043) or CAD (96.8±8.1%, P=0.0081) groups, these differences were not considerable in magnitude. The median of fibrin fiber diameter measured in this study was significantly higher in CAD thrombi compared to AIS or PAD samples (Figure 21).
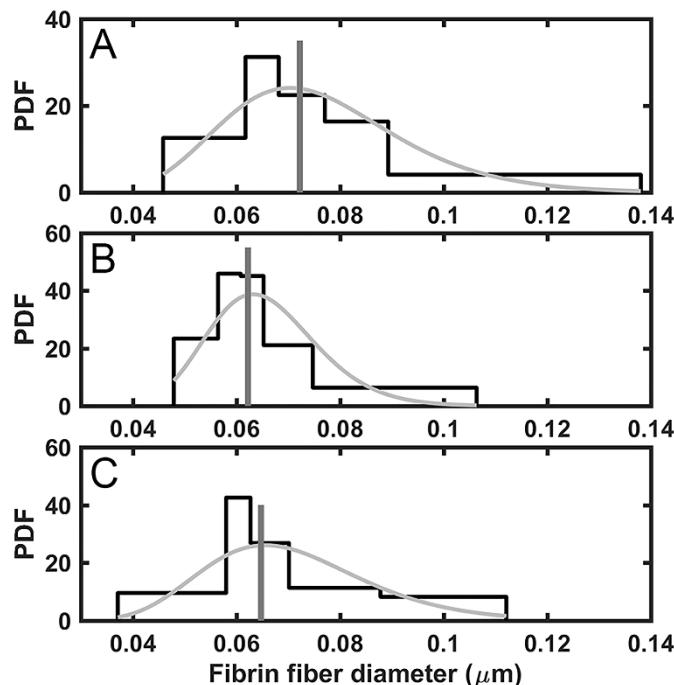

Figure 21. Fibrin fiber diameter in thrombi removed from different localizations. Manual measurement of 300 fibrin fiber diameters was performed on 5 SEM images of each thrombus, followed by evaluation of their distribution as described in chapter 3.5.1. A: Coronary artery disease (CAD), B: Peripheral artery disease (PAD), C: Acute ischemic stroke (AIS). The graphs show the probability density function (PDF) of the empiric distribution (black histogram) and the fitted theoretical lognormal distribution (gray curve). Median values are indicated by vertical lines. The number of thrombi in each group was n_{CAD}=62, n_{PAD}=61, n_{AIS}=77. Both the PAD (P=0.0026) and the AIS group (P=0.0132) had a significantly lower median fibrin fiber diameter, as compared to CAD samples according to one-tailed hypothesis test (significant if P-value less than 0.05) using Bootstrap resampling of n'=10,000.

These tendencies in the fiber size of the three main groups were due to the structural pattern of fibrin in male patients (median fiber diameter in CAD: 76.3 nm [67.2-90.8, n=41; AIS: 64.1 nm [58.6-85.3] n=46, P=0.0093 compared to CAD; PAD: 62.1 nm [57.4-75.2], n=34, P=0.0002 compared to CAD), whereas fiber diameter did not differ in females from these groups. Chronic acetylsalicylic acid (ASA) treatment prior to the acute ischemic event was associated with an increased fiber diameter only in males (No ASA: 64.4 nm [58.6-78.4] n=45; ASA: 70.9 nm [61.9-88.8] n=68, P=0.022). ASA had no other significant effects on the measured structural parameters.

Regarding comorbidities, accompanying malignant neoplasms reduced fibrin fiber thickness only in PAD (No malignant comorbidity: 64.3 nm [59.2-73.8] n=53 vs. malignant comorbidity: 57.9 nm [54.1-58.7], n=7, P=0.018), but not in AIS and CAD.

Out of the three main groups only in AIS thrombi, a parabolic dependence of fibrin fiber median on CRP was found with a minimum at about 5 mg/L CRP (n=16, R^2_{adj}=0.48, P_{ANOVA}=1.1×10^{-6}). CAD thrombi showed a similar correlation between the median diameter of fibrin fibers in thrombi and another acute-phase protein, the plasma fibrinogen, with a minimum at 4.0 g/L (n=35, R^2_{adj}=0.35, P_{ANOVA}=1.9×10^{-4}, Table 7 in the previous chapter and Figure 22).
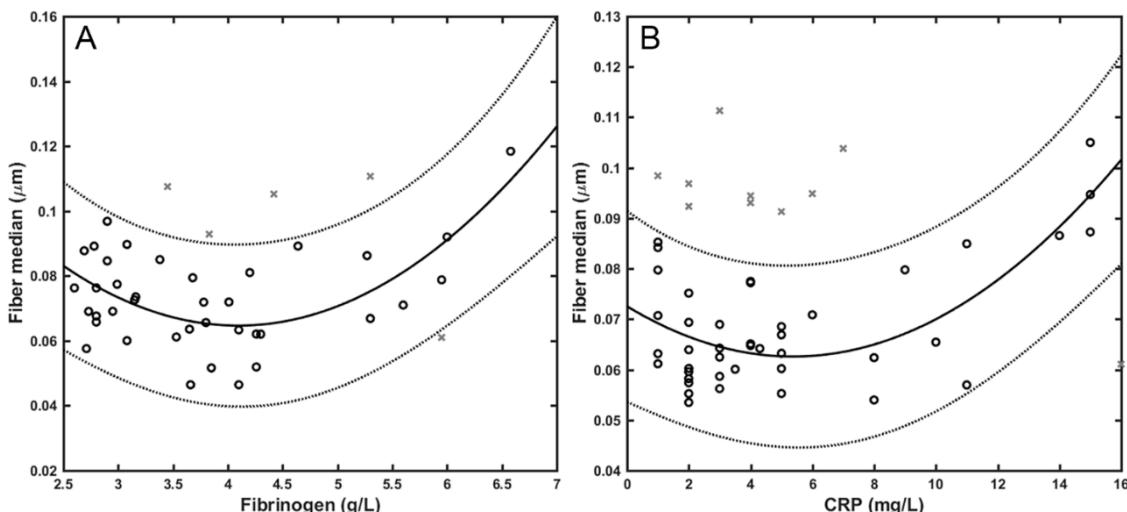
Figure 22. Associations between fibrin fiber diameter median and fibrinogen in coronary artery disease (A), C-reactive protein (B) in acute ischemic stroke. Fibrin fiber median determined by morphometric analysis of scanning electron micrographs shown as a function of blood fibrinogen level for coronary artery disease (A) and C-reactive protein (CRP) in acute ischemic stroke (B) thrombi. The regression curve (solid line) according to the model equation in Table 7 with 95% confidence intervals (dashed lines) is shown for data points (o) after outlier (x) rejection.

Interestingly, plasma fibrinogen level also showed a correlation with symptom-to-intervention time (Figure 23 and Table 7). A strong parabolic regression (n=35, $R^2_{adj}=0.34$, $P_{ANOVA}=8.3\times10^{-8}$) was observed in thrombi retrieved in less than 24 hours after the onset of symptoms, with the minimum value at about 6 hours. CRP showed no significant association with time. Similarly, we did not identify any significant associations between symptom-to-intervention time and fiber diameter, FD50, or FH50.
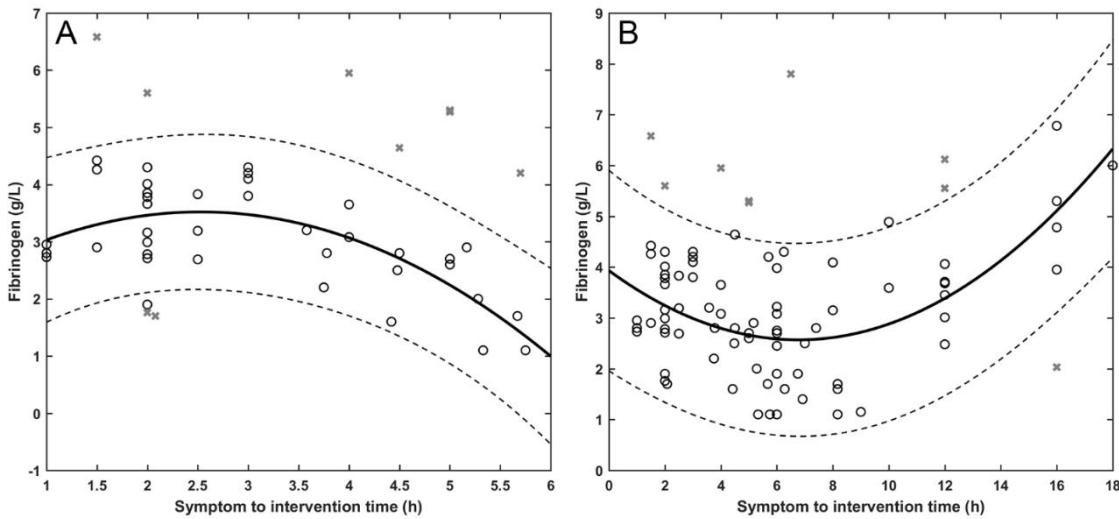
Figure 23. Associations between symptom to intervention time and plasma fibrinogen concentration, including all groups. Symptom to intervention time less than 6 hours (A), or 24 hours (B). Regression curve (solid line) with 95% confidence intervals (dashed lines) is shown for data points (o) after outlier (x) rejection.

4.2.3. Thrombi from mice bearing human pancreatic tumors

We measured the extracellular (cell-free) DNA and cH3 content in thrombi from mice bearing human pancreatic tumors and in thrombi from controls using immunofluorescence. Thrombi from tumor-bearing mice had increased levels of cell-free DNA and cH3 compared with levels of these bio-markers in thrombi from control mice (Figure 24). This was consistent with the data from the western blot analysis of our collaborators: thrombi from tumor-bearing mice had higher levels of histone H3, and cH3 compared with the levels in thrombi from control mice [3](358).
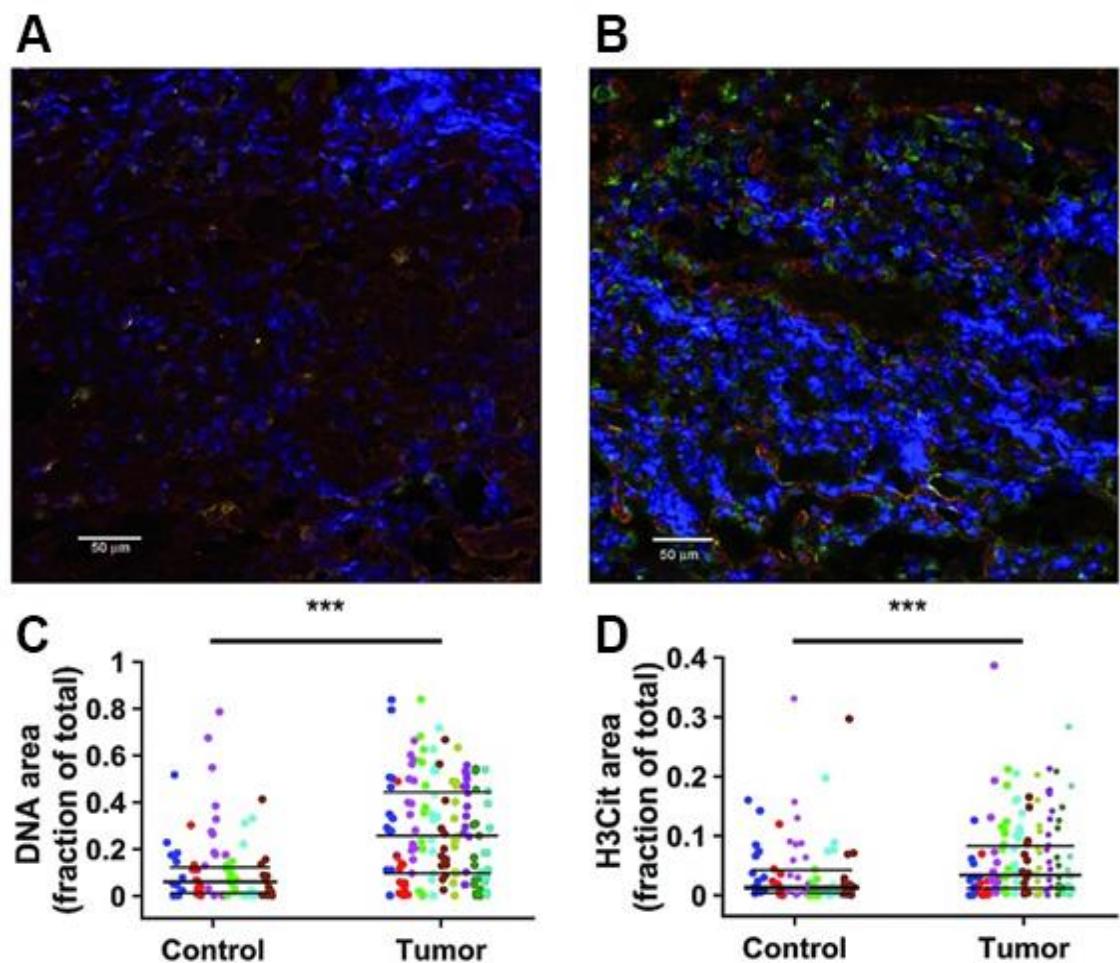
Figure 24. Analysis of thrombi by immunofluorescence. Thrombus sections from control (A) and tumor-bearing (B) mice were stained for cell-free DNA (TOTO-3, blue), citrullinated histone H3 (H3Cit; immunostained, green), and fibrin (immunostained, red) and examined with confocal laser scanning microscopy (Zeiss LSM 710, Carl Zeiss, Jena, Germany). The area occupied by the DNA (C) and H3Cit (D) signal was quantified in 15 randomly selected images from each thrombus shown with the same color. Lines indicate the median values of the bottom, median, and top quartiles calculated from the data of 90 images from six animals of the control group (shown in different colors) and 150 images from ten animals of the tumor group (shown in different colors). The statistical analysis was performed using 90 or 150 input data (Bootstrap Kuiper test P<0.001 for all three quartiles of the datasets in panels C and D). ***P<0.001

4.2.4. Citrullinated fibrinogen (CitFg)

4.2.4.1. Effects of citrullination on fibrin structure

Given its abundance in thrombi (according to our results from a mice model, (359)), we tested the effects of CitFg on clot structure in a purified *in vitro* system. SEM demonstrated that progressive citrullination of fibrinogen led to a decrease in fibrin fiber diameters following thrombin-induced clotting (Figure 25).
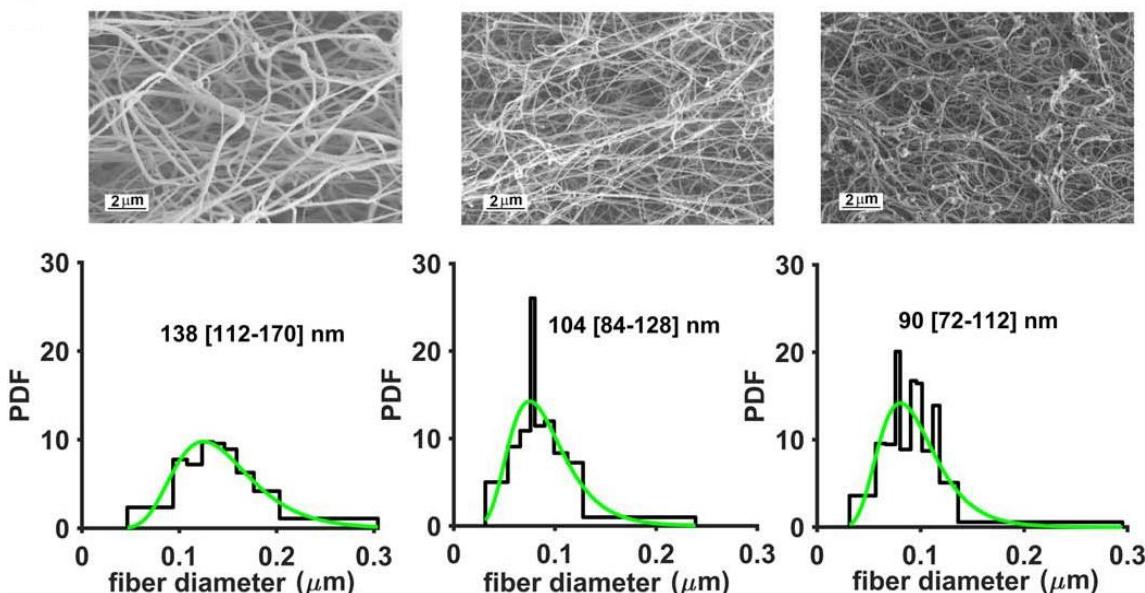

Figure 25. The effects of citrullination on fibrin fiber diameter. (A) Upper panel: representative SEM images of fibrin clots prepared from 6 µmol/L fibrinogen pre-treated with 1.15 mg/L PAD4 for 0/6/8 h (upper left-middle-right panel, respectively) clotted with 15 nmol/L thrombin for 2 h at 37 °C. Scale bar = 2 µm. Lower panel: the diameter of 300 fibers per image was measured from 4-6 SEM images per clot type using the algorithms described in chapter 3.5.1. The graphs present the probability density function (PDF) of the empiric distribution (histogram) and the fitted theoretical distribution (green curves). The numbers show the median, as well as the bottom and the top quartile values (in brackets) of the fitted theoretical distributions. All differences are significant at $P<0.005$ level according to Kuiper's test for identity of distributions (360).

The finding of increased convolution of citrullinated fibers was strengthened by SAXS analysis which indicated a significant rise in the mass fractal dimension (from 0.9 for native fibrin to 1.6 for maximally citrullinated fibrin, Figure 26). It is noteworthy that the changes in the space-filling pattern of the clots were accompanied by essentially similar

scattering correlation peaks with central positions corresponding to the known cross-sectional periodicity of ~7 nm and longitudinal periodicity of ~22 nm of native fibrin (Figure 26), suggesting conserved intrafibrillar monomer assembly - up to a critical degree of citrullination at which fibrin polymerization ceased (361).
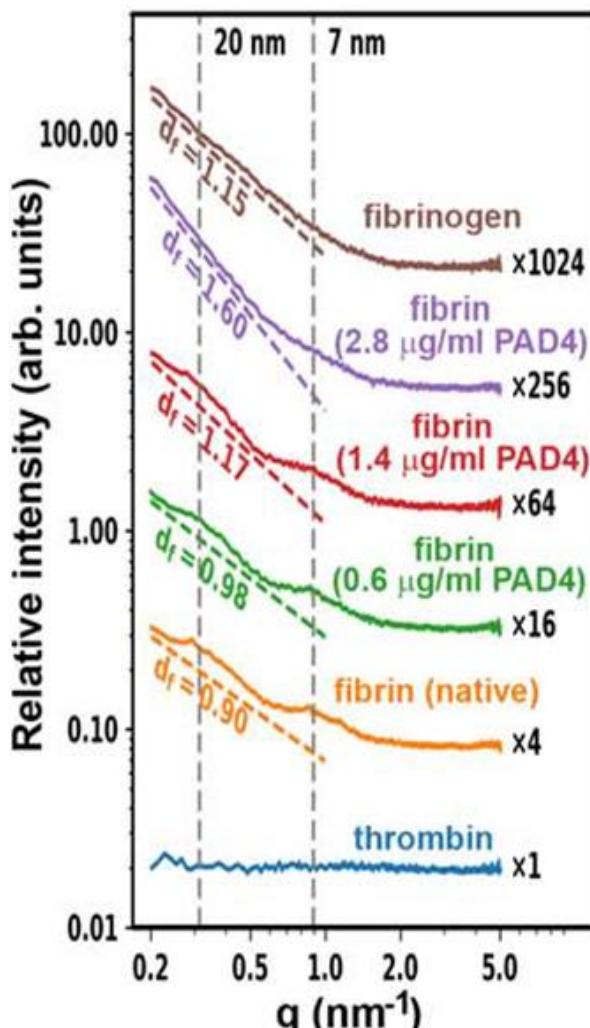
Figure 26. The effects of citrullination on the molecular structure of fibrin clots. Small-angle X-ray scattering in fibrin clots formed with fibrinogen pre-treated with 8 µmol/L citrullinated by 0/0.6/1.4/2.8 mg/L PAD4 for 1 h and clotted with 10 nmol/L thrombin (n=3). Fibrinogen and thrombin solutions were used as a reference. The normalized scattering intensity (dΣ/d) is plotted as a function of the momentum transfer (q), and empirical curves are fitted to the raw data, as described in chapter 3.5.2. Curves are shifted vertically by the indicated factors for better visualization. The vertical lines indicate the positions of the scattering peaks corresponding to periodicity of ~7 nm and ~20 nm.

LSM has been used for fibrin fiber density measurements in previous studies (349). According to our LSM observations, citrullination resulted in a fibrin network with increased density (from 44.0 ± 1.9 in control to 52.9 ± 2.9 and $56.4\pm2.0/120$ μm in samples preincubated with 0.4 mg/L PAD4 for 3 and 4 h, respectively, Figure 27) in line with the increase in the mass fractal dimension of the clots revealed by the SAXS data.
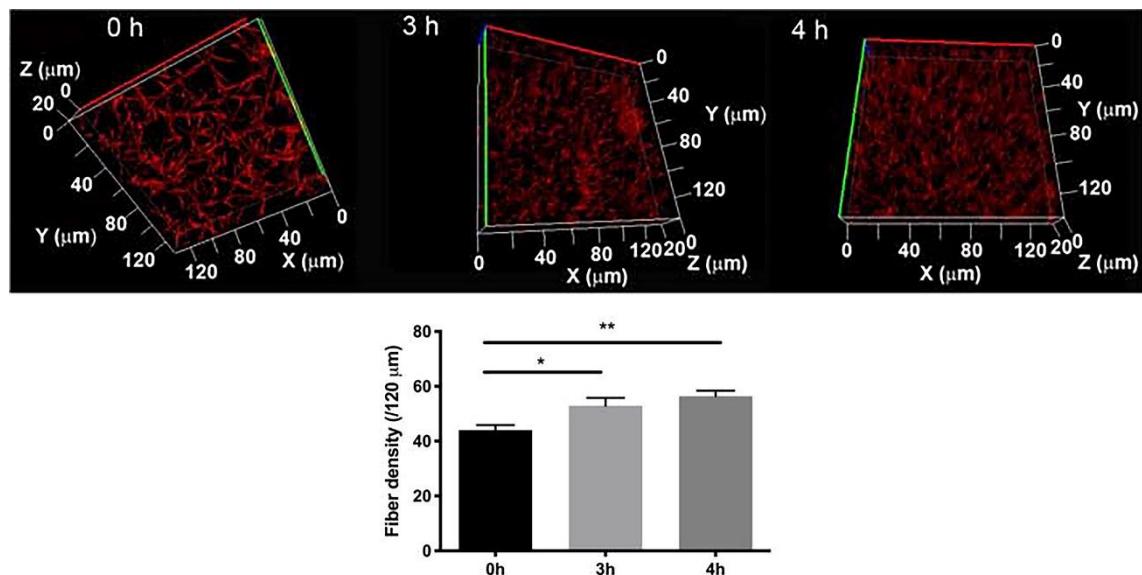
Figure 27. The effects of citrullination on fibrin fiber density. Laser scanning confocal microscopy images of 3.6 µmol/L fibrinogen (citrullinated with 0.4 mg/L PAD4 for the indicated times) clotted with 16 nmol/L thrombin in the presence of 1.5% Alexa Fluor® 546-conjugated fibrinogen. Images were taken after 30 min incubation at room temperature. Optical z-stacks (every 1 μm over 20 μm) were combined to construct 3D images (upper panel). Lower panel: fiber density was determined by counting the number of fibers crossing 120 μm long sections of 2D-projected LSM images. Error bars represent the standard error of the mean. Each clot was prepared in duplicate, and two density measurements were performed in each (n=4). *P<0.05, **P<0.01.

The formation of a finer but denser fibrin network was confirmed by an almost 50% decreased turbidity of fibrin clots formed with fibrinogen citrullinated for 8 h at 1.1 mg/L PAD, as well as with a mix of citrullinated and native fibrinogen (Figure 28).
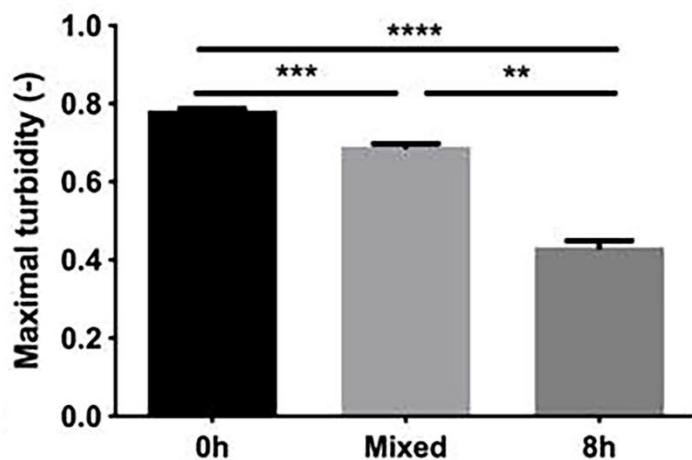
Figure 28. The effects of citrullination on clot turbidity. Turbidity of clots formed with 6 µmol/L fibrinogen (native, pre-treated with 1.15 mg/L PAD4 for 8 h, or a 1:1 mixture of the two) was clotted with 15 nmol/L thrombin for 2 h. Mean maximal light absorbance (measured at 340 nm at 37 °C) and standard error of mean were calculated from 12-13 individual turbidity curves originating from 3 independent experiments. **P<0.01, ***P<0.001,****P<0.0001.

Permeability measurements demonstrated that the increase in fiber density was accompanied by lower permeability (almost 50% decrease in the K_S of fibrin clots formed with fibrinogen pre-treated with 0.6 mg/L PAD4 for 1.5 h, Figure 29).
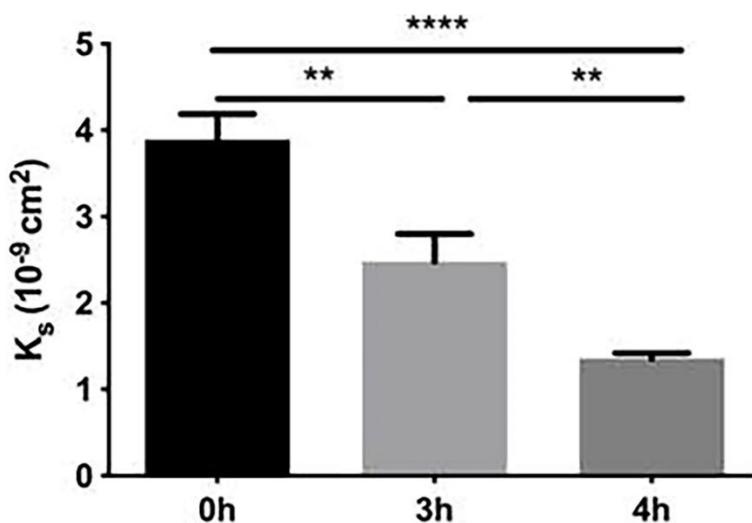
Figure 29. The effects of citrullination on clot permeability. Permeability of clots prepared from fibrinogen at 8 µmol/L pretreated with 0.6 mg/L PAD4 for the indicated times and clotted with 16 nmol/L thrombin. The permeability coefficient (K_S) was calculated as described in chapter 3.5.3. K_S values and standard error of mean were calculated from at least 8 samples originating from 3 independent experiments. **P<0.01, ****P<0.0001.

4.2.4.2. Mechanical consequences of fibrin citrullination

The marked effects of CitFg on the formed fibrin structure warranted further investigations into the mechanical properties of clots (Figure 30 on the next page). In terms of viscoelasticity, oscillation rheometry showed a drastic decline in the mechanical resilience of clots in parallel with increasing citrullination of fibrin(ogen). At the end of the clotting phase, both the storage modulus (G') and the loss modulus (G'') stabilized at significantly lower values in citrullinated clots compared to control (Figure 30B, C). As the decrease in G' was more prominent, the overall loss tangent (G''/G') increased, which indicates an increased energy loss during deformation due to structural rearrangements of fibrin. As observed in Figure 30, the flow curves of the softer citrullinated clot structures

presented lower dynamic viscosity values throughout the measurement, and gel/fluid transition occurred at a lower critical stress ($\tau 0$, Figure 30A, E).
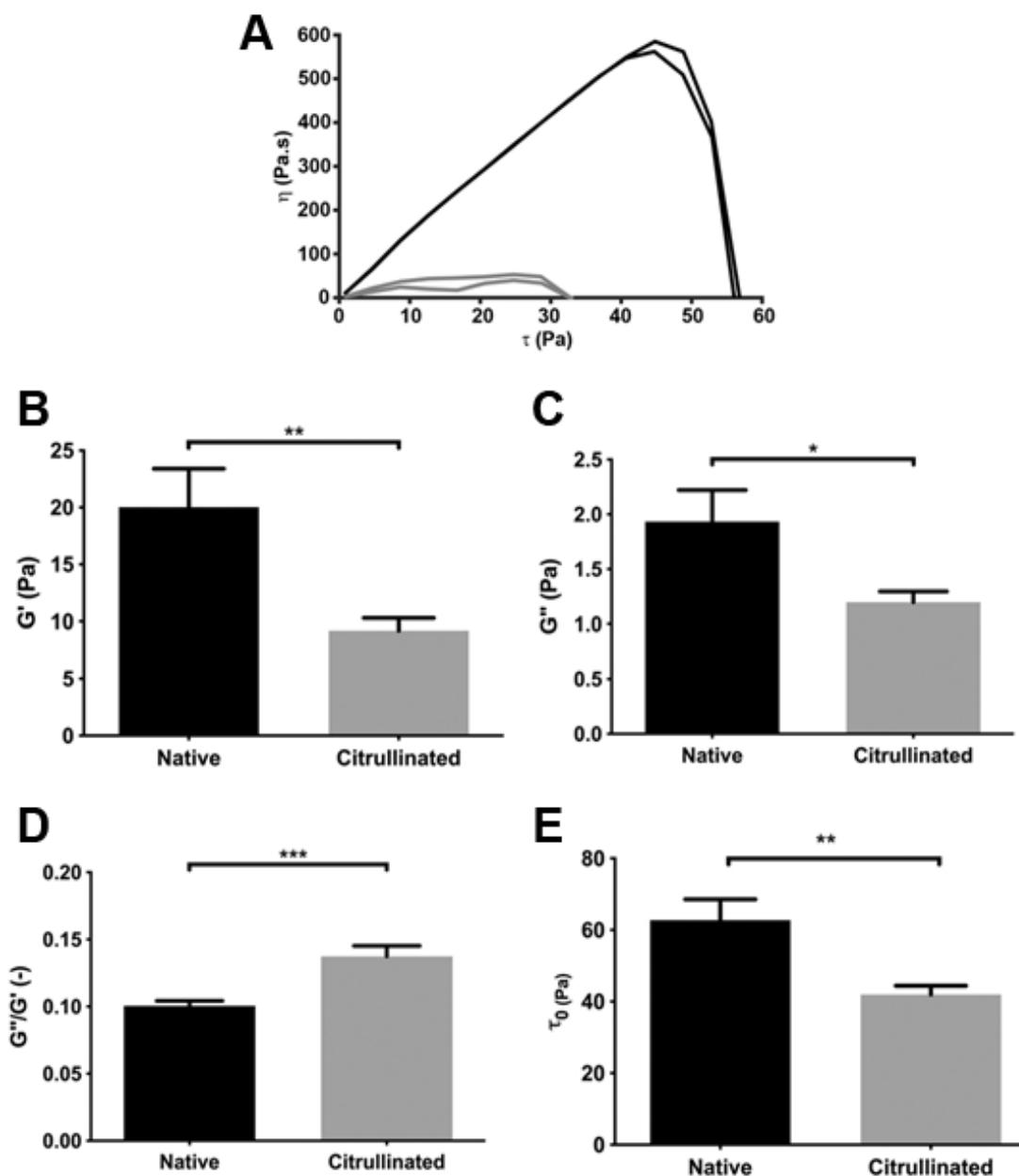
Figure 30. Effects of fibrinogen citrullination on mechanical attributes of fibrin clots. (A) Representative rheometry flow curves depict the viscosity (η) of fibrin clots formed with thrombin and fibrinogen (native-black lines or PAD4-pretreated-gray lines) as they are probed by applying increasing shear stress (τ). (B-D) Storage modulus (G'), loss modulus (G") and loss tangent (G"/G') were calculated from the clotting phase in

oscillation rheometry, while critical shear stress ($\tau 0$, panel E) values (at which viscosity falls to a theoretically zero value) were calculated based on 3-5 replicas of curves illustrated in panel A. *P<0.05, **P<0.01, ***P<0.001.

4.2.4.3. Effects of citrullination on clot resistance to lysis

Turbidimetry analysis showed decelerated plasmin-initiated lysis in fibrin clots formed with CitFg (37% increase in relative t50 = the time needed to reduce the turbidity of clots to 50% of the maximal value). Similar trends were observed in clots formed with a 1:1 mix of citrullinated and native fibrinogen, which showed intermediate times until 50% lysis (Figure 31A and B). To better mimic *in vivo* conditions, tPA-induced lysis was tested in plasma clots spiked with native or CitFg (citrullination was stopped prior to the addition of plasma to rule out off-target PAD4 effects, Figure 31C). In this system, clots supplemented with CitFg showed decreased lysis front movement (0.51±0.03 and 0.54±0.04 RU for clots supplemented with fibrinogen citrullinated at 1.1 mg/L PAD4 for 3 and 4 h respectively, versus 0.65±0.04 RU for plasma clots supplemented with control fibrinogen, Figure 31C and D).
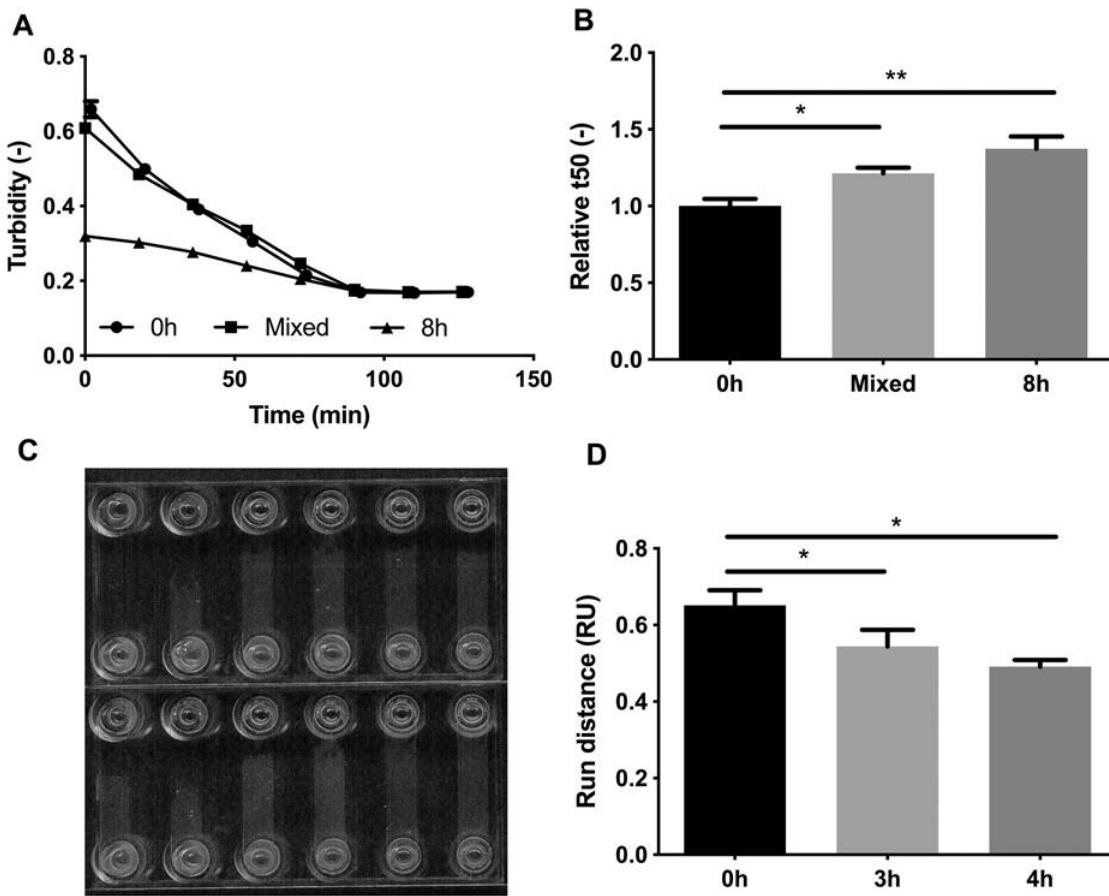
Figure 31. Effects of citrullination on the lysis of fibrin and plasma clots. (A) Representative curves of plasmin-induced lysis of fibrin clots were measured using a turbidimetry setup (absorbance measured at 340 nm). Circles represent fibrin clots clotted with native fibrinogen. Triangles refer to clots formed with fibrinogen pre-treated with 1.15 mg/L PAD4 for 8 h, while squares represent clots formed with a 1:1 mixture of citrullinated and native fibrinogen. Every 10th measurement point is shown. (B) The time needed to reduce the turbidity of clots to 50% of the maximal value (t50) is presented in relative units: the mean value of the t50 for fibrin clotted from native fibrinogen in each independent set of measurement was considered 1. Values presented are calculated from 8-11 curves depicted in panel A, originating from 3 independent experiments. *P<0.05, **P<0.01. (C) tPA-induced lysis of plasma clots supplemented with native (left two channels) or PAD4-pretreated fibrinogen (middle two and right two channels pretreated with 1.15 µg/mL PAD4 for 3 and 4 h, respectively). tPA was injected through the upper orifices, and images were taken after 45 min lysis. (D) Lysis front movement was registered every 15 minutes by photoscanning the samples, and the measured run

distances of the lysis front (opaque clot/transparent fluid interface) at 45 min were normalized for the distance of centers of opposite orifices (13 mm) to give relative units (RU). Mean values and standard error of mean of at least 7 runs from three independent experiments are shown. *P<0.05.

5. Discussion

5.1. Staphylocoagulase

The pathogenicity of *S. aureus* is largely dependent on its ability to exploit the host hemostatic system for bacterial colonization through the vasculature (362). Our study provided novel data on the structural and functional characteristics of the coagulum generated by an isolated key protein (staphylocoagulase) from the *S. aureus* arsenal of factors used to manipulate the hemostatic mechanisms for more efficient pathogenic invasion.

In pure fibrin clots, both SCG-PT and SCG-T lead to an altered fibrin meshwork compared to thrombin, suggesting that SCG not only forms staphylothrombin but also alters the thrombin catalyzed fibrinogen cleavage and/or fibrin polymerization, consistent with the different clotting profiles observed for thrombin and SCG-T [2](363). As SCG increased fibrin fiber thickness in a similar manner with both thrombin and PT, it is possible that SCG itself interferes with fibrin polymerization after binding to fibrinogen (176, 177). Our published results show that there is an equivalence in amidolytic activity between thrombin and SCG-T [2](363) that further implicates SCG-binding to fibrinogen as being responsible for differences in fibrin polymerization and structural properties. The lower amidolytic activity of SCG-PT and further reduced clotting activity relative to SCG-T suggests the contribution of differences in enzyme activity between thrombin and SCG-PT is additive to the effect of fibrinogen-binding [2](363).

Our results showed that when pure fibrinogen was clotted with thrombin, a thicker fiber matrix was associated with a more porous clot structure, which is similar to previously reported data (357). This trend, however, was not seen in fibrin generated by SCG-(P)T. The different trend of SCG-(P)T clot permeability and fiber size could be attributed to an earlier finding that SCG produces a greater amount of background debris compared to thrombin (364), which can explain the formation of thinner fibers – at higher SCG concentrations – without any reduction of the pore size or even allowing for increased porosity. Fibrin clots formed by SCG were more permeable compared to thrombin which probably allows lytic enzymes to penetrate the bacterial coagulum easier (in line with the reported increased tPA potency in SCG clots). At the concentrations used in the rheology studies, both SCG-PT and SCG-T promoted the formation of thicker fibrin fibers

(increased median fiber diameter by 10–15 nm). Ryan et al. described the relation between fiber thickness and elasticity (56) and found that there is an optimal, intermediate (75–90 nm) diameter that is also accompanied by an intermediate branchpoint density and results in maximal G′ values. In our study, fiber thickness exceeds this point; thus, the expected reduced branching can explain the loss of elasticity of the fibrin structure when SCG was present. However, the most striking difference was the decreased resistance of these clots against shear stress, thus a tendency to disrupt easier and form emboli.

As there are many factors (e.g., plasma proteins, clotting factors) in blood plasma interfering with both fibrinogen and thrombin and altering the structural and mechanical properties of a forming clot, it was of interest to evaluate the coagulum properties in this more complex and physiological system. Our findings suggest that coagulation will be finely tuned in the presence of SCG-T and/or SCG-PT at the site of infection or in a bacterial vegetation. When SCG-T is dominant, a thicker and more porous matrix is formed compared to thrombin. The structural trends seen in the presence of SCG-PT were more complex, and its effects were concentration-dependent. Critical shear stress values were dominantly lower in the presence of SCG than with thrombin, indicating that clots formed by either SCG-T or SCG-PT are easier to disrupt. Interestingly, in plasma, SCG increased both elasticity and viscosity of thrombi (when compared to thrombin control), which is the contrary of SCG effects in pure fibrin. In the case of SCG-T, the discrepancy can be explained by the additional interactions of thrombin in plasma (e.g., activation of coagulation factor XIII and the cross-linking of fibers leads to increased elasticity (365)). SCG-PT, on the other hand, does not interact with other partners of thrombin. Thus, the changes observed in the viscoelastic parameters might imply a direct effect on the fibrin network, independent of fiber thickness. We also cannot rule out the possibility of other plasma proteins being bound and trapped into the polymerizing matrix in the presence of SCG. Independently from the increased viscoelastic parameters, the plasma clots also appeared more fragile (as evidenced by the significantly lower τ_0 values) than the respective thrombin controls – suggesting an increased risk for thrombus fragmentation and septic embolization – which mirrored our results from the purified fibrin system.

Although the presence of staphylocoagulase in endocardial vegetations was proved by other groups (177), some studies imply that it is not crucial for the development of these

structures (366, 367). Nevertheless, our results show that when present, it will have a definite effect on the final properties of the lesion. Our study has its limitations as staphylocoagulase is not the sole player at the site of infection. Lipoteichoic acid from *S. aureus* might also change fibrin structure through amyloidogenesis (368). Furthermore, the innate immune system is activated upon a *S. aureus* infection and vegetation formation (362), and it is already reported with *Streptococcus mutans* that bacterial endocarditis can be accompanied by NET formation (369). *S. aureus* also has the capability to induce the release of such traps (194), which also modify clot structure and increase its mechanical stability (269). Thus, the structure of the vegetations, their fragmentation, and the resulting septic embolisms highly depend on the local concentration of clot components (e.g., SCG-T, SCG-PT, NET, or even cellular, bacterial components) in different regions of the lesion.

5.2. Neutrophil extracellular traps and the structure of *ex vivo* thrombi

5.2.1. NET constituents in heart, brain, and peripheral arterial thrombi

Our previous *in vitro* (269) and *ex vivo* (271) study provided evidence that NET components (DNA, histones) modify the structure of fibrin, increase its mechanical stability and render clots less sensitive to lysis with tPA/plasminogen. In line with the recently reported findings in ischemic stroke thrombi (271, 370), our work confirmed the presence of NET components in AIS thrombi, but we also demonstrated that the DNA content of AIS thrombi is similar to CAD and considerably lower than PAD thrombi. Thus, compared to other artery locations, in AIS, the NET meshwork impedes the fibrinolytic therapeutic approach the least to restore the patency of occluded vessels. During the early phase of NETosis, the arginine residues of histone proteins are deiminated (citrullinated) by the enzyme PAD4. Thus cH3 is considered to be a specific marker of NETs (246). This antigen was present in all clots – in line with the recently reported findings in ischemic stroke thrombi (370). No significant quantitative differences were observed between cH3 content at different vascular locations, which could be attributed to the role of citrullination limited to triggering NET formation. Thus, differences in the minuscule quantities of citrullinated histones (sufficient to initiate NETosis) are not necessarily detectable after the completion of the process – well after we performed the observations. Because thrombin is able to degrade citrullinated histones (286), extracellular DNA appears to be a more stable marker of NETosis in thrombi. Such an interpretation of the FD50 and FH50 findings is in line with our results regarding the effects of oral anticoagulants, as the treatment with such drugs leads to a two-fold higher relative cH3 content in all thrombi. In view of the stabilizing impact of NETs on thrombi, an important observation from our work was that both the DNA and the cH3 content, as hallmarks of NETs, correlated positively with the patients' age (except for cH3 in AIS). Our data suggest the local inflammatory process accompanied by NET release in thrombi is associated with a mild to moderate increase in the systemic signs of inflammation (WBC, CRP), whereas their extremely high systemic levels are probably related to additional loci, distinct from the thrombi.

Because histones are known to confer mechanical and lytic resistance to fibrin (269), our result from the patients' age at the intervention can be interpreted as an age-dependent clot-stabilizing effect, which suggests an improved response to lytic treatment in younger

patients, as well as that stabilization of the structure in older patients could favor the success of mechanical intervention. In addition, in PAD, the strength of association between the NET content of thrombi and patients' age was increased by atherosclerotic etiology or systemic indicators of inflammation (CRP, leukocytosis, plasma fibrinogen). The age trend in FH50 of AIS patients was reinforced by malignant co-morbidities, known to exert an independent NET-promoting effect (321), which points to increased lytic resistance in this subgroup of patients. The role of malignancy in NETosis was further strengthened by our results in venous thrombi from mice bearing human pancreatic tumor cells (358). We found increased levels of plasma biomarkers that either increase neutrophil counts, such as G-CSF, or are biomarkers of activated neutrophils and NET, such as NE and H3Cit, in tumor-bearing mice compared with controls. We also observed increased levels of the neutrophil biomarker Ly6G and the NET biomarker H3Cit in thrombi from tumor-bearing mice. Taken together, these data suggest that neutrophils contribute to increased venous thrombosis observed in tumor-bearing mice.

We found that tumor-bearing mice have increased levels of mouse G-CSF and there was a significant positive correlation between levels of mouse G-CSF and neutrophil numbers. This suggests that increased levels of G-CSF drive the increase in neutrophil numbers. At present, we do not know the cellular source of G-CSF in tumor-bearing mice, but this cytokine is normally expressed by endothelial cells, macrophages and immune cells (371). In support of this, mice with murine breast 4T1 tumors exhibit increased plasma levels of G-CSF and administration of an anti-G-CSF antibody reduces neutrophil counts (321). G-CSF level and neutrophil count may, therefore, represent novel biomarkers of VTE risk in cancer patients.

It has been hypothesized that G-CSF primes neutrophils to undergo NET formation in tumor-bearing mice (321, 372). In one study it was found that the percentage of H3Cit-positive neutrophils was increased in tumor-bearing mice compared with controls (321). Furthermore, neutrophils isolated from mice bearing murine 4T1 tumors treated with an anti-G-CSF antibody had significantly less NET formation compared with those from tumor-bearing mice treated with an isotype control (321). In addition, administration of recombinant G-CSF to mice bearing murine melanoma B16 tumors, which do not produce G-CSF, increased H3Cit in tumors in a PAD4-dependent manner (372, 373). We observed a large variation in the H3Cit/H3 ratio in thrombi from tumor-bearing mice

which appears to be due to different levels of H3Cit in the thrombi. At present, we do not know the reason for this range of H3Cit in thrombi from tumor-bearing mice, but it may reflect differences in G-CSF levels and the degree of neutrophil priming in the different tumor-bearing mice.

Plasma cfDNA and the NET biomarker, H3Cit, were increased in tumor-bearing mice compared with controls. Tumors are known to release cfDNA into the blood (374). In addition, we observed that BxPc-3 cells express PAD4 and therefore tumors may also contribute to the plasma levels of H3Cit. Thrombi from tumor-bearing mice also had increased levels of cfDNA and H3Cit compared with thrombi from controls. Importantly, administration of DNase I reduced thrombus size in tumor-bearing mice but not in control mice. Similarly, a previous study showed that DNase I did not affect jugular vein occlusion times in control mice but prolonged the time to occlusion in 4T1 tumor-bearing mice (322). We observed that DNase I reduced thrombus size more effectively than depletion of neutrophils. It is possible that DNase I is more effective than neutrophil depletion because it digests not only NET but also cfDNA, which may also be released by cancer cells and may enhance thrombosis by activating factor XII (266, 375).

5.2.2. Fibrin structure in thrombi

Because of the known effects of NET components on purified fibrin structure (269), in the present study, we investigated the alterations in fibrin content and fiber thickness in thrombi. Although the fibrin fiber occupancy was statistically higher in PAD thrombi (98.1±5.6%) compared to AIS (97.1±7.93%, P=0.043) or CAD (96.8±8.1%, P=0.0081) groups, these differences were not considerable in magnitude, and thus fibrin content could be used as a reference value for the content of NET constituents (justifying the interpretation of the FD50 and FH50 ratio values as measures of DNA and cH3 content of thrombi). Fibrin fiber thickness has a direct effect on the viscoelastic properties of the clots and their mechanical stability (376). The median of fibrin fiber diameter measured in this study was significantly higher in CAD thrombi compared to AIS or PAD samples. These tendencies in the fiber size of the three main groups were due to the structural pattern of fibrin in male patients (median fiber diameter in CAD: 76.3 nm [67.2-90.8, n=41; AIS: 64.1 nm [58.6-85.3] n=46, P=0.0093 compared to CAD; PAD: 62.1 nm [57.4-75.2], n=34, P=0.0002 compared to CAD), whereas fiber diameter did not differ in

females from these groups. Because the mechanical stability of thicker fibrin fibers is higher (376), this data indicates that thrombi of male CAD are the most stable. Furthermore, chronic acetylsalicylic acid (ASA) treatment prior to the acute ischemic event was associated with an increased fiber diameter only in males.

The alterations in fibrin structure cannot be attributed to the effect of NETs because PAD thrombi showed the highest relative DNA and cH3 content and the thinnest fibers, whereas, in purified fibrin clots, DNA and histones increase the fiber diameter (269). This discrepancy could be explained at least in part by differences in pre-procedural medication. While all CAD patients received chronic ASA prophylaxis, only a quarter of the AIS and half of the PAD patients were treated with ASA prior to the acute intervention. ASA is known to have platelet-independent effects, such as fibrin acetylation, which leads to thicker fibers (377, 378). Clinical trials demonstrate sex differences in response to ASA treatment (379), which is in agreement with our data showing that ASA treatment results in thicker fibrin fibers only in male patients.

The previously reported data on the association of fibrin structure and CRP are inconsistent and controversial with studies variably showing that: 1) CRP-treated fibrin clots had thicker fibrin fibers (380); 2) a lower CRP (<2 mg/L) was associated with greater fibrin fiber diameters compared to CRP>5 mg/L in thrombi removed from CAD (381). In our study, fibrin fiber diameters did not differ significantly in CAD patients with low CRP (<5 mg/L), compared to those with higher values (71.88 nm [63.34-86.24] n=43 vs. 72.26 nm [61.12-98.48], n=18, P=0.4825) probably due to the dominant ASA effect discussed above.

5.2.3. Citrullinated fibrinogen

We have shown that altered fibrin structure formed with CitFg results in a mechanically destabilized but chemically resistant clot.

Mounting evidence underlines the clinical prognostic value of clot structure (57, 382, 383). Patients with deep vein thrombosis (DVT) have decreased plasma clot permeability compared to controls without a DVT history, and densely packed fibrin fibers have been detected in distal pulmonary emboli (360, 384). Because of the similarity in the low-flow hydrodynamic conditions at the sites of thrombus formation (venous stasis and dysrhythmic heart, respectively), findings gained from venous thrombi could provide

clues for a better understanding of thrombi causing cardioembolic stroke, presenting the most common known stroke etiology (~20% stroke cases) (385). Clot structure, however, depends on a multitude of factors, including the concentration of thrombin and fibrinogen. In our system, both effective thrombin and fibrinogen concentrations might have decreased since CitFg is an uncompetitive inhibitor of thrombin (333). Moreover, the formation of CitFg occurs at the expense of effective fibrinogen concentrations since thrombin cleaves next to native peptidyl-arginine only (334). The net effects of these (and possibly other) factors might have contributed to the decreased median fiber diameter in clots containing CitFg, which is in alignment with the single preliminary study on CitFg with SEM investigations (334). Here we confirm the SEM findings with an independent method that adds structural insights on the level of individual fibers. SAXS indicated that the decrease in fiber thickness did not result from a change in intra-fiber protofibril density, as the scatter curve peak ranging from 0.6-1.5 nm^{-1} (corresponding to the cross-sectional fiber periodicity) (269) was preserved in clots containing various concentrations of CitFg. The measured fiber-level biomechanical parameters are in line with this finding: the Young modulus of citrullinated fibrin remained in the same order of magnitude as that of control fibrin [4](359), suggesting that the decreased fiber stiffness (decreased G') of citrullinated fibrin was primarily a consequence of a thinner fiber structure and not due to a change in the mechanical properties of individual fibrin protofibrils. Generally, the formation of thinner fibrin fibers leads to a decrease in clot porosity (57), which is in line with decreased Ks (permeability constant) values observed by us and the more compact space-filling pattern of the clots supported by increased fiber density (LSM) and increased mass fractal dimension (SAXS).

In pure fibrin clots, thinner fibers and lower porosity typically result in slower fibrinolysis, even though mathematical modeling of this system has shown more complexity (386). This phenomenon is traditionally explained with the different ratios of two processes, namely, inter-fiber diffusion of plasmin (slower) versus cutting across individual fibers (faster) in dense vs. coarse fibrin (114). In addition to the altered fibrin structure seen in our turbidimetry experiments, a loss of plasmin cleavage sites may play a role in the lower rate of fibrinolysis. While plasmin cleaves overwhelmingly next to lysine residues, there is some evidence that it may generate fibrinogen-derived peptides upon cleavage next to peptidyl-arginine (387, 388). As earlier work has shown decreased

efficiency of plasmin on soluble CitFg (333), it is plausible that fibrin formed with CitFg may show similarly decreased susceptibility to plasmin. Taking this experimental setting one step closer to the *in vivo* scenario, we demonstrated that plasma clots are resolved slower when supplemented even with a low % of CitFg: given that citrullination was submaximal (confirmed by coagulometry experiments performed in parallel), the ratio of citrullinated to native fibrinogen was probably well below 5% in this setup.

Perhaps even more prominent than the effects on chemical stability, the presence of CitFg resulted in markedly altered clot mechanics, as our study uniquely demonstrates. Clots formed with CitFg were mechanically less stable, as revealed by the decrease in the critical shear stress causing gel/fluid transition (rheometry) in the current study. These are in line with previous studies, which showed that thinner fibrin fiber networks were associated with decreased G' (56, 389) and an increase in the loss tangent (G''/G') in the presence of calcium (389). In the present study, the combination of methods analyzing fiber-level structures and macroscopic viscoelasticity revealed that the convoluted fibers of citrullinated fibrin (which bear lower bending rigidity seen as decreased persistence length) [4](359) allowed for a relatively higher energy loss than energy storage upon deformation (increased G''/G'). Thus, in terms of biomechanics, citrullination increased the deformability and decreased the stability of fibrin. In *in vivo* thrombi, such a decrease in mechanical stability might lead to a propensity for rupture of deep venous thrombi and consequential formation of emboli (390, 391).

While we and others have previously demonstrated the inhibitory effects of DNA, histones, and NETs on clot lysis (258, 268, 269), our current findings point to another potential mechanism through which neutrophils could influence clot structure and stability, namely, the generation of CitFg via neutrophil-derived PAD enzymes. The mechanisms described by us could contribute to decreased *in vivo* fibrinolytic susceptibility, with implications for thrombolytic efficacy in DVT studies.

CitFg has been detected previously alongside PAD4 in a murine model of wound healing (392) as well as in human atherosclerotic plaques – the rupture of which often trigger thrombosis – and in the synovia and serum of patients with rheumatoid arthritis (330, 331), a condition associated with a higher risk for cardiovascular disease (393). Furthermore, PAD4-catalyzed CitFg formation might attract attention from a therapeutic perspective. Even though the exact role of PAD4 in NETosis is still debated (394),

inhibition of PAD4 has shown promising *in vitro* results in inhibiting NET formation (395) and, in a previous study using the IVC stenosis model, genetic knockout of PAD4 decreased the likelihood of thrombosis (316). However, therapeutic inhibition of PAD in the circulation would not only silence NETosis but also likely affect the amount of citrullinated plasma proteins such as fibrinogen. With specific regards to thrombosis, it is tempting to visualize cell-impermeable PAD inhibitors that hinder the formation of the antifibrinolytic CitFg but avoid the hazards of disturbed gene expression stemming from altered histone modification. Future studies will decide if this vision becomes a reality.

6. Conclusions

Our most important conclusions are the following:

1. Staphylocoagulase has an impact not only on prothrombin but also alters thrombin catalyzed fibrin polymerization.

2. Concerning fibrin structure, we observed a general trend for SCG to produce a fibrin matrix with thicker individual fibers, preserved intrafibrillar density, and increased clot porosity.

3. Fibrin clots formed in the presence of SCG have lower elasticity and viscosity. Plasma clots showed opposing results: increased elasticity and viscosity.

4. When present, SCG renders clots less resistant to mechanical forces and shear stress.

5. Lysis of both plasma and pure fibrin clots is generally potentiated in SCG-formed clots – with a more accentuated effect with SCG-PT.

6. NETs are present in arterial clots and the NET content of thrombi varies at different locations (brain, heart, peripheral arteries).

7. DNA and citrullinated histones in thrombi correlate with patient age and systemic inflammatory markers.

8. Thicker fibrin fibers are formed in coronaries, unlike those formed in brain and peripheral arteries.

9. Markers of NETs are present in higher amounts in thrombi from mice bearing human pancreatic tumors.

10. Citrullinated fibrinogen leads to the formation of a thinner fiber matrix with increased fibrin fiber density and lower permeability.

11. Clots with CitFg are less elastic, less viscous, and show decreased resistance against mechanical forces and shear stress but increased lytic resistance.

Implications:

1.   Our lysis results of clots formed in the presence of SCG suggest a shorter lifespan of these clots *in vivo.*

2.   The opposing results of the viscoelastic properties of fibrin and plasma clots can be the result of the direct effects of SCG on fibrin(ogen).

3.   Clots formed in the presence of SCG tend to disrupt easier and form emboli.

4.   Certain routine laboratory findings may have a predictive value for NET content and the structure of thrombi. These findings could lead to better therapeutic strategies, but the predictive model must be further tested.

5.   Neutrophils and NET formation enhance venous thrombosis in pancreatic cancer.

6.   Therapeutic inhibition of PAD in the circulation would not only silence NETosis but also likely affect the amount of citrullinated plasma proteins such as fibrinogen.

7.   Cell-impermeable PAD inhibitors might hinder the formation of the antifibrinolytic CitFg but avoid the hazards of disturbed gene expression stemming from altered histone modification.

7. Summary

The mortality rates of thromboembolic diseases remain high despite the continuous expansion of treatment options. For better prognosis, novel therapeutic targets are needed. We studied the interrelations of the immune and the hemostatic systems to identify such molecular mechanisms; we examined the structural, mechanical, and lytic behavior of thrombi and determined novel determinants of thrombus structure.

Staphylococcus aureus is a Gram-positive coccal bacterium that can cause a broad palette of pathologies. One of its virulence factors is staphylocoagulase, a protein that binds to prothrombin, and the formed SCG-PT complex expresses thrombin-like proteolytic activity through a non-proteolytic zymogen activation of prothrombin. Our results showed that thrombi formed in the presence of staphylocoagulase are chemically less resistant against plasmin-mediated lysis, partially explained by the fibrin matrix made up from thicker individual fibers in the presence of SCG-(P)T. These clots had increased porosity and decreased resistance against shear stress, which makes them prone to disruption and emboli formation.

Neutrophil extracellular traps (NETs) are net-like structures composed of decondensed chromatin, and antimicrobial peptides emitted to the extracellular space by polymorphonuclear cells during NETosis. Previous results show that NETs render clots more resistant against lytic and mechanical forces. Examining thrombi removed during therapeutic intervention from coronary, peripheral artery disease and acute ischemic stroke patients, we showed not only that NETs are present in varying amounts in arterial thrombi from different localizations, but also found associations of NET content with systemic inflammatory markers and patient age. Furthermore, malignancy increased the NET content of clots in a murine *in vivo* venous thrombosis model.

Peptidyl-arginine-deiminase 4 can citrullinate fibrinogen upon NETosis. Our results showed that thrombi formed in the presence of such fibrinogen have thinner fiber matrix, with increased fiber density and lower permeability. These clots were less elastic, less viscous, and showed decreased resistance against mechanical forces and shear stress. These findings were accompanied by increased lytic resistance.

In summary, our findings improved the understanding of the molecular links between inflammation and thrombosis and pave the way to novel diagnostic and therapeutic options in cardiovascular diseases.

8. Összefoglalás

A bővülő terápiás lehetőségek ellenére a trombotikus betegségek halálozási aránya továbbra is magas, a jobb prognózis érdekében új terápiás célpontokra van szükség. Munkánk során az immun- és véralvadási rendszer kapcsolatait tanulmányoztuk ilyen lehetőségek feltérképezése céljából. Alvadékok szerkezeti, mechanikai és lítikus tulajdonságait vizsgáltuk, új, trombusszerkezetet meghatározó faktorokat írtunk le.

A *Staphylococcus aureus* egy Gram-pozitív baktérium, amely számos patológiás állapotért felelős. Egyik fontos virulencia-faktora a stafilokoaguláz, egy fehérje, amely protrombinhoz kötődik. A létrejövő SCG-PT komplex a protrombin nem-enzimatikus zimogén aktivációját követően trombin-szerű aktivitással rendelkezik. A stafilokoaguláz jelenlétében létrejött alvadékok kevésbé rezisztensek plazmin általi lízissel szemben, amit részben az SCG-(P)T jelenlétében létrejött vastagabb szálakból álló fibrinmátrix magyarázhat. Ez fokozott porozitással, nyíróerőkkel szemben kisebb ellenállással társult, ami az ilyen alvadékok könnyebb dezintegrációjához, embolusképződéshez vezethet.

A neutrofil extracelluláris csapdák (NETek) hálószerű struktúrák, melyek dekondenzált kromatinból és antimikrobiális fehérjékből állnak, amiket polimorfonukleáris sejtek bocsájtanak ki az extracelluláris térbe NETózis során. A NET-ek az alvadékok lítikus és mechanikai erőkkel szembeni ellenállását is képesek fokozni. Szívkoszorúér- és perifériás artériás betegségben szenvedő betegekből, valamint stroke-on átesett betegekből intervenciós módszerekkel eltávolított vérrögöket vizsgáltunk, melyekben a NET komponensek változó mértékben voltak jelen, emellett azok mennyisége összefüggést mutatott szisztémás gyulladásos paraméterekkel és a betegek életkorával. Továbbá *in vivo* egér vénás trombózis modellünkben tumor jelenléte fokozta a trombusok NET-tartalmát. A NETózis során aktiválódó peptidil-arginin-deimináz 4 képes a fibrinogént citrullinálni. A citrullinált fibrinogén jelenlétében képződött alvadékok vékonyabb fibrinszálakból épülnek fel nagyobb száldenzitással, melyhez kisebb permeabilitás (porozitás) társul. Az alvadékok kevésbé elasztikusak és viszkózusak, emellett csökkent mechanikai ellenállást mutatnak, megnövekedett lítikus rezisztenciával.

Összefoglalva, munkánk elősegíti a trombózis és gyulladás közötti kapcsolatok pontosabb megértését, utat nyitva ezáltal újabb diagnosztikai és terápiás módszerek fejlesztéséhez kardiovaszkuláris betegségekben.

9. Bibliography

1   World Health Organization - The top 10 causes of death. Available at: https://www.who.int/news-room/fact-sheets/detail/the-top-10-causes-of-death Accessed 2021 Apr 13.

2   Longstaff C, Varju I, Sotonyi P, Szabo L, Krumrey M, Hoell A, Bota A, Varga Z, Komorowicz E, Kolev K. (2013) Mechanical stability and fibrinolytic resistance of clots containing fibrin, DNA, and histones. J Biol Chem. 288: 6946-56.

3   Wood JP, Silveira JR, Maille NM, Haynes LM, Tracy PB. (2011) Prothrombin activation on the activated platelet surface optimizes expression of procoagulant activity. Blood. 117: 1710-8.

4   Mann KG, Nesheim ME, Church WR, Haley P, Krishnaswamy S. (1990) Surface-dependent reactions of the vitamin K-dependent enzyme complexes. Blood. 76: 1-16.

5   Heldebrant CM, Butkowski RJ, Bajaj SP, Mann KG. (1973) The activation of prothrombin. II. Partial reactions, physical and chemical characterization of the intermediates of activation. J Biol Chem. 248: 7149-63.

6   Davie EW, Kulman JD. (2006) An overview of the structure and function of thrombin. Semin Thromb Hemost. 32 Suppl 1: 3-15.

7   Huntington JA. (2014) Natural inhibitors of thrombin. Thromb Haemost. 111: 583-9.

8   Pechik I, Madrazo J, Mosesson MW, Hernandez I, Gilliland GL, Medved L. (2004) Crystal structure of the complex between thrombin and the central "E" region of fibrin. Proc Natl Acad Sci U S A. 101: 2718-23.

9   Fuentes-Prior P, Iwanaga Y, Huber R, Pagila R, Rumennik G, Seto M, Morser J, Light DR, Bode W. (2000) Structural basis for the anticoagulant activity of the thrombin-thrombomodulin complex. Nature. 404: 518-25.

10   Gandhi PS, Chen Z, Di Cera E. (2010) Crystal structure of thrombin bound to the uncleaved extracellular fragment of PAR1. J Biol Chem. 285: 15393-8.

11   Myles T, Yun TH, Hall SW, Leung LL. (2001) An extensive interaction interface between thrombin and factor V is required for factor V activation. J Biol Chem. 276: 25143-9.

12   Myles T, Yun TH, Leung LL. (2002) Structural requirements for the activation of human factor VIII by thrombin. Blood. 100: 2820-6.

13   Bukys MA, Orban T, Kim PY, Beck DO, Nesheim ME, Kalafatis M. (2006) The structural integrity of anion binding exosite I of thrombin is required and sufficient for timely cleavage and activation of factor V and factor VIII. J Biol Chem. 281: 18569-80.

14   Hall SW, Nagashima M, Zhao L, Morser J, Leung LL. (1999) Thrombin interacts with thrombomodulin, protein C, and thrombin-activatable fibrinolysis inhibitor via specific and distinct domains. J Biol Chem. 274: 25510-6.

15   Janus TJ, Lewis SD, Lorand L, Shafer JA. (1983) Promotion of thrombin-catalyzed activation of factor XIII by fibrinogen. Biochemistry. 22: 6269-72.

16   De Cristofaro R, De Candia E, Landolfi R, Rutella S, Hall SW. (2001) Structural and functional mapping of the thrombin domain involved in the binding to the platelet glycoprotein Ib. Biochemistry. 40: 13268-73.

17   Celikel R, McClintock RA, Roberts JR, Mendolicchio GL, Ware J, Varughese KI, Ruggeri ZM. (2003) Modulation of alpha-thrombin function by distinct interactions with platelet glycoprotein Ibalpha. Science. 301: 218-21.

18   Dumas JJ, Kumar R, Seehra J, Somers WS, Mosyak L. (2003) Crystal structure of the GpIbalpha-thrombin complex essential for platelet aggregation. Science. 301: 222-6.

19   Nogami K, Zhou Q, Myles T, Leung LL, Wakabayashi H, Fay PJ. (2005) Exosite-interactive regions in the A1 and A2 domains of factor VIII facilitate thrombin-catalyzed cleavage of heavy chain. J Biol Chem. 280: 18476-87.

20   Segers K, Dahlback B, Bock PE, Tans G, Rosing J, Nicolaes GA. (2007) The role of thrombin exosites I and II in the activation of human coagulation factor V. J Biol Chem. 282: 33915-24.

21   Shore JD, Day DE, Francis-Chmura AM, Verhamme I, Kvassman J, Lawrence DA, Ginsburg D. (1995) A fluorescent probe study of plasminogen activator inhibitor-1. Evidence for reactive center loop insertion and its role in the inhibitory mechanism. J Biol Chem. 270: 5395-8.

22   Stratikos E, Gettins PG. (1999) Formation of the covalent serpin-proteinase complex involves translocation of the proteinase by more than 70 A and full insertion of the reactive center loop into beta-sheet A. Proc Natl Acad Sci U S A. 96: 4808-13.

23   Hagglof P, Bergstrom F, Wilczynska M, Johansson LB, Ny T. (2004) The reactive-center loop of active PAI-1 is folded close to the protein core and can be partially inserted. J Mol Biol. 335: 823-32.

24   Lawrence DA, Ginsburg D, Day DE, Berkenpas MB, Verhamme IM, Kvassman JO, Shore JD. (1995) Serpin-protease complexes are trapped as stable acyl-enzyme intermediates. J Biol Chem. 270: 25309-12.

25   Lawrence DA, Strandberg L, Ericson J, Ny T. (1990) Structure-function studies of the SERPIN plasminogen activator inhibitor type 1. Analysis of chimeric strained loop mutants. J Biol Chem. 265: 20293-301.

26   Huntington JA, Read RJ, Carrell RW. (2000) Structure of a serpin-protease complex shows inhibition by deformation. Nature. 407: 923-6.

27   Egelund R, Petersen TE, Andreasen PA. (2001) A serpin-induced extensive proteolytic susceptibility of urokinase-type plasminogen activator implicates distortion of the proteinase substrate-binding pocket and oxyanion hole in the serpin inhibitory mechanism. Eur J Biochem. 268: 673-85.

28   Huntington JA. (2013) Thrombin inhibition by the serpins. J Thromb Haemost. 11 Suppl 1: 254-64.

29   Rau JC, Beaulieu LM, Huntington JA, Church FC. (2007) Serpins in thrombosis, hemostasis and fibrinolysis. J Thromb Haemost. 5 Suppl 1: 102-15.

30   Gettins PG. (2002) Serpin structure, mechanism, and function. Chem Rev. 102: 4751-804.

31   Baglin TP, Carrell RW, Church FC, Esmon CT, Huntington JA. (2002) Crystal structures of native and thrombin-complexed heparin cofactor II reveal a multistep allosteric mechanism. Proc Natl Acad Sci U S A. 99: 11079-84.

32   Li W, Adams TE, Nangalia J, Esmon CT, Huntington JA. (2008) Molecular basis of thrombin recognition by protein C inhibitor revealed by the 1.6-A structure of the heparin-bridged complex. Proc Natl Acad Sci U S A. 105: 4661-6.

33   Li W, Huntington JA. (2012) Crystal structures of protease nexin-1 in complex with heparin and thrombin suggest a 2-step recognition mechanism. Blood. 120: 459-67.

34   Li W, Johnson DJ, Esmon CT, Huntington JA. (2004) Structure of the antithrombin-thrombin-heparin ternary complex reveals the antithrombotic mechanism of heparin. Nat Struct Mol Biol. 11: 857-62.

35   Weisel JW, Litvinov RI. (2017) Fibrin Formation, Structure and Properties. Subcell Biochem. 82: 405-56.

36   Weisel JW. (2005) Fibrinogen and fibrin. Adv Protein Chem. 70: 247-99.

37   Mosesson MW. (2005) Fibrinogen and fibrin structure and functions. J Thromb Haemost. 3: 1894-904.

38   Zhmurov A, Brown AE, Litvinov RI, Dima RI, Weisel JW, Barsegov V. (2011) Mechanism of fibrin(ogen) forced unfolding. Structure. 19: 1615-24.

39   Henschen A, Lottspeich F, Kehl M, Southan C. (1983) Covalent structure of fibrinogen. Ann N Y Acad Sci. 408: 28-43.

40   Henschen A, Mcdonagh, J. Fibrinogen, fibrin and factor XIII. In: Zwaal R, Hemker H (Ed.), Blood coagulation. Elsevier Science, Amsterdam, 1986:

41   Weisel JW, Veklich Y, Gorkun O. (1993) The sequence of cleavage of fibrinopeptides from fibrinogen is important for protofibril formation and enhancement of lateral aggregation in fibrin clots. J Mol Biol. 232: 285-97.

42   Medved L, Weisel JW, Fibrinogen, Factor XSoSSCoISoT, Haemostasis. (2009) Recommendations for nomenclature on fibrinogen and fibrin. J Thromb Haemost. 7: 355-9.

43   Ferry JD. (1952) The Mechanism of Polymerization of Fibrinogen. Proc Natl Acad Sci U S A. 38: 566-9.

44   Krakow W, Endres GF, Siegel BM, Scheraga HA. (1972) An electron microscopic investigation of the polymerization of bovine fibrin monomer. J Mol Biol. 71: 95-103.

45   Fowler WE, Hantgan RR, Hermans J, Erickson HP. (1981) Structure of the fibrin protofibril. Proc Natl Acad Sci U S A. 78: 4872-6.

46   Muller MF, Ris H, Ferry JD. (1984) Electron microscopy of fine fibrin clots and fine and coarse fibrin films. Observations of fibers in cross-section and in deformed states. J Mol Biol. 174: 369-84.

47   Spraggon G, Everse SJ, Doolittle RF. (1997) Crystal structures of fragment D from human fibrinogen and its crosslinked counterpart from fibrin. Nature. 389: 455-62.

48   Brown JH, Volkmann N, Jun G, Henschen-Edman AH, Cohen C. (2000) The crystal structure of modified bovine fibrinogen. Proc Natl Acad Sci U S A. 97: 85-90.

49   Weisel JW. (1986) The electron microscope band pattern of human fibrin: various stains, lateral order, and carbohydrate localization. J Ultrastruct Mol Struct Res. 96: 176-88.

50   Blomback B, Hessel B, Hogg D, Therkildsen L. (1978) A two-step fibrinogen--fibrin transition in blood coagulation. Nature. 275: 501-5.

51   Yang Z, Mochalkin I, Doolittle RF. (2000) A model of fibrin formation based on crystal structures of fibrinogen and fibrin fragments complexed with synthetic peptides. Proc Natl Acad Sci U S A. 97: 14156-61.

52   Okumura N, Terasawa F, Hirota-Kawadobora M, Yamauchi K, Nakanishi K, Shiga S, Ichiyama S, Saito M, Kawai M, Nakahata T. (2006) A novel variant fibrinogen, deletion of Bbeta111Ser in coiled-coil region, affecting fibrin lateral aggregation. Clin Chim Acta. 365: 160-7.

53   Langer BG, Weisel JW, Dinauer PA, Nagaswami C, Bell WR. (1988) Deglycosylation of fibrinogen accelerates polymerization and increases lateral aggregation of fibrin fibers. J Biol Chem. 263: 15056-63.

54   Weisel JW, Medved L. (2001) The structure and function of the alpha C domains of fibrinogen. Ann N Y Acad Sci. 936: 312-27.

55   Baradet TC, Haselgrove JC, Weisel JW. (1995) Three-dimensional reconstruction of fibrin clot networks from stereoscopic intermediate voltage electron microscope images and analysis of branching. Biophys J. 68: 1551-60.

56   Ryan EA, Mockros LF, Weisel JW, Lorand L. (1999) Structural origins of fibrin clot rheology. Biophys J. 77: 2813-26.

57   Weisel JW, Litvinov RI. (2013) Mechanisms of fibrin polymerization and clinical implications. Blood. 121: 1712-9.

58   Blomback B, Banerjee D, Carlsson K, Hamsten A, Hessel B, Procyk R, Silveira A, Zacharski L. (1990) Native fibrin gel networks and factors influencing their formation in health and disease. Adv Exp Med Biol. 281: 1-23.

59   Matveyev M, Domogatsky SP. (1992) Penetration of macromolecules into contracted blood clot. Biophys J. 63: 862-3.

60   Okada M, Blomback B. (1983) Factors influencing fibrin gel structure studied by flow measurement. Ann N Y Acad Sci. 408: 233-53.

61   Spero RC, Sircar RK, Schubert R, Taylor RM, 2nd, Wolberg AS, Superfine R. (2011) Nanoparticle diffusion measures bulk clot permeability. Biophys J. 101: 943-50.

62   Weisel JW, Nagaswami C. (1992) Computer modeling of fibrin polymerization kinetics correlated with electron microscope and turbidity observations: clot structure and assembly are kinetically controlled. Biophys J. 63: 111-28.

63   Cohen C, Parry DA. (1990) Alpha-helical coiled coils and bundles: how to design an alpha-helical protein. Proteins. 7: 1-15.

64   Litvinov RI, Faizullin DA, Zuev YF, Weisel JW. (2012) The alpha-helix to beta-sheet transition in stretched and compressed hydrated fibrin clots. Biophys J. 103: 1020-7.

65   Zhmurov A, Kononova O, Litvinov RI, Dima RI, Barsegov V, Weisel JW. (2012) Mechanical transition from alpha-helical coiled coils to beta-sheets in fibrin(ogen). J Am Chem Soc. 134: 20396-402.

66   Lim BB, Lee EH, Sotomayor M, Schulten K. (2008) Molecular basis of fibrin clot elasticity. Structure. 16: 449-59.

67   Brown AE, Litvinov RI, Discher DE, Weisel JW. (2007) Forced unfolding of coiled-coils in fibrinogen by single-molecule AFM. Biophys J. 92: L39-41.

68   Kolev K, Longstaff C, Machovich R. (2005) Fibrinolysis at the fluid-solid interface of thrombi. Curr Med Chem Cardiovasc Hematol Agents. 3: 341-55.

69   Fay WP, Garg N, Sunkar M. (2007) Vascular functions of the plasminogen activation system. Arterioscler Thromb Vasc Biol. 27: 1231-7.

70   Pennica D, Holmes WE, Kohr WJ, Harkins RN, Vehar GA, Ward CA, Bennett WF, Yelverton E, Seeburg PH, Heyneker HL, Goeddel DV, Collen D. (1983) Cloning and expression of human tissue-type plasminogen activator cDNA in E. coli. Nature. 301: 214-21.

71   van Hinsbergh VW. (1988) Regulation of the synthesis and secretion of plasminogen activators by endothelial cells. Haemostasis. 18: 307-27.

72   Weisel JW, Litvinov RI. (2008) The biochemical and physical process of fibrinolysis and effects of clot structure and stability on the lysis rate. Cardiovasc Hematol Agents Med Chem. 6: 161-80.

73   Tachias K, Madison EL. (1997) Converting tissue type plasminogen activator into a zymogen. Important role of Lys156. J Biol Chem. 272: 28-31.

74   Thelwell C, Longstaff C. (2007) The regulation by fibrinogen and fibrin of tissue plasminogen activator kinetics and inhibition by plasminogen activator inhibitor 1. J Thromb Haemost. 5: 804-11.

75   Horrevoets AJ, Smilde A, de Vries C, Pannekoek H. (1994) The specific roles of finger and kringle 2 domains of tissue-type plasminogen activator during in vitro fibrinolysis. J Biol Chem. 269: 12639-44.

76   Bakker AH, Weening-Verhoeff EJ, Verheijen JH. (1995) The role of the lysyl binding site of tissue-type plasminogen activator in the interaction with a forming fibrin clot. J Biol Chem. 270: 12355-60.

77   Medved L, Nieuwenhuizen W. (2003) Molecular mechanisms of initiation of fibrinolysis by fibrin. Thromb Haemost. 89: 409-19.

78   Kasai S, Arimura H, Nishida M, Suyama T. (1985) Primary structure of single-chain pro-urokinase. J Biol Chem. 260: 12382-9.

79   Vassalli JD, Dayer JM, Wohlwend A, Belin D. (1984) Concomitant secretion of prourokinase and of a plasminogen activator-specific inhibitor by cultured human monocytes-macrophages. J Exp Med. 159: 1653-68.

80   Clowes AW, Clowes MM, Au YP, Reidy MA, Belin D. (1990) Smooth muscle cells express urokinase during mitogenesis and tissue-type plasminogen activator during migration in injured rat carotid artery. Circ Res. 67: 61-7.

81   Sappino AP, Huarte J, Vassalli JD, Belin D. (1991) Sites of synthesis of urokinase and tissue-type plasminogen activators in the murine kidney. J Clin Invest. 87: 962-70.

82   Pepper MS, Sappino AP, Stocklin R, Montesano R, Orci L, Vassalli JD. (1993) Upregulation of urokinase receptor expression on migrating endothelial cells. J Cell Biol. 122: 673-84.

83   Lijnen HR, Collen D. (1986) Stimulation by heparin of the plasmin-mediated conversion of single-chain to two-chain urokinase-type plasminogen activator. Thromb Res. 43: 687-90.

84   Gunzler WA, Steffens GJ, Otting F, Buse G, Flohe L. (1982) Structural relationship between human high and low molecular mass urokinase. Hoppe Seylers Z Physiol Chem. 363: 133-41.

85   Appella E, Robinson EA, Ullrich SJ, Stoppelli MP, Corti A, Cassani G, Blasi F. (1987) The receptor-binding sequence of urokinase. A biological function for the growth-factor module of proteases. J Biol Chem. 262: 4437-40.

86   Irigoyen JP, Munoz-Canoves P, Montero L, Koziczak M, Nagamine Y. (1999) The plasminogen activator system: biology and regulation. Cell Mol Life Sci. 56: 104-32.

87   Alfano D, Franco P, Vocca I, Gambi N, Pisa V, Mancini A, Caputi M, Carriero MV, Iaccarino I, Stoppelli MP. (2005) The urokinase plasminogen activator and its receptor: role in cell growth and apoptosis. Thromb Haemost. 93: 205-11.

88   McClintock DK, Bell PH. (1971) The mechanism of activation of human plasminogen by streptokinase. Biochem Biophys Res Commun. 43: 694-702.

89   Reddy KN, Markus G. (1972) Mechanism of activation of human plasminogen by streptokinase. Presence of active center in streptokinase-plasminogen complex. J Biol Chem. 247: 1683-91.

90   Schick LA, Castellino FJ. (1974) Direct evidence for the generation of an active site in the plasminogen moiety of the streptokinase-human plasminogen activator complex. Biochem Biophys Res Commun. 57: 47-54.

91   Boxrud PD, Bock PE. (2004) Coupling of conformational and proteolytic activation in the kinetic mechanism of plasminogen activation by streptokinase. J Biol Chem. 279: 36642-9.

92   Boxrud PD, Verhamme IM, Bock PE. (2004) Resolution of conformational activation in the kinetic mechanism of plasminogen activation by streptokinase. J Biol Chem. 279: 36633-41.

93   Ohlenschlager O, Ramachandran R, Guhrs KH, Schlott B, Brown LR. (1998) Nuclear magnetic resonance solution structure of the plasminogen-activator protein staphylokinase. Biochemistry. 37: 10635-42.

94   Lijnen HR, Van Hoef B, De Cock F, Okada K, Ueshima S, Matsuo O, Collen D. (1991) On the mechanism of fibrin-specific plasminogen activation by staphylokinase. J Biol Chem. 266: 11826-32.

95   Sakai M, Watanuki M, Matsuo O. (1989) Mechanism of fibrin-specific fibrinolysis by staphylokinase: participation of alpha 2-plasmin inhibitor. Biochem Biophys Res Commun. 162: 830-7.

96   Okada K, Ueshima S, Takaishi T, Yuasa H, Fukao H, Matsuo O. (1996) Effects of fibrin and alpha2-antiplasmin on plasminogen activation by staphylokinase. Am J Hematol. 53: 151-7.

97   Sakharov DV, Lijnen HR, Rijken DC. (1996) Interactions between staphylokinase, plasmin(ogen), and fibrin. Staphylokinase discriminates between free plasminogen and plasminogen bound to partially degraded fibrin. J Biol Chem. 271: 27912-8.

98   Wiman B, Wallen P. (1975) On the primary structure of human plasminogen and plasmin. Purification and characterization of cyanogen-bromide fragments. Eur J Biochem. 57: 387-94.

99   Raum D, Marcus D, Alper CA, Levey R, Taylor PD, Starzl TE. (1980) Synthesis of human plasminogen by the liver. Science. 208: 1036-7.

100   Castellino FJ, McCance SG. (1997) The kringle domains of human plasminogen. Ciba Found Symp. 212: 46-60; discussion -5.

101   Fredenburgh JC, Nesheim ME. (1992) Lys-plasminogen is a significant intermediate in the activation of Glu-plasminogen during fibrinolysis in vitro. J Biol Chem. 267: 26150-6.

102   Ellis V, Behrendt N, Dano K. (1991) Plasminogen activation by receptor-bound urokinase. A kinetic study with both cell-associated and isolated receptor. J Biol Chem. 266: 12752-8.

103   Higgins DL, Bennett WF. (1990) Tissue plasminogen activator: the biochemistry and pharmacology of variants produced by mutagenesis. Annu Rev Pharmacol Toxicol. 30: 91-121.

104   Fleury V, Loyau S, Lijnen HR, Nieuwenhuizen W, Angles-Cano E. (1993) Molecular assembly of plasminogen and tissue-type plasminogen activator on an evolving fibrin surface. Eur J Biochem. 216: 549-56.

105   Thorsen S. (1975) Differences in the binding to fibrin of native plasminogen and plasminogen modified by proteolytic degradation. Influence of omega-aminocarboxylic acids. Biochim Biophys Acta. 393: 55-65.

106   Lucas MA, Fretto LJ, McKee PA. (1983) The binding of human plasminogen to fibrin and fibrinogen. J Biol Chem. 258: 4249-56.

107   Robbins KC, Summaria L, Hsieh B, Shah RJ. (1967) The peptide chains of human plasmin. Mechanism of activation of human plasminogen to plasmin. J Biol Chem. 242: 2333-42.

108   Takada A, Ohashi H, Matsuda H, Takada Y. (1979) Effects of tranexamic acid, cis-AMCHA, and 6-aminohexanoic acid on the activation rate of plasminogen by urokinase in the presence of clot. Thromb Res. 14: 915-23.

109   Valnickova Z, Thogersen IB, Christensen S, Chu CT, Pizzo SV, Enghild JJ. (1996) Activated human plasma carboxypeptidase B is retained in the blood by binding to alpha2-macroglobulin and pregnancy zone protein. J Biol Chem. 271: 12937-43.

110   Sakharov DV, Nagelkerke JF, Rijken DC. (1996) Rearrangements of the fibrin network and spatial distribution of fibrinolytic components during plasma clot lysis. Study with confocal microscopy. J Biol Chem. 271: 2133-8.

111   Sakharov DV, Rijken DC. (1995) Superficial accumulation of plasminogen during plasma clot lysis. Circulation. 92: 1883-90.

112   Veklich Y, Francis CW, White J, Weisel JW. (1998) Structural studies of fibrinolysis by electron microscopy. Blood. 92: 4721-9.

113   Collet JP, Montalescot G, Lesty C, Weisel JW. (2002) A structural and dynamic investigation of the facilitating effect of glycoprotein IIb/IIIa inhibitors in dissolving platelet-rich clots. Circ Res. 90: 428-34.

114   Weisel JW, Veklich Y, Collet JP, Francis CW. (1999) Structural studies of fibrinolysis by electron and light microscopy. Thromb Haemost. 82: 277-82.

115   Weisel JW, Nagaswami C, Korsholm B, Petersen LC, Suenson E. (1994) Interactions of plasminogen with polymerizing fibrin and its derivatives, monitored with a photoaffinity cross-linker and electron microscopy. J Mol Biol. 235: 1117-35.

116   Meh DA, Mosesson MW, DiOrio JP, Siebenlist KR, Hernandez I, Amrani DL, Stojanovich L. (2001) Disintegration and reorganization of fibrin networks during tissue-type plasminogen activator-induced clot lysis. Blood Coagul Fibrinolysis. 12: 627-37.

117   Ferguson EW, Fretto LJ, McKee PA. (1975) A re-examination of the cleavage of fibrinogen and fibrin by plasmin. J Biol Chem. 250: 7210-8.

118   Walker JB, Nesheim ME. (1999) The molecular weights, mass distribution, chain composition, and structure of soluble fibrin degradation products released from a fibrin clot perfused with plasmin. J Biol Chem. 274: 5201-12.

119   Collet JP, Park D, Lesty C, Soria J, Soria C, Montalescot G, Weisel JW. (2000) Influence of fibrin network conformation and fibrin fiber diameter on fibrinolysis speed: dynamic and structural approaches by confocal microscopy. Arterioscler Thromb Vasc Biol. 20: 1354-61.

120   Collet JP, Soria J, Mirshahi M, Hirsch M, Dagonnet FB, Caen J, Soria C. (1993) Dusart syndrome: a new concept of the relationship between fibrin clot architecture and fibrin clot degradability: hypofibrinolysis related to an abnormal clot structure. Blood. 82: 2462-9.

121   van Mourik JA, Lawrence DA, Loskutoff DJ. (1984) Purification of an inhibitor of plasminogen activator (antiactivator) synthesized by endothelial cells. J Biol Chem. 259: 14914-21.

122   Sprengers ED, Kluft C. (1987) Plasminogen activator inhibitors. Blood. 69: 381-7.

123   Fay WP. (2004) Plasminogen activator inhibitor 1, fibrin, and the vascular response to injury. Trends Cardiovasc Med. 14: 196-202.

124   Brogren H, Karlsson L, Andersson M, Wang L, Erlinge D, Jern S. (2004) Platelets synthesize large amounts of active plasminogen activator inhibitor 1. Blood. 104: 3943-8.

125   Hekman CM, Loskutoff DJ. (1988) Bovine plasminogen activator inhibitor 1: specificity determinations and comparison of the active, latent, and guanidine-activated forms. Biochemistry. 27: 2911-8.

126   Declerck PJ, De Mol M, Alessi MC, Baudner S, Paques EP, Preissner KT, Muller-Berghaus G, Collen D. (1988) Purification and characterization of a plasminogen activator inhibitor 1 binding protein from human plasma. Identification as a multimeric form of S protein (vitronectin). J Biol Chem. 263: 15454-61.

127   Schar CR, Jensen JK, Christensen A, Blouse GE, Andreasen PA, Peterson CB. (2008) Characterization of a site on PAI-1 that binds to vitronectin outside of the somatomedin B domain. J Biol Chem. 283: 28487-96.

128   Podor TJ, Campbell S, Chindemi P, Foulon DM, Farrell DH, Walton PD, Weitz JI, Peterson CB. (2002) Incorporation of vitronectin into fibrin clots. Evidence for a binding interaction between vitronectin and gamma A/gamma' fibrinogen. J Biol Chem. 277: 7520-8.

129   Keijer J, Ehrlich HJ, Linders M, Preissner KT, Pannekoek H. (1991) Vitronectin governs the interaction between plasminogen activator inhibitor 1 and tissue-type plasminogen activator. J Biol Chem. 266: 10700-7.

130   Zhou A, Huntington JA, Pannu NS, Carrell RW, Read RJ. (2003) How vitronectin binds PAI-1 to modulate fibrinolysis and cell migration. Nat Struct Biol. 10: 541-4.

131   Herz J, Clouthier DE, Hammer RE. (1992) LDL receptor-related protein internalizes and degrades uPA-PAI-1 complexes and is essential for embryo implantation. Cell. 71: 411-21.

132   Wohlwend A, Belin D, Vassalli JD. (1987) Plasminogen activator-specific inhibitors produced by human monocytes/macrophages. J Exp Med. 165: 320-39.

133   Astedt B, Hagerstrand I, Lecander I. (1986) Cellular localisation in placenta of placental type plasminogen activator inhibitor. Thromb Haemost. 56: 63-5.

134   Feinberg RF, Kao LC, Haimowitz JE, Queenan JT, Jr., Wun TC, Strauss JF, 3rd, Kliman HJ. (1989) Plasminogen activator inhibitor types 1 and 2 in human trophoblasts. PAI-1 is an immunocytochemical marker of invading trophoblasts. Lab Invest. 61: 20-6.

135   Kruithof EK, Baker MS, Bunn CL. (1995) Biological and clinical aspects of plasminogen activator inhibitor type 2. Blood. 86: 4007-24.

136   Jensen PH, Lorand L, Ebbesen P, Gliemann J. (1993) Type-2 plasminogen-activator inhibitor is a substrate for trophoblast transglutaminase and factor XIIIa. Transglutaminase-catalyzed cross-linking to cellular and extracellular structures. Eur J Biochem. 214: 141-6.

137   Ritchie H, Lawrie LC, Mosesson MW, Booth NA. (2001) Characterization of crosslinking sites in fibrinogen for plasminogen activator inhibitor 2 (PAI-2). Ann N Y Acad Sci. 936: 215-8.

138   Collen D, Wiman B. (1979) Turnover of antiplasmin, the fast-acting plasmin inhibitor of plasma. Blood. 53: 313-24.

139   Mast AE, Enghild JJ, Pizzo SV, Salvesen G. (1991) Analysis of the plasma elimination kinetics and conformational stabilities of native, proteinase-complexed, and reactive site cleaved serpins: comparison of alpha 1-proteinase inhibitor, alpha 1-antichymotrypsin, antithrombin III, alpha 2-antiplasmin, angiotensinogen, and ovalbumin. Biochemistry. 30: 1723-30.

140   Sakata Y, Aoki N. (1982) Significance of cross-linking of alpha 2-plasmin inhibitor to fibrin in inhibition of fibrinolysis and in hemostasis. J Clin Invest. 69: 536-42.

141   Reed GL, 3rd, Matsueda GR, Haber E. (1990) Inhibition of clot-bound alpha 2-antiplasmin enhances in vivo thrombolysis. Circulation. 82: 164-8.

142   Reed GL, Matsueda GR, Haber E. (1992) Platelet factor XIII increases the fibrinolytic resistance of platelet-rich clots by accelerating the crosslinking of alpha 2-antiplasmin to fibrin. Thromb Haemost. 68: 315-20.

143   Kimura S, Aoki N. (1986) Cross-linking site in fibrinogen for alpha 2-plasmin inhibitor. J Biol Chem. 261: 15591-5.

144   Wiman B, Collen D. (1979) On the mechanism of the reaction between human alpha 2-antiplasmin and plasmin. J Biol Chem. 254: 9291-7.

145   Lin Z, Lo A, Simeone DM, Ruffin MT, Lubman DM. (2012) An N-glycosylation Analysis of Human Alpha-2-Macroglobulin Using an Integrated Approach. J Proteomics Bioinform. 5: 127-34.

146   Meyer C, Hinrichs W, Hahn U. (2012) Human alpha2-macroglobulin--another variation on the venus flytrap. Angew Chem Int Ed Engl. 51: 5045-7.

147   Barrera DI, Matheus LM, Stigbrand T, Arbelaez LF. (2007) Proteolytic hydrolysis and purification of the LRP/alfa-2-macroglobulin receptor domain from alpha-macroglobulins. Protein Expr Purif. 53: 112-8.

148   Lin YC, Vaseeharan B, Chen JC. (2008) Molecular cloning and phylogenetic analysis on alpha2-macroglobulin (alpha2-M) of white shrimp Litopenaeus vannamei. Dev Comp Immunol. 32: 317-29.

149   Borth W. (1992) Alpha 2-macroglobulin, a multifunctional binding protein with targeting characteristics. FASEB J. 6: 3345-53.

150   Eaton DL, Malloy BE, Tsai SP, Henzel W, Drayna D. (1991) Isolation, molecular cloning, and partial characterization of a novel carboxypeptidase B from human plasma. J Biol Chem. 266: 21833-8.

151   Buelens K, Hillmayer K, Compernolle G, Declerck PJ, Gils A. (2008) Biochemical importance of glycosylation in thrombin activatable fibrinolysis inhibitor. Circ Res. 102: 295-301.

152   Willemse JL, Heylen E, Hendriks DF. (2007) The intrinsic enzymatic activity of procarboxypeptidase U (TAFI) does not significantly influence the fibrinolysis rate: a rebuttal. J Thromb Haemost. 5: 1334-6.

153   Valnickova Z, Thogersen IB, Potempa J, Enghild JJ. (2007) The intrinsic enzymatic activity of procarboxypeptidase U (TAFI) does not significantly influence the fibrinolytic rate: reply to a rebuttal. J Thromb Haemost. 5: 1336-7.

154   Schatteman KA, Goossens FJ, Scharpe SS, Hendriks DF. (2000) Proteolytic activation of purified human procarboxypeptidase U. Clin Chim Acta. 292: 25-40.

155   Bajzar L, Morser J, Nesheim M. (1996) TAFI, or plasma procarboxypeptidase B, couples the coagulation and fibrinolytic cascades through the thrombin-thrombomodulin complex. J Biol Chem. 271: 16603-8.

156   Nesheim M, Wang W, Boffa M, Nagashima M, Morser J, Bajzar L. (1997) Thrombin, thrombomodulin and TAFI in the molecular link between coagulation and fibrinolysis. Thromb Haemost. 78: 386-91.

157   Sakharov DV, Plow EF, Rijken DC. (1997) On the mechanism of the antifibrinolytic activity of plasma carboxypeptidase B. J Biol Chem. 272: 14477-82.

158   Wang W, Nagashima M, Schneider M, Morser J, Nesheim M. (2000) Elements of the primary structure of thrombomodulin required for efficient thrombin-activable fibrinolysis inhibitor activation. J Biol Chem. 275: 22942-7.

159   Mao SS, Cooper CM, Wood T, Shafer JA, Gardell SJ. (1999) Characterization of plasmin-mediated activation of plasma procarboxypeptidase B. Modulation by glycosaminoglycans. J Biol Chem. 274: 35046-52.

160   Marx PF. (2004) Thrombin-activatable fibrinolysis inhibitor. Curr Med Chem. 11: 2335-48.

161   Hoylaerts M, Rijken DC, Lijnen HR, Collen D. (1982) Kinetics of the activation of plasminogen by human tissue plasminogen activator. Role of fibrin. J Biol Chem. 257: 2912-9.

162   Wang W, Boffa MB, Bajzar L, Walker JB, Nesheim ME. (1998) A study of the mechanism of inhibition of fibrinolysis by activated thrombin-activable fibrinolysis inhibitor. J Biol Chem. 273: 27176-81.

163   Schneider M, Nesheim M. (2004) A study of the protection of plasmin from antiplasmin inhibition within an intact fibrin clot during the course of clot lysis. J Biol Chem. 279: 13333-9.

164   Valnickova Z, Enghild JJ. (1998) Human procarboxypeptidase U, or thrombin-activable fibrinolysis inhibitor, is a substrate for transglutaminases. Evidence for transglutaminase-catalyzed cross-linking to fibrin. J Biol Chem. 273: 27220-4.

165   Boffa MB, Bell R, Stevens WK, Nesheim ME. (2000) Roles of thermal instability and proteolytic cleavage in regulation of activated thrombin-activable fibrinolysis inhibitor. J Biol Chem. 275: 12868-78.

166   Marx PF, Hackeng TM, Dawson PE, Griffin JH, Meijers JC, Bouma BN. (2000) Inactivation of active thrombin-activable fibrinolysis inhibitor takes place by a process that involves conformational instability rather than proteolytic cleavage. J Biol Chem. 275: 12410-5.

167   Grundmann H, Aires-de-Sousa M, Boyce J, Tiemersma E. (2006) Emergence and resurgence of meticillin-resistant Staphylococcus aureus as a public-health threat. Lancet. 368: 874-85.

168   Lowy FD. (1998) Staphylococcus aureus infections. N Engl J Med. 339: 520-32.

169   Tong SY, Davis JS, Eichenberger E, Holland TL, Fowler VG, Jr. (2015) Staphylococcus aureus infections: epidemiology, pathophysiology, clinical manifestations, and management. Clin Microbiol Rev. 28: 603-61.

170   Hoerr V, Franz M, Pletz MW, Diab M, Niemann S, Faber C, Doenst T, Schulze PC, Deinhardt-Emmer S, Loffler B. (2018) S. aureus endocarditis: Clinical aspects and experimental approaches. Int J Med Microbiol. 308: 640-52.

171   Friedrich R, Panizzi P, Fuentes-Prior P, Richter K, Verhamme I, Anderson PJ, Kawabata S, Huber R, Bode W, Bock PE. (2003) Staphylocoagulase is a prototype for the mechanism of cofactor-induced zymogen activation. Nature. 425: 535-9.

172   Bode W, Huber R. (1976) Induction of the bovine trypsinogen-trypsin transition by peptides sequentially similar to the N-terminus of trypsin. FEBS Lett. 68: 231-6.

173   Bas BM, Muller AD, Hemker HC. (1975) Purification and properties of staphylocoagulase. Biochim Biophys Acta. 379: 164-71.

174   Panizzi P, Friedrich R, Fuentes-Prior P, Bode W, Bock PE. (2004) The staphylocoagulase family of zymogen activator and adhesion proteins. Cell Mol Life Sci. 61: 2793-8.

175   Thomer L, Emolo C, Thammavongsa V, Kim HK, McAdow ME, Yu W, Kieffer M, Schneewind O, Missiakas D. (2016) Antibodies against a secreted product of Staphylococcus aureus trigger phagocytic killing. J Exp Med. 213: 293-301.

176   Ko YP, Kang M, Ganesh VK, Ravirajan D, Li B, Hook M. (2016) Coagulase and Efb of Staphylococcus aureus Have a Common Fibrinogen Binding Motif. mBio. 7: e01885-15.

177   Panizzi P, Nahrendorf M, Figueiredo JL, Panizzi J, Marinelli B, Iwamoto Y, Keliher E, Maddur AA, Waterman P, Kroh HK, Leuschner F, Aikawa E, Swirski FK, Pittet MJ, Hackeng TM, Fuentes-Prior P, Schneewind O, Bock PE, Weissleder R. (2011) In vivo detection of Staphylococcus aureus endocarditis by targeting pathogen-specific prothrombin activation. Nat Med. 17: 1142-6.

178   Panizzi P, Friedrich R, Fuentes-Prior P, Richter K, Bock PE, Bode W. (2006) Fibrinogen substrate recognition by staphylocoagulase.(pro)thrombin complexes. J Biol Chem. 281: 1179-87.

179   Hijikata-Okunomiya A, Kataoka N. (2003) Argatroban inhibits staphylothrombin. J Thromb Haemost. 1: 2060-1.

180   Cheng AG, McAdow M, Kim HK, Bae T, Missiakas DM, Schneewind O. (2010) Contribution of coagulases towards Staphylococcus aureus disease and protective immunity. PLoS Pathog. 6: e1001036.

181   Klein M, Wang A. (2016) Infective Endocarditis. J Intensive Care Med. 31: 151-63.

182   Claes J, Liesenborghs L, Peetermans M, Veloso TR, Missiakas D, Schneewind O, Mancini S, Entenza JM, Hoylaerts MF, Heying R, Verhamme P, Vanassche T. (2017) Clumping factor A, von Willebrand factor-binding protein and von Willebrand factor anchor Staphylococcus aureus to the vessel wall. J Thromb Haemost. 15: 1009-19.

183   Bjerketorp J, Nilsson M, Ljungh A, Flock JI, Jacobsson K, Frykberg L. (2002) A novel von Willebrand factor binding protein expressed by Staphylococcus aureus. Microbiology (Reading). 148: 2037-44.

184   Herrmann M, Hartleib J, Kehrel B, Montgomery RR, Sixma JJ, Peters G. (1997) Interaction of von Willebrand factor with Staphylococcus aureus. J Infect Dis. 176: 984-91.

185   Pappelbaum KI, Gorzelanny C, Grassle S, Suckau J, Laschke MW, Bischoff M, Bauer C, Schorpp-Kistner M, Weidenmaier C, Schneppenheim R, Obser T, Sinha B, Schneider SW. (2013) Ultralarge von Willebrand factor fibers mediate luminal Staphylococcus aureus adhesion to an intact endothelial cell layer under shear stress. Circulation. 128: 50-9.

186   Claes J, Vanassche T, Peetermans M, Liesenborghs L, Vandenbriele C, Vanhoorelbeke K, Missiakas D, Schneewind O, Hoylaerts MF, Heying R, Verhamme P. (2014) Adhesion of Staphylococcus aureus to the vessel wall under flow is mediated by von Willebrand factor-binding protein. Blood. 124: 1669-76.

187   Vanassche T, Verhaegen J, Peetermans WE, J VANR, Cheng A, Schneewind O, Hoylaerts MF, Verhamme P. (2011) Inhibition of staphylothrombin by dabigatran reduces Staphylococcus aureus virulence. J Thromb Haemost. 9: 2436-46.

188   Vanassche T, Peetermans M, Van Aelst LN, Peetermans WE, Verhaegen J, Missiakas DM, Schneewind O, Hoylaerts MF, Verhamme P. (2013) The role of staphylothrombin-mediated fibrin deposition in catheter-related Staphylococcus aureus infections. J Infect Dis. 208: 92-100.

189   Thiene G, Basso C. (2006) Pathology and pathogenesis of infective endocarditis in native heart valves. Cardiovasc Pathol. 15: 256-63.

190   Veloso TR, Que YA, Chaouch A, Giddey M, Vouillamoz J, Rousson V, Moreillon P, Entenza JM. (2015) Prophylaxis of experimental endocarditis with antiplatelet and antithrombin agents: a role for long-term prevention of infective endocarditis in humans? J Infect Dis. 211: 72-9.

191   Brinkmann V, Reichard U, Goosmann C, Fauler B, Uhlemann Y, Weiss DS, Weinrauch Y, Zychlinsky A. (2004) Neutrophil extracellular traps kill bacteria. Science. 303: 1532-5.

192   Takei H, Araki A, Watanabe H, Ichinose A, Sendo F. (1996) Rapid killing of human neutrophils by the potent activator phorbol 12-myristate 13-acetate (PMA) accompanied by changes different from typical apoptosis or necrosis. J Leukoc Biol. 59: 229-40.

193   Brinkmann V, Zychlinsky A. (2007) Beneficial suicide: why neutrophils die to make NETs. Nat Rev Microbiol. 5: 577-82.

194   Fuchs TA, Abed U, Goosmann C, Hurwitz R, Schulze I, Wahn V, Weinrauch Y, Brinkmann V, Zychlinsky A. (2007) Novel cell death program leads to neutrophil extracellular traps. J Cell Biol. 176: 231-41.

195   Steinberg BE, Grinstein S. (2007) Unconventional roles of the NADPH oxidase: signaling, ion homeostasis, and cell death. Sci STKE. 2007: pe11.

196   Yipp BG, Kubes P. (2013) NETosis: how vital is it? Blood. 122: 2784-94.

197   Fink SL, Cookson BT. (2005) Apoptosis, pyroptosis, and necrosis: mechanistic description of dead and dying eukaryotic cells. Infect Immun. 73: 1907-16.

198   Remijsen Q, Vanden Berghe T, Wirawan E, Asselbergh B, Parthoens E, De Rycke R, Noppen S, Delforge M, Willems J, Vandenabeele P. (2011) Neutrophil extracellular trap cell death requires both autophagy and superoxide generation. Cell Res. 21: 290-304.

199   Pilsczek FH, Salina D, Poon KK, Fahey C, Yipp BG, Sibley CD, Robbins SM, Green FH, Surette MG, Sugai M, Bowden MG, Hussain M, Zhang K, Kubes P. (2010) A novel mechanism of rapid nuclear neutrophil extracellular trap formation in response to Staphylococcus aureus. J Immunol. 185: 7413-25.

200   Yousefi S, Mihalache C, Kozlowski E, Schmid I, Simon HU. (2009) Viable neutrophils release mitochondrial DNA to form neutrophil extracellular traps. Cell Death Differ. 16: 1438-44.

201   Branzk N, Papayannopoulos V. (2013) Molecular mechanisms regulating NETosis in infection and disease. Semin Immunopathol. 35: 513-30.

202   Dabrowska D, Jablonska E, Garley M, Ratajczak-Wrona W, Iwaniuk A. (2016) New Aspects of the Biology of Neutrophil Extracellular Traps. Scand J Immunol. 84: 317-22.

203   Krautgartner WD, Klappacher M, Hannig M, Obermayer A, Hartl D, Marcos V, Vitkov L. (2010) Fibrin mimics neutrophil extracellular traps in SEM. Ultrastruct Pathol. 34: 226-31.

204   Brinkmann V, Zychlinsky A. (2012) Neutrophil extracellular traps: is immunity the second function of chromatin? J Cell Biol. 198: 773-83.

205   Urban CF, Ermert D, Schmid M, Abu-Abed U, Goosmann C, Nacken W, Brinkmann V, Jungblut PR, Zychlinsky A. (2009) Neutrophil extracellular traps contain

calprotectin, a cytosolic protein complex involved in host defense against Candida albicans. PLoS Pathog. 5: e1000639.

206 Varju I, Kolev K. (2019) Networks that stop the flow: A fresh look at fibrin and neutrophil extracellular traps. Thromb Res. 182: 1-11.

207 Parseghian MH, Luhrs KA. (2006) Beyond the walls of the nucleus: the role of histones in cellular signaling and innate immunity. Biochem Cell Biol. 84: 589-604.

208 Christophorou MA, Castelo-Branco G, Halley-Stott RP, Oliveira CS, Loos R, Radzisheuskaya A, Mowen KA, Bertone P, Silva JC, Zernicka-Goetz M, Nielsen ML, Gurdon JB, Kouzarides T. (2014) Citrullination regulates pluripotency and histone H1 binding to chromatin. Nature. 507: 104-8.

209 Yousefi S, Gold JA, Andina N, Lee JJ, Kelly AM, Kozlowski E, Schmid I, Straumann A, Reichenbach J, Gleich GJ, Simon HU. (2008) Catapult-like release of mitochondrial DNA by eosinophils contributes to antibacterial defense. Nat Med. 14: 949-53.

210 Cho JH, Fraser IP, Fukase K, Kusumoto S, Fujimoto Y, Stahl GL, Ezekowitz RA. (2005) Human peptidoglycan recognition protein S is an effector of neutrophil-mediated innate immunity. Blood. 106: 2551-8.

211 Wartha F, Beiter K, Normark S, Henriques-Normark B. (2007) Neutrophil extracellular traps: casting the NET over pathogenesis. Curr Opin Microbiol. 10: 52-6.

212 O'Donoghue AJ, Jin Y, Knudsen GM, Perera NC, Jenne DE, Murphy JE, Craik CS, Hermiston TW. (2013) Global substrate profiling of proteases in human neutrophil extracellular traps reveals consensus motif predominantly contributed by elastase. PLoS One. 8: e75141.

213 Nathan C. (2006) Neutrophils and immunity: challenges and opportunities. Nat Rev Immunol. 6: 173-82.

214 Zasloff M. (2002) Antimicrobial peptides of multicellular organisms. Nature. 415: 389-95.

215 Nauseef WM. (2007) How human neutrophils kill and degrade microbes: an integrated view. Immunol Rev. 219: 88-102.

216 Selsted ME, Ouellette AJ. (2005) Mammalian defensins in the antimicrobial immune response. Nat Immunol. 6: 551-7.

217   von Kockritz-Blickwede M, Goldmann O, Thulin P, Heinemann K, Norrby-Teglund A, Rohde M, Medina E. (2008) Phagocytosis-independent antimicrobial activity of mast cells by means of extracellular trap formation. Blood. 111: 3070-80.

218   Garcia-Romo GS, Caielli S, Vega B, Connolly J, Allantaz F, Xu Z, Punaro M, Baisch J, Guiducci C, Coffman RL, Barrat FJ, Banchereau J, Pascual V. (2011) Netting neutrophils are major inducers of type I IFN production in pediatric systemic lupus erythematosus. Sci Transl Med. 3: 73ra20.

219   Lande R, Ganguly D, Facchinetti V, Frasca L, Conrad C, Gregorio J, Meller S, Chamilos G, Sebasigari R, Riccieri V, Bassett R, Amuro H, Fukuhara S, Ito T, Liu YJ, Gilliet M. (2011) Neutrophils activate plasmacytoid dendritic cells by releasing self-DNA-peptide complexes in systemic lupus erythematosus. Sci Transl Med. 3: 73ra19.

220   Zawrotniak M, Rapala-Kozik M. (2013) Neutrophil extracellular traps (NETs) - formation and implications. Acta Biochim Pol. 60: 277-84.

221   Goldmann O, Medina E. (2012) The expanding world of extracellular traps: not only neutrophils but much more. Front Immunol. 3: 420.

222   Drescher B, Bai F. (2013) Neutrophil in viral infections, friend or foe? Virus Res. 171: 1-7.

223   Itakura A, McCarty OJ. (2013) Pivotal role for the mTOR pathway in the formation of neutrophil extracellular traps via regulation of autophagy. Am J Physiol Cell Physiol. 305: C348-54.

224   Gupta AK, Joshi MB, Philippova M, Erne P, Hasler P, Hahn S, Resink TJ. (2010) Activated endothelial cells induce neutrophil extracellular traps and are susceptible to NETosis-mediated cell death. FEBS Lett. 584: 3193-7.

225   Kessenbrock K, Krumbholz M, Schonermarck U, Back W, Gross WL, Werb Z, Grone HJ, Brinkmann V, Jenne DE. (2009) Netting neutrophils in autoimmune small-vessel vasculitis. Nat Med. 15: 623-5.

226   Delbosc S, Alsac JM, Journe C, Louedec L, Castier Y, Bonnaure-Mallet M, Ruimy R, Rossignol P, Bouchard P, Michel JB, Meilhac O. (2011) Porphyromonas gingivalis participates in pathogenesis of human abdominal aortic aneurysm by neutrophil activation. Proof of concept in rats. PLoS One. 6: e18679.

227   Parker H, Dragunow M, Hampton MB, Kettle AJ, Winterbourn CC. (2012) Requirements for NADPH oxidase and myeloperoxidase in neutrophil extracellular trap formation differ depending on the stimulus. J Leukoc Biol. 92: 841-9.

228   Veras FP, Pontelli MC, Silva CM, Toller-Kawahisa JE, de Lima M, Nascimento DC, Schneider AH, Caetite D, Tavares LA, Paiva IM, Rosales R, Colon D, Martins R, Castro IA, Almeida GM, Lopes MIF, Benatti MN, Bonjorno LP, Giannini MC, Luppino-Assad R, Almeida SL, Vilar F, Santana R, Bollela VR, Auxiliadora-Martins M, Borges M, Miranda CH, Pazin-Filho A, da Silva LLP, Cunha LD, Zamboni DS, Dal-Pizzol F, Leiria LO, Siyuan L, Batah S, Fabro A, Mauad T, Dolhnikoff M, Duarte-Neto A, Saldiva P, Cunha TM, Alves-Filho JC, Arruda E, Louzada-Junior P, Oliveira RD, Cunha FQ. (2020) SARS-CoV-2-triggered neutrophil extracellular traps mediate COVID-19 pathology. J Exp Med. 217.

229   Neeli I, Khan SN, Radic M. (2008) Histone deimination as a response to inflammatory stimuli in neutrophils. J Immunol. 180: 1895-902.

230   Martinelli S, Urosevic M, Daryadel A, Oberholzer PA, Baumann C, Fey MF, Dummer R, Simon HU, Yousefi S. (2004) Induction of genes mediating interferon-dependent extracellular trap formation during neutrophil differentiation. J Biol Chem. 279: 44123-32.

231   Munks MW, McKee AS, Macleod MK, Powell RL, Degen JL, Reisdorph NA, Kappler JW, Marrack P. (2010) Aluminum adjuvants elicit fibrin-dependent extracellular traps in vivo. Blood. 116: 5191-9.

232   Saitoh T, Komano J, Saitoh Y, Misawa T, Takahama M, Kozaki T, Uehata T, Iwasaki H, Omori H, Yamaoka S, Yamamoto N, Akira S. (2012) Neutrophil extracellular traps mediate a host defense response to human immunodeficiency virus-1. Cell Host Microbe. 12: 109-16.

233   Clark SR, Ma AC, Tavener SA, McDonald B, Goodarzi Z, Kelly MM, Patel KD, Chakrabarti S, McAvoy E, Sinclair GD, Keys EM, Allen-Vercoe E, Devinney R, Doig CJ, Green FH, Kubes P. (2007) Platelet TLR4 activates neutrophil extracellular traps to ensnare bacteria in septic blood. Nat Med. 13: 463-9.

234   Kaplan MJ, Radic M. (2012) Neutrophil extracellular traps: double-edged swords of innate immunity. J Immunol. 189: 2689-95.

235   Papayannopoulos V, Metzler KD, Hakkim A, Zychlinsky A. (2010) Neutrophil elastase and myeloperoxidase regulate the formation of neutrophil extracellular traps. J Cell Biol. 191: 677-91.

236   Akong-Moore K, Chow OA, von Kockritz-Blickwede M, Nizet V. (2012) Influences of chloride and hypochlorite on neutrophil extracellular trap formation. PLoS One. 7: e42984.

237   Wang Y, Li M, Stadler S, Correll S, Li P, Wang D, Hayama R, Leonelli L, Han H, Grigoryev SA, Allis CD, Coonrod SA. (2009) Histone hypercitrullination mediates chromatin decondensation and neutrophil extracellular trap formation. J Cell Biol. 184: 205-13.

238   Wang Y, Wysocka J, Sayegh J, Lee YH, Perlin JR, Leonelli L, Sonbuchner LS, McDonald CH, Cook RG, Dou Y, Roeder RG, Clarke S, Stallcup MR, Allis CD, Coonrod SA. (2004) Human PAD4 regulates histone arginine methylation levels via demethylimination. Science. 306: 279-83.

239   Hakkim A, Fuchs TA, Martinez NE, Hess S, Prinz H, Zychlinsky A, Waldmann H. (2011) Activation of the Raf-MEK-ERK pathway is required for neutrophil extracellular trap formation. Nat Chem Biol. 7: 75-7.

240   Lim MB, Kuiper JW, Katchky A, Goldberg H, Glogauer M. (2011) Rac2 is required for the formation of neutrophil extracellular traps. J Leukoc Biol. 90: 771-6.

241   Khan MA, Farahvash A, Douda DN, Licht JC, Grasemann H, Sweezey N, Palaniyar N. (2017) JNK Activation Turns on LPS- and Gram-Negative Bacteria-Induced NADPH Oxidase-Dependent Suicidal NETosis. Sci Rep. 7: 3409.

242   Mastronardi FG, Wood DD, Mei J, Raijmakers R, Tseveleki V, Dosch HM, Probert L, Casaccia-Bonnefil P, Moscarello MA. (2006) Increased citrullination of histone H3 in multiple sclerosis brain and animal models of demyelination: a role for tumor necrosis factor-induced peptidylarginine deiminase 4 translocation. J Neurosci. 26: 11387-96.

243   Tanikawa C, Espinosa M, Suzuki A, Masuda K, Yamamoto K, Tsuchiya E, Ueda K, Daigo Y, Nakamura Y, Matsuda K. (2012) Regulation of histone modification and chromatin structure by the p53-PADI4 pathway. Nat Commun. 3: 676.

244   Andrade F, Darrah E, Gucek M, Cole RN, Rosen A, Zhu X. (2010) Autocitrullination of human peptidyl arginine deiminase type 4 regulates protein citrullination during cell activation. Arthritis Rheum. 62: 1630-40.

245   Slack JL, Jones LE, Jr., Bhatia MM, Thompson PR. (2011) Autodeimination of protein arginine deiminase 4 alters protein-protein interactions but not activity. Biochemistry. 50: 3997-4010.

246   Leshner M, Wang S, Lewis C, Zheng H, Chen X, Santy L, Wang Y. (2012) PAD4 mediated histone hypercitrullination induces heterochromatin decondensation and chromatin unfolding to form neutrophil extracellular trap-like structures. Front Immunol. 3.

247   Douda DN, Khan MA, Grasemann H, Palaniyar N. (2015) SK3 channel and mitochondrial ROS mediate NADPH oxidase-independent NETosis induced by calcium influx. Proc Natl Acad Sci U S A. 112: 2817-22.

248   Neeli I, Radic M. (2013) Opposition between PKC isoforms regulates histone deimination and neutrophil extracellular chromatin release. Front Immunol. 4: 38.

249   Ravindran M, Khan MA, Palaniyar N. (2019) Neutrophil Extracellular Trap Formation: Physiology, Pathology, and Pharmacology. Biomolecules. 9.

250   Bratton DL, Henson PM. (2011) Neutrophil clearance: when the party is over, clean-up begins. Trends Immunol. 32: 350-7.

251   Lacks SA. (1981) Deoxyribonuclease I in mammalian tissues. Specificity of inhibition by actin. J Biol Chem. 256: 2644-8.

252   Napirei M, Ricken A, Eulitz D, Knoop H, Mannherz HG. (2004) Expression pattern of the deoxyribonuclease 1 gene: lessons from the Dnase1 knockout mouse. Biochem J. 380: 929-37.

253   Takeshita H, Yasuda T, Nakajima T, Hosomi O, Nakashima Y, Kishi K. (1997) Mouse deoxyribonuclease I (DNase I): biochemical and immunological characterization, cDNA structure and tissue distribution. Biochem Mol Biol Int. 42: 65-75.

254   Shiokawa D, Tanuma S. (2001) Characterization of human DNase I family endonucleases and activation of DNase gamma during apoptosis. Biochemistry. 40: 143-52.

255   Napirei M, Wulf S, Mannherz HG. (2004) Chromatin breakdown during necrosis by serum Dnase1 and the plasminogen system. Arthritis Rheum. 50: 1873-83.

256   Napirei M, Ludwig S, Mezrhab J, Klockl T, Mannherz HG. (2009) Murine serum nucleases--contrasting effects of plasmin and heparin on the activities of DNase1 and DNase1-like 3 (DNase1l3). FEBS J. 276: 1059-73.

257   Harvima RJ, Yabe K, Fraki JE, Fukuyama K, Epstein WL. (1988) Hydrolysis of histones by proteinases. Biochem J. 250: 859-64.

258   Varju I, Longstaff C, Szabo L, Farkas AZ, Varga-Szabo VJ, Tanka-Salamon A, Machovich R, Kolev K. (2015) DNA, histones and neutrophil extracellular traps exert anti-fibrinolytic effects in a plasma environment. Thromb Haemost. 113: 1289-98.

259   Xu J, Zhang X, Pelayo R, Monestier M, Ammollo CT, Semeraro F, Taylor FB, Esmon NL, Lupu F, Esmon CT. (2009) Extracellular histones are major mediators of death in sepsis. Nat Med. 15: 1318-21.

260   Serhan CN. (2005) Novel omega -- 3-derived local mediators in anti-inflammation and resolution. Pharmacol Ther. 105: 7-21.

261   Engelmann B, Massberg S. (2013) Thrombosis as an intravascular effector of innate immunity. Nat Rev Immunol. 13: 34-45.

262   Naudin C, Burillo E, Blankenberg S, Butler L, Renne T. (2017) Factor XII Contact Activation. Semin Thromb Hemost. 43: 814-26.

263   Semeraro F, Ammollo CT, Morrissey JH, Dale GL, Friese P, Esmon NL, Esmon CT. (2011) Extracellular histones promote thrombin generation through platelet-dependent mechanisms: involvement of platelet TLR2 and TLR4. Blood. 118: 1952-61.

264   Muller F, Mutch NJ, Schenk WA, Smith SA, Esterl L, Spronk HM, Schmidbauer S, Gahl WA, Morrissey JH, Renne T. (2009) Platelet polyphosphates are proinflammatory and procoagulant mediators in vivo. Cell. 139: 1143-56.

265   Vu TT, Leslie BA, Stafford AR, Zhou J, Fredenburgh JC, Weitz JI. (2016) Histidine-rich glycoprotein binds DNA and RNA and attenuates their capacity to activate the intrinsic coagulation pathway. Thromb Haemost. 115: 89-98.

266   Noubouossie DF, Whelihan MF, Yu YB, Sparkenbaugh E, Pawlinski R, Monroe DM, Key NS. (2017) In vitro activation of coagulation by human neutrophil DNA and histone proteins but not neutrophil extracellular traps. Blood. 129: 1021-9.

267   Komissarov AA, Florova G, Idell S. (2011) Effects of extracellular DNA on plasminogen activation and fibrinolysis. J Biol Chem. 286: 41949-62.

268   Gould TJ, Vu TT, Stafford AR, Dwivedi DJ, Kim PY, Fox-Robichaud AE, Weitz JI, Liaw PC. (2015) Cell-Free DNA Modulates Clot Structure and Impairs Fibrinolysis in Sepsis. Arterioscler Thromb Vasc Biol. 35: 2544-53.

269   Longstaff C, Varju I, Sotonyi P, Szabo L, Krumrey M, Hoell A, Bota A, Varga Z, Komorowicz E, Kolev K. (2013) Mechanical Stability and Fibrinolytic Resistance of Clots Containing Fibrin, DNA, and Histones. J Biol Chem. 288: 6946-56.

270   Mangold A, Alias S, Scherz T, Hofbauer M, Jakowitsch J, Panzenbock A, Simon D, Laimer D, Bangert C, Kammerlander A, Mascherbauer J, Winter MP, Distelmaier K, Adlbrecht C, Preissner KT, Lang IM. (2015) Coronary neutrophil extracellular trap burden and deoxyribonuclease activity in ST-elevation acute coronary syndrome are predictors of ST-segment resolution and infarct size. Circ Res. 116: 1182-92.

271   Ducroux C, Di Meglio L, Loyau S, Delbosc S, Boisseau W, Deschildre C, Ben Maacha M, Blanc R, Redjem H, Ciccio G, Smajda S, Fahed R, Michel JB, Piotin M, Salomon L, Mazighi M, Ho-Tin-Noe B, Desilles JP. (2018) Thrombus Neutrophil Extracellular Traps Content Impair tPA-Induced Thrombolysis in Acute Ischemic Stroke. Stroke. 49: 754-7.

272   Giannitsis DJ, St P. (1974) Role of leukocyte neclei in blood coagulation. Naturwissenschaften. 61: 690.

273   Pereira LF, Marco FM, Boimorto R, Caturla A, Bustos A, De la Concha EG, Subiza JL. (1994) Histones interact with anionic phospholipids with high avidity; its relevance for the binding of histone-antihistone immune complexes. Clin Exp Immunol. 97: 175-80.

274   Kleine TJ, Gladfelter A, Lewis PN, Lewis SA. (1995) Histone-induced damage of a mammalian epithelium: the conductive effect. Am J Physiol. 268: C1114-25.

275   Saffarzadeh M, Juenemann C, Queisser MA, Lochnit G, Barreto G, Galuska SP, Lohmeyer J, Preissner KT. (2012) Neutrophil extracellular traps directly induce epithelial and endothelial cell death: a predominant role of histones. PLoS One. 7: e32366.

276   Michels A, Albanez S, Mewburn J, Nesbitt K, Gould TJ, Liaw PC, James PD, Swystun LL, Lillicrap D. (2016) Histones link inflammation and thrombosis through the induction of Weibel-Palade body exocytosis. J Thromb Haemost. 14: 2274-86.

277   Abrams ST, Zhang N, Manson J, Liu T, Dart C, Baluwa F, Wang SS, Brohi K, Kipar A, Yu W, Wang G, Toh CH. (2013) Circulating histones are mediators of trauma-associated lung injury. Am J Respir Crit Care Med. 187: 160-9.

278   Kleine TJ, Lewis PN, Lewis SA. (1997) Histone-induced damage of a mammalian epithelium: the role of protein and membrane structure. Am J Physiol. 273: C1925-36.

279   Gamberucci A, Fulceri R, Marcolongo P, Pralong WF, Benedetti A. (1998) Histones and basic polypeptides activate Ca2+/cation influx in various cell types. Biochem J. 331 (Pt 2): 623-30.

280   Crittenden JR, Bergmeier W, Zhang Y, Piffath CL, Liang Y, Wagner DD, Housman DE, Graybiel AM. (2004) CalDAG-GEFI integrates signaling for platelet aggregation and thrombus formation. Nat Med. 10: 982-6.

281   Carestia A, Rivadeneyra L, Romaniuk MA, Fondevila C, Negrotto S, Schattner M. (2013) Functional responses and molecular mechanisms involved in histone-mediated platelet activation. Thromb Haemost. 110: 1035-45.

282   Darbousset R, Thomas GM, Mezouar S, Frere C, Bonier R, Mackman N, Renne T, Dignat-George F, Dubois C, Panicot-Dubois L. (2012) Tissue factor-positive neutrophils bind to injured endothelial wall and initiate thrombus formation. Blood. 120: 2133-43.

283   Fuchs TA, Bhandari AA, Wagner DD. (2011) Histones induce rapid and profound thrombocytopenia in mice. Blood. 118: 3708-14.

284   Whelihan MF, Zachary V, Orfeo T, Mann KG. (2012) Prothrombin activation in blood coagulation: the erythrocyte contribution to thrombin generation. Blood. 120: 3837-45.

285   Semeraro F, Ammollo CT, Esmon NL, Esmon CT. (2014) Histones induce phosphatidylserine exposure and a procoagulant phenotype in human red blood cells. J Thromb Haemost. 12: 1697-702.

286   Barranco-Medina S, Pozzi N, Vogt AD, Di Cera E. (2013) Histone H4 promotes prothrombin autoactivation. J Biol Chem. 288: 35749-57.

287   Ammollo CT, Semeraro F, Xu J, Esmon NL, Esmon CT. (2011) Extracellular histones increase plasma thrombin generation by impairing thrombomodulin-dependent protein C activation. J Thromb Haemost. 9: 1795-803.

288   Glaser CB, Morser J, Clarke JH, Blasko E, McLean K, Kuhn I, Chang RJ, Lin JH, Vilander L, Andrews WH, Light DR. (1992) Oxidation of a specific methionine in thrombomodulin by activated neutrophil products blocks cofactor activity. A potential rapid mechanism for modulation of coagulation. J Clin Invest. 90: 2565-73.

289   Abe H, Okajima K, Okabe H, Takatsuki K, Binder BR. (1994) Granulocyte proteases and hydrogen peroxide synergistically inactivate thrombomodulin of endothelial cells in vitro. J Lab Clin Med. 123: 874-81.

290   Biezunski N, Shafrir E, De Vries A, Katchalski E. (1955) The action of poly-lysine on the conversion of fibrinogen into fibrin by coagulase thrombin. Biochem J. 59: 55-8.

291   Machovich R, Owen WG. (1989) An elastase-dependent pathway of plasminogen activation. Biochemistry. 28: 4517-22.

292   Kolev K, Tenekedjiev K, Komorowicz E, Machovich R. (1997) Functional evaluation of the structural features of proteases and their substrate in fibrin surface degradation. J Biol Chem. 272: 13666-75.

293   Plow EF. (1980) The major fibrinolytic proteases of human leukocytes. Biochim Biophys Acta. 630: 47-56.

294   Wohner N, Kovacs A, Machovich R, Kolev K. (2012) Modulation of the von Willebrand factor-dependent platelet adhesion through alternative proteolytic pathways. Thromb Res. 129: e41-6.

295   Papareddy P, Rydengard V, Pasupuleti M, Walse B, Morgelin M, Chalupka A, Malmsten M, Schmidtchen A. (2010) Proteolysis of human thrombin generates novel host defense peptides. PLoS Pathog. 6: e1000857.

296   Massberg S, Grahl L, von Bruehl ML, Manukyan D, Pfeiler S, Goosmann C, Brinkmann V, Lorenz M, Bidzhekov K, Khandagale AB, Konrad I, Kennerknecht E, Reges K, Holdenrieder S, Braun S, Reinhardt C, Spannagl M, Preissner KT, Engelmann B. (2010) Reciprocal coupling of coagulation and innate immunity via neutrophil serine proteases. Nat Med. 16: 887-96.

297   Jochum M, Lander S, Heimburger N, Fritz H. (1981) Effect of human granulocytic elastase on isolated human antithrombin III. Hoppe Seylers Z Physiol Chem. 362: 103-12.

298   Wohner N, Keresztes Z, Sotonyi P, Szabo L, Komorowicz E, Machovich R, Kolev K. (2010) Neutrophil granulocyte-dependent proteolysis enhances platelet adhesion to the arterial wall under high-shear flow. J Thromb Haemost. 8: 1624-31.

299   Moir E, Robbie LA, Bennett B, Booth NA. (2002) Polymorphonuclear leucocytes have two opposing roles in fibrinolysis. Thromb Haemost. 87: 1006-10.

300   Clark RA, Stone PJ, El Hag A, Calore JD, Franzblau C. (1981) Myeloperoxidase-catalyzed inactivation of alpha 1-protease inhibitor by human neutrophils. J Biol Chem. 256: 3348-53.

301   Stavrou EX, Fang C, Bane KL, Long AT, Naudin C, Kucukal E, Gandhi A, Brett-Morris A, Mumaw MM, Izadmehr S, Merkulova A, Reynolds CC, Alhalabi O, Nayak L, Yu WM, Qu CK, Meyerson HJ, Dubyak GR, Gurkan UA, Nieman MT, Sen Gupta A, Renne T, Schmaier AH. (2018) Factor XII and uPAR upregulate neutrophil functions to influence wound healing. J Clin Invest. 128: 944-59.

302   de Bont CM, Boelens WC, Pruijn GJM. (2019) NETosis, complement, and coagulation: a triangular relationship. Cell Mol Immunol. 16: 19-27.

303   Csomos K, Kristof E, Jakob B, Csomos I, Kovacs G, Rotem O, Hodrea J, Bagoly Z, Muszbek L, Balajthy Z, Csosz E, Fesus L. (2016) Protein cross-linking by chlorinated polyamines and transglutamylation stabilizes neutrophil extracellular traps. Cell Death Dis. 7: e2332.

304   Ward CM, Tetaz TJ, Andrews RK, Berndt MC. (1997) Binding of the von Willebrand factor A1 domain to histone. Thromb Res. 86: 469-77.

305   Grassle S, Huck V, Pappelbaum KI, Gorzelanny C, Aponte-Santamaria C, Baldauf C, Grater F, Schneppenheim R, Obser T, Schneider SW. (2014) von Willebrand factor directly interacts with DNA from neutrophil extracellular traps. Arterioscler Thromb Vasc Biol. 34: 1382-9.

306   Martinod K, Wagner DD. (2014) Thrombosis: tangled up in NETs. Blood. 123: 2768-76.

307   Timp JF, Braekkan SK, Versteeg HH, Cannegieter SC. (2013) Epidemiology of cancer-associated venous thrombosis. Blood. 122: 1712-23.

308   Horsted F, West J, Grainge MJ. (2012) Risk of venous thromboembolism in patients with cancer: a systematic review and meta-analysis. PLoS Med. 9: e1001275.

309   Hisada Y, Mackman N. (2017) Cancer-associated pathways and biomarkers of venous thrombosis. Blood. 130: 1499-506.

310   Khorana AA, Kuderer NM, Culakova E, Lyman GH, Francis CW. (2008) Development and validation of a predictive model for chemotherapy-associated thrombosis. Blood. 111: 4902-7.

311   Pabinger I, Posch F. (2014) Flamethrowers: blood cells and cancer thrombosis risk. Hematology Am Soc Hematol Educ Program. 2014: 410-7.

312   Blix K, Jensvoll H, Braekkan SK, Hansen JB. (2013) White blood cell count measured prior to cancer development is associated with future risk of venous thromboembolism--the Tromso study. PLoS One. 8: e73447.

313   Kasuga I, Makino S, Kiyokawa H, Katoh H, Ebihara Y, Ohyashiki K. (2001) Tumor-related leukocytosis is linked with poor prognosis in patients with lung carcinoma. Cancer. 92: 2399-405.

314   Esmon CT. (2004) Interactions between the innate immune and blood coagulation systems. Trends Immunol. 25: 536-42.

315   Osterud B. (1998) Tissue factor expression by monocytes: regulation and pathophysiological roles. Blood Coagul Fibrinolysis. 9 Suppl 1: S9-14.

316   Martinod K, Demers M, Fuchs TA, Wong SL, Brill A, Gallant M, Hu J, Wang Y, Wagner DD. (2013) Neutrophil histone modification by peptidylarginine deiminase 4 is critical for deep vein thrombosis in mice. Proc Natl Acad Sci U S A. 110: 8674-9.

317   Mauracher LM, Posch F, Martinod K, Grilz E, Daullary T, Hell L, Brostjan C, Zielinski C, Ay C, Wagner DD, Pabinger I, Thaler J. (2018) Citrullinated histone H3, a biomarker of neutrophil extracellular trap formation, predicts the risk of venous thromboembolism in cancer patients. J Thromb Haemost. 16: 508-18.

318   Oklu R, Sheth RA, Wong KHK, Jahromi AH, Albadawi H. (2017) Neutrophil extracellular traps are increased in cancer patients but does not associate with venous thrombosis. Cardiovasc Diagn Ther. 7: S140-S9.

319   Hisada Y, Ay C, Auriemma AC, Cooley BC, Mackman N. (2017) Human pancreatic tumors grown in mice release tissue factor-positive microvesicles that increase venous clot size. J Thromb Haemost. 15: 2208-17.

320   DuPre SA, Redelman D, Hunter KW, Jr. (2007) The mouse mammary carcinoma 4T1: characterization of the cellular landscape of primary tumours and metastatic tumour foci. Int J Exp Pathol. 88: 351-60.

321   Demers M, Krause DS, Schatzberg D, Martinod K, Voorhees JR, Fuchs TA, Scadden DT, Wagner DD. (2012) Cancers predispose neutrophils to release extracellular DNA traps that contribute to cancer-associated thrombosis. Proc Natl Acad Sci U S A. 109: 13076-81.

322   Leal AC, Mizurini DM, Gomes T, Rochael NC, Saraiva EM, Dias MS, Werneck CC, Sielski MS, Vicente CP, Monteiro RQ. (2017) Tumor-Derived Exosomes Induce the Formation of Neutrophil Extracellular Traps: Implications For The Establishment of Cancer-Associated Thrombosis. Sci Rep. 7: 6438.

323   Giri J, Sista AK, Weinberg I, Kearon C, Kumbhani DJ, Desai ND, Piazza G, Gladwin MT, Chatterjee S, Kobayashi T, Kabrhel C, Barnes GD. (2019) Interventional Therapies for Acute Pulmonary Embolism: Current Status and Principles for the Development of Novel Evidence: A Scientific Statement From the American Heart Association. Circulation. 140: e774-e801.

324   Spengler J, Lugonja B, Ytterberg AJ, Zubarev RA, Creese AJ, Pearson MJ, Grant MM, Milward M, Lundberg K, Buckley CD, Filer A, Raza K, Cooper PR, Chapple IL, Scheel-Toellner D. (2015) Release of Active Peptidyl Arginine Deiminases by Neutrophils Can Explain Production of Extracellular Citrullinated Autoantigens in Rheumatoid Arthritis Synovial Fluid. Arthritis Rheumatol. 67: 3135-45.

325   Zhou Y, Chen B, Mittereder N, Chaerkady R, Strain M, An LL, Rahman S, Ma W, Low CP, Chan D, Neal F, Bingham CO, 3rd, Sampson K, Darrah E, Siegel RM, Hasni S, Andrade F, Vousden KA, Mustelin T, Sims GP. (2017) Spontaneous Secretion of the Citrullination Enzyme PAD2 and Cell Surface Exposure of PAD4 by Neutrophils. Front Immunol. 8: 1200.

326   Nakayama-Hamada M, Suzuki A, Kubota K, Takazawa T, Ohsaka M, Kawaida R, Ono M, Kasuya A, Furukawa H, Yamada R, Yamamoto K. (2005) Comparison of enzymatic properties between hPADI2 and hPADI4. Biochem Biophys Res Commun. 327: 192-200.

327   Litvinov RI, Nabiullina RM, Zubairova LD, Shakurova MA, Andrianova IA, Weisel JW. (2019) Lytic Susceptibility, Structure, and Mechanical Properties of Fibrin in Systemic Lupus Erythematosus. Front Immunol. 10: 1626.

328   Binder V, Bergum B, Jaisson S, Gillery P, Scavenius C, Spriet E, Nyhaug AK, Roberts HM, Chapple ILC, Hellvard A, Delaleu N, Mydel P. (2017) Impact of fibrinogen carbamylation on fibrin clot formation and stability. Thromb Haemost. 117: 899-910.

329   Hood JE, Yesudasan S, Averett RD. (2018) Glucose Concentration Affects Fibrin Clot Structure and Morphology as Evidenced by Fluorescence Imaging and Molecular Simulations. Clin Appl Thromb Hemost. 24: 104S-16S.

330   Masson-Bessiere C, Sebbag M, Girbal-Neuhauser E, Nogueira L, Vincent C, Senshu T, Serre G. (2001) The major synovial targets of the rheumatoid arthritis-specific antifilaggrin autoantibodies are deiminated forms of the alpha- and beta-chains of fibrin. J Immunol. 166: 4177-84.

331   Sokolove J, Brennan MJ, Sharpe O, Lahey LJ, Kao AH, Krishnan E, Edmundowicz D, Lepus CM, Wasko MC, Robinson WH. (2013) Brief report: citrullination within the atherosclerotic plaque: a potential target for the anti-citrullinated protein antibody response in rheumatoid arthritis. Arthritis Rheum. 65: 1719-24.

332   Sharma M, Damgaard D, Senolt L, Svensson B, Bay-Jensen AC, Nielsen CH, Hagglund P. (2019) Expanding the citrullinome of synovial fibrinogen from rheumatoid arthritis patients. J Proteomics. 208: 103484.

333   Nakayama-Hamada M, Suzuki A, Furukawa H, Yamada R, Yamamoto K. (2008) Citrullinated fibrinogen inhibits thrombin-catalysed fibrin polymerization. J Biochem. 144: 393-8.

334   Okumura N, Haneishi A, Terasawa F. (2009) Citrullinated fibrinogen shows defects in FPA and FPB release and fibrin polymerization catalyzed by thrombin. Clin Chim Acta. 401: 119-23.

335   Damiana T, Damgaard D, Sidelmann JJ, Nielsen CH, de Maat MPM, Munster AB, Palarasah Y. (2020) Citrullination of fibrinogen by peptidylarginine deiminase 2 impairs fibrin clot structure. Clin Chim Acta. 501: 6-11.

336   Chang X, Yamada R, Sawada T, Suzuki A, Kochi Y, Yamamoto K. (2005) The inhibition of antithrombin by peptidylarginine deiminase 4 may contribute to pathogenesis of rheumatoid arthritis. Rheumatology (Oxford). 44: 293-8.

337   Tilvawala R, Nguyen SH, Maurais AJ, Nemmara VV, Nagar M, Salinger AJ, Nagpal S, Weerapana E, Thompson PR. (2018) The Rheumatoid Arthritis-Associated Citrullinome. Cell Chem Biol. 25: 691-704 e6.

338   Sorvillo N, Mizurini DM, Coxon C, Martinod K, Tilvawala R, Cherpokova D, Salinger AJ, Seward RJ, Staudinger C, Weerapana E, Shapiro NI, Costello CE, Thompson PR, Wagner DD. (2019) Plasma Peptidylarginine Deiminase IV Promotes VWF-Platelet String Formation and Accelerates Thrombosis After Vessel Injury. Circ Res. 125: 507-19.

339   Kovacs A, Sotonyi P, Nagy AI, Tenekedjiev K, Wohner N, Komorowicz E, Kovacs E, Nikolova N, Szabo L, Kovalszky I, Machovich R, Szelid Z, Becker D, Merkely B, Kolev K. (2015) Ultrastructure and composition of thrombi in coronary and peripheral artery disease: correlations with clinical and laboratory findings. Thromb Res. 135: 760-6.

340   Geddings J, Aleman MM, Wolberg A, von Bruhl ML, Massberg S, Mackman N. (2014) Strengths and weaknesses of a new mouse model of thrombosis induced by inferior vena cava stenosis: communication from the SSC of the ISTH. J Thromb Haemost. 12: 571-3.

341   Wrobleski SK, Farris DM, Diaz JA, Myers DD, Jr., Wakefield TW. (2011) Mouse complete stasis model of inferior vena cava thrombosis. J Vis Exp.

342   Diaz JA, Obi AT, Myers DD, Jr., Wrobleski SK, Henke PK, Mackman N, Wakefield TW. (2012) Critical review of mouse models of venous thrombosis. Arterioscler Thromb Vasc Biol. 32: 556-62.

343   Varju I, Sotonyi P, Machovich R, Szabo L, Tenekedjiev K, Silva MM, Longstaff C, Kolev K. (2011) Hindered dissolution of fibrin formed under mechanical stress. J Thromb Haemost. 9: 979-86.

344   Nikolova N, Toneva-Zheynova D, Tenekedjiev K, Kolev K. Monte Carlo Statistical Tests for Identity of Theoretical and Empirical Distributions of Experimental Data. In: Chan WKV (Ed.), Theory and Applications of Monte Carlo Simulations. InTech, London, 2013: 1-26.

345   Yeromonahos C, Polack B, Caton F. (2010) Nanostructure of the fibrin clot. Biophys J. 99: 2018-27.

346   Wacha A, Zoltán V, Attila B. (2014) CREDO: a new general-purpose laboratory instrument forsmall-angle X-ray scattering. J Appl Cryst 47: 1749-54.

347   Wacha A. (2015) Optimized pinhole geometry for small-angle scattering. J Appl Cryst. 48: 1843-8.

348   Woodhead JL, Nagaswami C, Matsuda M, Arocha-Pinango CL, Weisel JW. (1996) The ultrastructure of fibrinogen Caracas II molecules, fibers, and clots. J Biol Chem. 271: 4946-53.

349   Duval C, Allan P, Connell SD, Ridger VC, Philippou H, Ariens RA. (2014) Roles of fibrin alpha- and gamma-chain specific cross-linking by FXIIIa in fibrin structure and function. Thromb Haemost. 111: 842-50.

350   Longstaff C, fibrinolysis Tso. (2017) Development of Shiny app tools to simplify and standardize the analysis of hemostasis assay data: communication from the SSC of the ISTH. J Thromb Haemost. 15: 1044-6.

351   Daas A. Combistats v5. Available at: www.combistats.eu Accessed 2021 Jul 17.

352   Nikolova N, Chai S, Ivanova SD, Kolev K, Tenekedjiev K. (2015) Bootstrap Kuiper Testing of the Identity of 1D Continuous Distributions using Fuzzy Samples. International Journal of Computational Intelligence Systems. 8 (Suppl. 2): 63-75.

353   Efron B, Tibshirani RJ. An Introduction to the Bootstrap. Chapman&Hall, New York, NY, USA, 1993: 220-223.

354   Nikolova N, Mihaylova N, Tenekedjiev K. (2015) Bootstrap tests for mean value differences over fuzzy samples. IFAC-PapersOnLine. 48: 7-14.

355   Benjamini Y, Yekutieli D. (2001) The control of the false discovery rate in multiple testing under dependency. Ann Statist. 29: 1165-88.

356   Longstaff C, Kolev K. (2015) Basic mechanisms and regulation of fibrinolysis. J Thromb Haemost. 13 Suppl 1: S98-105.

357   Blomback B, Carlsson K, Hessel B, Liljeborg A, Procyk R, Aslund N. (1989) Native fibrin gel networks observed by 3D microscopy, permeation and turbidity. Biochim Biophys Acta. 997: 96-110.

358   Hisada Y, Grover SP, Maqsood A, Houston R, Ay C, Noubouossie DF, Cooley BC, Wallen H, Key NS, Thalin C, Farkas AZ, Farkas VJ, Tenekedjiev K, Kolev K, Mackman N. (2020) Neutrophils and neutrophil extracellular traps enhance venous thrombosis in mice bearing human pancreatic tumors. Haematologica. 105: 218-25.

359   Varju I, Sorvillo N, Cherpokova D, Farkas AZ, Farkas VJ, Komorowicz E, Feller T, Kiss B, Kellermayer MZ, Szabo L, Wacha A, Bota A, Longstaff C, Wagner DD, Kolev K. (2021) Citrullinated Fibrinogen Renders Clots Mechanically Less Stable, but Lysis-Resistant. Circ Res. 129: 342-4.

360   Mazur P, Sobczynski R, Zabczyk M, Babiarczyk P, Sadowski J, Undas A. (2013) Architecture of fibrin network inside thrombotic material obtained from the right atrium and pulmonary arteries: flow and location matter. J Thromb Thrombolysis. 35: 127-9.

361   Feller T, Harsfalvi J, Csanyi C, Kiss B, Kellermayer M. (2018) Plasmin-driven fibrinolysis in a quasi-two-dimensional nanoscale fibrin matrix. J Struct Biol. 203: 273-80.

362   Liesenborghs L, Verhamme P, Vanassche T. (2018) Staphylococcus aureus, master manipulator of the human hemostatic system. J Thromb Haemost. 16: 441-54.

363   Farkas AZ, Farkas VJ, Szabo L, Wacha A, Bota A, Csehi L, Kolev K, Thelwell C. (2019) Structure, Mechanical, and Lytic Stability of Fibrin and Plasma Coagulum Generated by Staphylocoagulase From Staphylococcus aureus. Front Immunol. 10: 2967.

364   King MJ, Morris MS, Tager M. (1975) The comparative ultrastructure of fibrin induced by thrombin and by staphylocoagulase. Thromb Diath Haemorrh. 34: 223-35.

365   Liu W, Jawerth LM, Sparks EA, Falvo MR, Hantgan RR, Superfine R, Lord ST, Guthold M. (2006) Fibrin fibers have extraordinary extensibility and elasticity. Science. 313: 634.

366   Moreillon P, Entenza JM, Francioli P, McDevitt D, Foster TJ, Francois P, Vaudaux P. (1995) Role of Staphylococcus aureus coagulase and clumping factor in pathogenesis of experimental endocarditis. Infect Immun. 63: 4738-43.

367   Baddour LM, Tayidi MM, Walker E, McDevitt D, Foster TJ. (1994) Virulence of coagulase-deficient mutants of Staphylococcus aureus in experimental endocarditis. J Med Microbiol. 41: 259-63.

368   Pretorius E, Page MJ, Hendricks L, Nkosi NB, Benson SR, Kell DB. (2018) Both lipopolysaccharide and lipoteichoic acids potently induce anomalous fibrin amyloid formation: assessment with novel Amytracker stains. J R Soc Interface. 15.

369   Jung CJ, Yeh CY, Hsu RB, Lee CM, Shun CT, Chia JS. (2015) Endocarditis pathogen promotes vegetation formation by inducing intravascular neutrophil extracellular traps through activated platelets. Circulation. 131: 571-81.

370   Laridan E, Denorme F, Desender L, Francois O, Andersson T, Deckmyn H, Vanhoorelbeke K, De Meyer SF. (2017) Neutrophil extracellular traps in ischemic stroke thrombi. Ann Neurol.

371   von Vietinghoff S, Ley K. (2008) Homeostatic regulation of blood neutrophil counts. J Immunol. 181: 5183-8.

372   Demers M, Wong SL, Martinod K, Gallant M, Cabral JE, Wang Y, Wagner DD. (2016) Priming of neutrophils toward NETosis promotes tumor growth. Oncoimmunology. 5: e1134073.

373   Cedervall J, Zhang Y, Huang H, Zhang L, Femel J, Dimberg A, Olsson AK. (2015) Neutrophil Extracellular Traps Accumulate in Peripheral Blood Vessels and Compromise Organ Function in Tumor-Bearing Animals. Cancer Res. 75: 2653-62.

374   Schwarzenbach H, Hoon DS, Pantel K. (2011) Cell-free nucleic acids as biomarkers in cancer patients. Nat Rev Cancer. 11: 426-37.

375   Swystun LL, Mukherjee S, Liaw PC. (2011) Breast cancer chemotherapy induces the release of cell-free DNA, a novel procoagulant stimulus. J Thromb Haemost. 9: 2313-21.

376   Weisel JW. (2007) Structure of fibrin: impact on clot stability. J Thromb Haemost. 5 Suppl 1: 116-24.

377   He S, Bark N, Wang H, Svensson J, Blomback M. (2009) Effects of acetylsalicylic acid on increase of fibrin network porosity and the consequent upregulation of fibrinolysis. J Cardiovasc Pharmacol. 53: 24-9.

378   Bjornsson TD, Schneider DE, Berger H, Jr. (1989) Aspirin acetylates fibrinogen and enhances fibrinolysis. Fibrinolytic effect is independent of changes in plasminogen activator levels. J Pharmacol Exp Ther. 250: 154-61.

379   Harris WH, Salzman EW, Athanasoulis CA, Waltman AC, DeSanctis RW. (1977) Aspirin prophylaxis of venous thromboembolism after total hip replacement. N Engl J Med. 297: 1246-9.

380   Li R, Ren M, Luo M, Chen N, Zhang Z, Luo B, Wu J. (2012) Monomeric C-reactive protein alters fibrin clot properties on endothelial cells. Thromb Res. 129: e251-6.

381   Undas A, Plicner D, Stepien E, Drwila R, Sadowski J. (2007) Altered fibrin clot structure in patients with advanced coronary artery disease: a role of C-reactive protein, lipoprotein(a) and homocysteine. J Thromb Haemost. 5: 1988-90.

382   Fatah K, Silveira A, Tornvall P, Karpe F, Blomback M, Hamsten A. (1996) Proneness to formation of tight and rigid fibrin gel structures in men with myocardial infarction at a young age. Thromb Haemost. 76: 535-40.

383   Schuett K, Savvaidis A, Maxeiner S, Lysaja K, Jankowski V, Schirmer SH, Dimkovic N, Boor P, Kaesler N, Dekker FW, Floege J, Marx N, Schlieper G. (2017) Clot Structure: A Potent Mortality Risk Factor in Patients on Hemodialysis. J Am Soc Nephrol. 28: 1622-30.

384   Undas A. (2017) Prothrombotic Fibrin Clot Phenotype in Patients with Deep Vein Thrombosis and Pulmonary Embolism: A New Risk Factor for Recurrence. Biomed Res Int. 2017: 8196256.

385   Putaala J, Haapaniemi E, Metso AJ, Metso TM, Artto V, Kaste M, Tatlisumak T. (2010) Recurrent ischemic events in young adults after first-ever ischemic stroke. Ann Neurol. 68: 661-71.

386   Bannish BE, Keener JP, Fogelson AL. (2014) Modelling fibrinolysis: a 3D stochastic multiscale model. Math Med Biol. 31: 17-44.

387   Koehn JA, Hurlet-Jensen A, Nossel HL, Canfield RE. (1983) Sequence of plasmin proteolysis at the NH2-terminus of the b beta-chain of human fibrinogen. Anal Biochem. 133: 502-10.

388   Kirschbaum NE, Budzynski AZ. (1990) A unique proteolytic fragment of human fibrinogen containing the A alpha COOH-terminal domain of the native molecule. J Biol Chem. 265: 13669-76.

389   Domingues MM, Macrae FL, Duval C, McPherson HR, Bridge KI, Ajjan RA, Ridger VC, Connell SD, Philippou H, Ariens RA. (2016) Thrombin and fibrinogen gamma' impact clot structure by marked effects on intrafibrillar structure and protofibril packing. Blood. 127: 487-95.

390   Schwartz RS, Burke A, Farb A, Kaye D, Lesser JR, Henry TD, Virmani R. (2009) Microemboli and microvascular obstruction in acute coronary thrombosis and sudden coronary death: relation to epicardial plaque histopathology. J Am Coll Cardiol. 54: 2167-73.

131

391   Rottenberger Z, Komorowicz E, Szabo L, Bota A, Varga Z, Machovich R, Longstaff C, Kolev K. (2013) Lytic and mechanical stability of clots composed of fibrin and blood vessel wall components. J Thromb Haemost. 11: 529-38.

392   Coudane F, Mechin MC, Huchenq A, Henry J, Nachat R, Ishigami A, Adoue V, Sebbag M, Serre G, Simon M. (2011) Deimination and expression of peptidylarginine deiminases during cutaneous wound healing in mice. Eur J Dermatol. 21: 376-84.

393   Hejblum BP, Cui J, Lahey LJ, Cagan A, Sparks JA, Sokolove J, Cai T, Liao KP. (2018) Association Between Anti-Citrullinated Fibrinogen Antibodies and Coronary Artery Disease in Rheumatoid Arthritis. Arthritis Care Res (Hoboken). 70: 1113-7.

394   Sorvillo N, Cherpokova D, Martinod K, Wagner DD. (2019) Extracellular DNA NET-Works With Dire Consequences for Health. Circ Res. 125: 470-88.

395   Lewis HD, Liddle J, Coote JE, Atkinson SJ, Barker MD, Bax BD, Bicker KL, Bingham RP, Campbell M, Chen YH, Chung CW, Craggs PD, Davis RP, Eberhard D, Joberty G, Lind KE, Locke K, Maller C, Martinod K, Patten C, Polyakova O, Rise CE, Rudiger M, Sheppard RJ, Slade DJ, Thomas P, Thorpe J, Yao G, Drewes G, Wagner DD, Thompson PR, Prinjha RK, Wilson DM. (2015) Inhibition of PAD4 activity is sufficient to disrupt mouse and human NET formation. Nat Chem Biol. 11: 189-91.

10. Bibliography of the candidate's publications

10.1. Publications related to the PhD thesis

[1] Farkas AZ*, Farkas VJ*, Gubucz I, Szabo L, Balint K, Tenekedjiev K, Nagy AI, Sotonyi P, Hidi L, Nagy Z, Szikora I, Merkely B and Kolev K. (2019) Neutrophil extracellular traps in thrombi retrieved during interventional treatment of ischemic arterial diseases. Thromb Res, 175: 46-52.

Impact factor: 2.869

[2] Farkas AZ, Farkas VJ, Szabo L, Wacha A, Bota A, Csehi L, Kolev K and Thelwell C. (2019) Structure, Mechanical, and Lytic Stability of Fibrin and Plasma Coagulum Generated by Staphylocoagulase From Staphylococcus aureus. Front Immunol, 10: 2967.

Impact factor: 5.085

[3] Hisada Y, Grover SP, Maqsood A, Houston R, Ay C, Noubouossie DF, Cooley BC, Wallen H, Key NS, Thalin C, Farkas AZ, Farkas VJ, Tenekedjiev K, Kolev K and Mackman N. (2020) Neutrophils and neutrophil extracellular traps enhance venous thrombosis in mice bearing human pancreatic tumors. Haematologica, 105: 218-225.

Impact factor: 9.941

[4] Varjú I, Sorvillo N, Cherpokova D, Farkas ÁZ, Farkas VJ, Komorowicz E, Feller T, Kiss B, Kellermayer M, Szabó L, Wacha A, Bóta A, Longstaff C, Wagner DD, Kolev K. (2021) Citrullinated fibrinogen renders clots mechanically less stable, but lysis-resistant. Circ Res, 2021; 129:342-344

Impact factor: 17.367

10.2. Publications not related to the PhD thesis

[1] Varju I, Longstaff C, Szabo L, Farkas AZ, Varga-Szabo VJ, Tanka-Salamon A, Machovich R and Kolev K. (2015) DNA, histones and neutrophil extracellular traps exert anti-fibrinolytic effects in a plasma environment. Thromb Haemost, 113: 1289-98.

[2] Varju I*, Farkas VJ*, Kohidai L, Szabo L, Farkas AZ, Polgar L, Chinopoulos C and Kolev K. (2018) Functional cyclophilin D moderates platelet adhesion, but enhances the lytic resistance of fibrin. Sci Rep, 8: 5366.

[3] Farkas ÁZ, Török S, Kovács JB, Piros L, Végső G, Kiss G, Korda D, Bibok A, Hartmann E, Deák ÁP, Doros A. (2019) Diagnosis and Management of a De Novo Urothelial Carcinoma in a Kidney Allograft: A Case Report. Transplant Proc. 51(4):1281-1285.

11. Acknowledgements

Finally, I am extending my heartfelt thanks to my family for their acceptance and patience during my research work and thesis preparation. I am very much thankful to my wife (who was also my colleague) for her love, understanding and continuing support to complete this research work.